PhD.31030

Diamond Schottky Barrier Diodes

Mihai Brezeanu

Churchill College
Department of Engineering
University of Cambridge

CAMBRIDGE
UNIVERSITY
LIBRARY

Dissertation submitted for consideration to the University of Cambridge towards the degree of Doctor of Philosophy

August 2007

Diamond Schottky Barrier Diodes
Mihai Brezeanu

Summary

Research on wide band gap semiconductors suitable for power electronic devices has spread rapidly in the last decade. The remarkable results exhibited by silicon carbide (SiC) Schottky barrier diodes (SBDs), commercially available since 2001, showed the potential of wide band gap semiconductors for replacing silicon (Si) in the range of medium to high voltage applications, where high frequency operation is required. With superior physical and electrical properties, diamond became a potential competitor to SiC soon after Element Six reported in 2002 the successful synthesis of single crystal plasma deposited diamond with high carrier mobility.

This thesis discusses the remarkable properties of diamond and introduces several device structures suitable for power electronics. The calculation of several figures of merit emphasize the advantages of diamond with respect to silicon and other wide band gap semiconductors and clearly identifies the areas where its impact would be most significant. Information regarding the first synthesis of diamond, which took place back in 1954, together with data regarding the modern technological process which leads nowadays to high-quality diamond crystals suitable for electronic devices, are reviewed. Models regarding the incomplete ionization of atomic dopants and the variation of carrier mobility with doping level and temperature have been elaborated and included in numerical simulators.

The study introduces the novel diamond M-i-P Schottky diode, a version of power Schottky diode which takes advantage of the extremely high intrinsic hole mobility. The structure overcomes the drawback induced by the high activation energies of acceptor dopants in diamond which yield poor hole concentration at room temperature. The complex shape of the on-state characteristic exhibited by diamond M-i-P Schottky structures is thoroughly investigated by means of experimental results, numerical simulations and theoretical considerations.

The fabrication of a ramp oxide termination on a diamond device is for the first time reported in this thesis. Both experimental and simulated results show the potential of this termination structure, previously built on Si and SiC power devices. A comprehensive comparison between the ramp oxide and two other versions of the field plate termination concept, the single step and the three-step structures, has been performed, considering aspects such as electrical performance, occupied area, complexity of technological process and cost.

Based on experimental results presented in this study, together with predictions made via simulations and theoretical models, it is concluded that diamond M-i-P Schottky diodes have the ability to deliver significantly higher performance compared to that of SiC SBDs if issues such as material defects, Schottky contact formation and measurement of reliable ionization coefficients are carefully addressed in the near future.

Acknowledgements

To Dr. Florin Udrea, my supervisor, for his never-ending enthusiasm, invaluable help, and flattering friendship

To Professor Gehan Amaratunga, my advisor, for all the ideas, good spirits, confidence and support

To Gates Cambridge Trust and Overseas Research Students Awards Scheme for their financial support

To Antonella Tajani and Richard Balmer from Element Six, to Lee Coulbeck and Tony Garraway from Dynex Semiconductors, to Nalin Rupesinghe, Jeremy Rashid and Tim Butler, for all the discussions regarding diamond devices and many other matters

To Professor Adrian Rusu at the University Politehnica Bucharest for the guidance during my undergraduate years

To all my colleagues in the High Voltage Microelectronics Laboratory, to Suat for showing La Dolce vita, to Mash-hud and the right to ask questions, to Marina Antoniou and her future Romanian villa, to Zeeshan and our twin PhD-routes, to Hatice and her heinous Bukowskian nights

To Alex and our Internautian nights which once happened in a Japanese morning, to Cristina and her unbeatable Frederic, to Dani and his stock exchange good luck, to Delia and her British happiness, to Doru and his weekly wanderings, to Letitia and her South-American white-dressed knight, to Maria and her exercises of admiration, to Mihnea and all the online matches, to Oana and her charmful, unalterable energy, to Puiu and his friendship, to Ramona&Silviu, the classy couple, to Razvan and our laughs together, to Voichita and the way she co-hosted that exibition in London, to Suzana and her willing to help

To Anca and her moody moods, to Bogdan, the scientist who has the passion and the strength to change the world, to Claudia and her jolly demission, to Valeria&Marco, the Italian way of saying "I love you", to Anne&Raph, for the Wolfsonian months and always surprising future, to Mircea and our endless conversation about Romania, to Danutz, ultimul fermion dashtept al verginei sutane, to Sorana&Alex and my kindergarten memories reborn during a night in London, to Miha&Cristi, "the apple and the pear / the lovely, happy pair / who love the teddy bear", to Andra and her belief in people

To Marina and my sweet childhood

To all those who are not to be named here, to all those who are watching from above, who are and always be part of my life

To all those long-time-ago forgotten ideas, feelings, mornings, smiles and dreams

To Andrei and those tears premeditated in dreams before happening in reality

To Lucian and his daily, brotherly being

To my grandmothers and everything they thought for me, to my father and his passion, to my mother and her dedication

To Laura and our love

Declaration

This thesis contains the results of my research work undertaken between October 2003 and August 2007 as a student in the High Voltage Microelectronics Laboratory, part of the Engineering Department, University of Cambridge. This is entirely my own research work and contains nothing done in collaboration, except where explicit acknowledgement is given.

No part of this thesis has been ever submitted towards any other degree.

Permission is hereby granted to consult or copy parts of this thesis for purpose of private study, but not for any other purposes.

This thesis contains approximately 25500 words, 102 figures, and 7 tables.

Mihai Brezeanu
Cambridge
August 2007

Contents

Contents i

1 **Introduction** 1

1.1 Semiconductors for power electronics: from germanium to diamond.. 2

1.2 Overview of the thesis 4

2 **Synthetic Single Crystal Diamond** 6

2.1 Brief history 7

2.2 Material properties 8

2.2.1 Physical properties 8

2.2.2 Electrical properties 12

2.2.3 Figures of merit 16

2.3 Process and fabrication issues 18

2.3.1 Synthesis of diamond 18

2.3.2 Ohmic and Schottky contacts 19

2.4 Diamond devices 20

2.4.1 Introduction 20

2.4.2 Schottky diodes 20

2.4.3 Field effect transistors 22

3 **Models used in numerical simulations** 25

3.1 Introduction 26

3.2 Incomplete ionization.. 28

3.3 Mobility versus doping 31

3.4 Mobility versus temperature.. 35

3.5 Ionization coefficients.. 36

4 **Schottky rectifiers.. 39**

4.1 Schottky contact essentials.. 40

4.2 Power rectifiers.. 50

4.2.1 Silicon power rectifiers.. 50

4.2.2 Silicon carbide power rectifiers...................................... 53

4.3 Diamond M-i-P Schottky diodes....................................... 56

5 **The on-state behaviour of the diamond M-i-P structure................ 64**

5.1 The shape of the forward characteristic................................ 65

5.2 The dispersion on the on-state characteristic........................... 71

5.3 Temperature variation.. 76

5.3.1 M-i-P structures.. 76

5.3.2 Experiment-simulation matching...................................... 78

5.3.3 Non M-i-P structures.. 81

5.4 Zero temperature coefficient point on the forward characteristic....... 86

6 **Termination structures suitable for diamond M-i-P diodes........ 89**

6.1 Introduction.. 90

6.2 Single step field plate termination..................................... 96

6.3 Three-step field plate termination....................................... 104

6.4 Ramp oxide termination.. 110

6.4.1 General consideration... 110

6.4.2 Structure optimisation... 111

6.4.3 Experimental results... 115

6.5 Comparison between different termination structures.................... 122

6.5.1 Electrical performance... 122

6.5.2 Area consumption comparison...................................... 123

6.5.3 Scaling with drift thickness.. 125

6.6 Use of high-k dielectrics for oxide ramp termination..................... 127

7 Conclusions and future work... 133

References.. 139

Appendix A - Diamond parameters implemented in ISE-TCAD simulator 147

Appendix B - List of publications and patents................................ 153

CHAPTER 1
Introduction

1.1 Semiconductors for power electronics: from germanium to diamond

Following its historical debut, which coincides with the invention of the bipolar transistor in 1947, the field of power electronics had a consistent and spectacular development. The first power electronic devices were built on germanium, which was by far the most preferred semiconductor material in those early times. In 1952, Hall presented the first power rectifier built on germanium, which had a breakdown voltage of 200V and an on-state current capability of 35A [1]. By the end of the 1950's, germanium started to be replaced by silicon. With excellent semiconducting properties, simple, diverse and cheap means methods of growth, and above all, having the best native oxide (SiO_2) among all known semiconductors, silicon soon won the battle against germanium and became the "supreme" semiconductor in electronics.

The remarkable technological achievements enabled the fabrication of silicon thyristors able to block more than 5000V and to conduct 2000A when forward-biased. However, due to their bipolar conduction mechanism, these devices suffered from serious limitations in terms of high frequency operation [2]. The replacement of the bipolar structure with MOS (Metal Oxide Semiconductor) power transistors allowed operation at high frequencies, but seriously affected the on- and off-state performance.

Most of Si Power MOSFETs (MOS Field Effect Transistors) are rated at breakdown voltages of less than 200V, which corresponds to the low voltage range of applications. Any increase in the off-state capability induces a drastic increase in the on-state resistance, thus leading to significant overall losses [3].

In the early 1980's, Baliga derived an equation for unipolar power devices, according to which the on-state resistance of such a device is proportional with the square

CAMBRIDGE UNIVERSITY LIBRARY

of the breakdown voltage, and reversely proportional with the carrier mobility and the cube of the critical electric field [4]. Based on this equation, the possibility of replacing silicon with wide band bap semiconductors with superior carrier mobility and critical electric field started to be investigated. Silicon carbide (SiC), and gallium nitride (GaN) were amongst the first wide band gap semiconductors considered for power devices. In order to keep the switching losses at low levels, the research has mainly focused on devices based on unipolar conduction. The aim was to replace silicon p-i-n diodes with wide band gap Schottky rectifiers and silicon bipolar transistors and thyristors with wide band gap power FETs [5, 6].

In the following two decades, the technology for the growth of high-purity, high-quality wide band gap materials, especially silicon carbide, constantly developed, culminating with the paper published by Toyota and Denso in Nature in 2004 [7] reporting the achievement of ultrahigh-quality silicon carbide single crystals. In terms of SiC devices, Schottky barrier diodes (SBDs) on 4H-SiC capable of blocking 600V became commercially available in 2001 [8], while now Cree and Infineon offer SiC SBDs with 1.2kV off-state capability and zero reverse-recovery losses [9, 10]. In terms of SiC transistors, the evolution was less spectacular, no commercial product being currently available. However, SiC FETs with breakdown voltages in the range of 5000V and low on-state resistance have been reported [11].

The consistent success in producing SiC power devices with clearly superior performance compared to that of their Si counterparts has consolidated the faith in the potential of wide band gap semiconductors for power electronics. A new chapter within this avant-garde field was opened by the announcement in 2002 made by Element Six in Science [12] regarding the synthesis of single crystal plasma deposited diamond with high carrier mobility. This high-quality synthetic diamond, with hole mobility nearly one order of magnitude higher than in Si, SiC or GaN, and with, by far, the largest critical field amongst semiconductors, looked like the perfect candidate for repeating in the near future the SiC success story [13].

1.2 Overview of the thesis

It is the purpose of this thesis to introduce diamond as a material suitable for power electronics and to present some of the device structures which yield promising results when built on diamond. A special attention is given to diamond Schottky diodes which are thoroughly investigated by means of new theoretical considerations, numerical simulations and experimental data. The diamond M-i-P Schottky diode, a version of the power SBD structure adapted to the diamond specific properties, is introduced and analysed, and models for its on-state behaviour, together with suitable termination structures, are also developed.

Chapter 2 presents the physical and electric properties of diamond. The outstanding theoretical properties of diamond are compared with the ones corresponding to its main semiconductor competitors. Well-known figures of merit for power devices exhibit extreme values in case of diamond, thus enhancing the remarkable 'charisma' of this wide band gap material. Considerations regarding the synthesis of the material, together with issues related to the deposition of both ohmic and Schottky contacts are also discussed. Several types of diamond Schottky diodes and field effect transistors, the most attractive categories of diamond devices, are also introduced in **Chapter 2**.

Due to its novelty in the family of semiconductors for electronic applications, diamond is not currently included in the default material library of the commercially available simulators. The extensive models which were considered in order to define diamond as a semiconductor in ISE-TCAD simulator are presented in **Chapter 3**. The variation of mobility with doping and temperature, and the incomplete ionization of dopants are some of the phenomena which were taken into consideration.

The diamond M-i-P Schottky structure, which represents the main focus and novelty in this thesis, is introduced in **Chapter 4**. A comprehensive analysis of the potential advantages of the diamond M-i-P diode with respect to that of the Si p-i-n diode

and the SiC SBD is made. Band diagrams drawn at different biases explicitly show the complex phenomena that occur within this type of Schottky diode.

The on-state behaviour of the diamond M-i-P diodes is the subject of **Chapter 5**. Three main regions can be delimited on the forward characteristics. For small forward biases, the current has an exponential increase with the voltage, obeying the thermionic emission theory. As the voltage increases, the current becomes space-charge limited and turn to a quadratic behaviour. Finally, for high current levels, the voltage drop on the internal resistances becomes predominant and the current has a linear variation with the voltage. The influence of the temperature and of the doping level on the forward characteristics is also investigated.

Chapter 6 in concerned with termination structures suitable for such diamond Schottky structures. The single-step and three-step field plate terminations, together with the ramp oxide structure are thoroughly investigated by means of numerical simulations. Experimental results of the profile and performance of the ramp oxide termination for the first time produced on a diamond device are reported here. The possibility of replacing SiO_2 as a field oxide layer with high-k dielectrics is also investigated.

The final conclusions of the thesis and ideas for further research are included in **Chapter 7**.

Chapter 2

Synthetic Single Crystal Diamond

CHAPTER 2

Synthetic Single Crystal Diamond

2.1 Brief history

For thousands of years, natural diamonds have sparked the imagination of people all around the world. Their capability to disperse light better than any other precious material, their amazing resistance to corrosion by acids and salts, and their outstanding hardness have fascinated people and given birth to numerous legends and myths [14]. In the 19th century, as the industry was developing rapidly, scientists became interested in using diamond's remarkable properties. However, the extremely high cost of natural diamond stones made their widespread industrial scale use almost prohibitively expensive. Thus, the need for synthetic diamond emerged.

Who produced the first synthetic diamond sample is still a controversial subject. Scientists at the General Electric Company's research laboratories in Schenectady, New York, are commonly acknowledged to have been the first to succeed in synthesizing diamond, in December 1954. The experiment was successfully repeated in the next two weeks [15] and the results were published on the 9th of July 1955, in Nature [16]. The first paragraph of the paper, entitled "Man-Made Diamonds", describes the atmosphere filled with extreme passion, great expectations and well hidden secrets, which surrounded the subject: "In the 1920's it was quite widely believed that diamond had been made from carbon under conditions of high heat and great pressure. The story was indeed one to capture the imagination. It involved famous chemists, a thoroughly fascinating subject and very striking experimental techniques" [16]. The essential key which enabled the General Electric scientists to successfully synthesize diamond was their ability to build high pressure, high temperature pressure vessels: "By developing some new ways of distributing stress and giving support to critical parts, our research group has succeeded in developing pressure vessels that operate at pressures up to at least 100,000 $kg*m/s^2$

and temperature in excess of 2300K for hours of continuous operation" [16]. The experiments were successfully repeated hundred of times within a couple of months, and yielded diamonds with dimensions varying from 100μm to 1mm along an edge. In order to convince the scientific community of the validity of their achievement, the authors of the paper presented four proofs: an X-ray showing the identity of crystal structure in man-made diamonds and natural diamonds, the result of a chemical analysis which showed that 86% of their produced samples was carbon, a picture presenting the scratches produced with the synthetic samples on the hardest face (111) of natural diamond, and the information that the synthesis was "repeated, entirely independently, by a number of workers in the General Electric Company" [16].

For many years, the General Electric team was unanimously considered as the first one to have ever produced synthetic diamond. However, it is now known that pieces of synthetic diamond were first obtained nearly two years earlier, on the 16th of February 1953, in Sweden [14], within a research project of the former Swedish company ASEA (ASEA is now part of the multinational ABB and during the 1970s their diamond synthesis unit was acquired by the British company Element Six). The machine used in the experiment had been designed by the inventor of the refrigerator, Baltzar von Platen, and was extremely complicated. Any mistake in its operation needed many days of effort before it could run again. Due to the lack of success in consistently reproducing the experiment and trying to avoid the synthesis procedure unravel, ASEA decided not to make their results public. This is the reason why the General Electric team is officially recognised as being the first to synthesize diamond.

2.2 Material properties

2.2.1 Physical properties

Diamond is the hardest known materials [17]. This is mainly due to the fact that is made of repeating units of carbon atoms joined to four other atoms via covalent bonds, which are the strongest chemical bonds. The distance between carbon atoms in diamond

is of 1.5445 Angstroms, while the angle between them is of 109^0. As a result, the central atom and its neighbors form a tetrahedron. The interlocking network of covalent bonds makes the diamond structure very rigid. In the diagram shown in **Fig. 2.1**, only a small part of the whole diamond structure is presented. Its giant covalent structure continues on and on in three dimensions. It's the extreme difficulty of breaking these 3D covalent bonds that makes diamond the hardest known material.

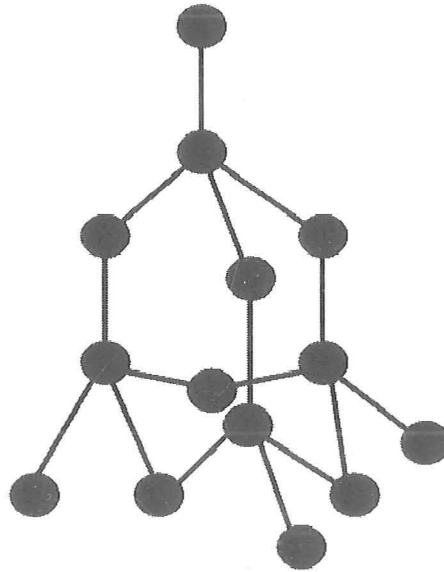

Fig. 2.1 – Crystalline structure of diamond

On Mohs scale, diamond is ranked 10, the hardest substance on the scale (**Fig. 2.2**). This scale, invented in 1812 by the German mineralogist Friedrich Mohs, characterizes the hardness of minerals. The hardness of a material is determined by scratching it against a reference mineral. If a material scratches the reference mineral, then it is of equal hardness or harder that it, otherwise it is softer. As it can be noticed, the intervals between minerals on this scale are irregular. Diamond is 1500 times harder than talc (ranked 1), while corundrum (ranked 9) is only 400 times harder. Diamond cannot be scratched by any other known material, therefore occupies the highest position on Mohs scale.

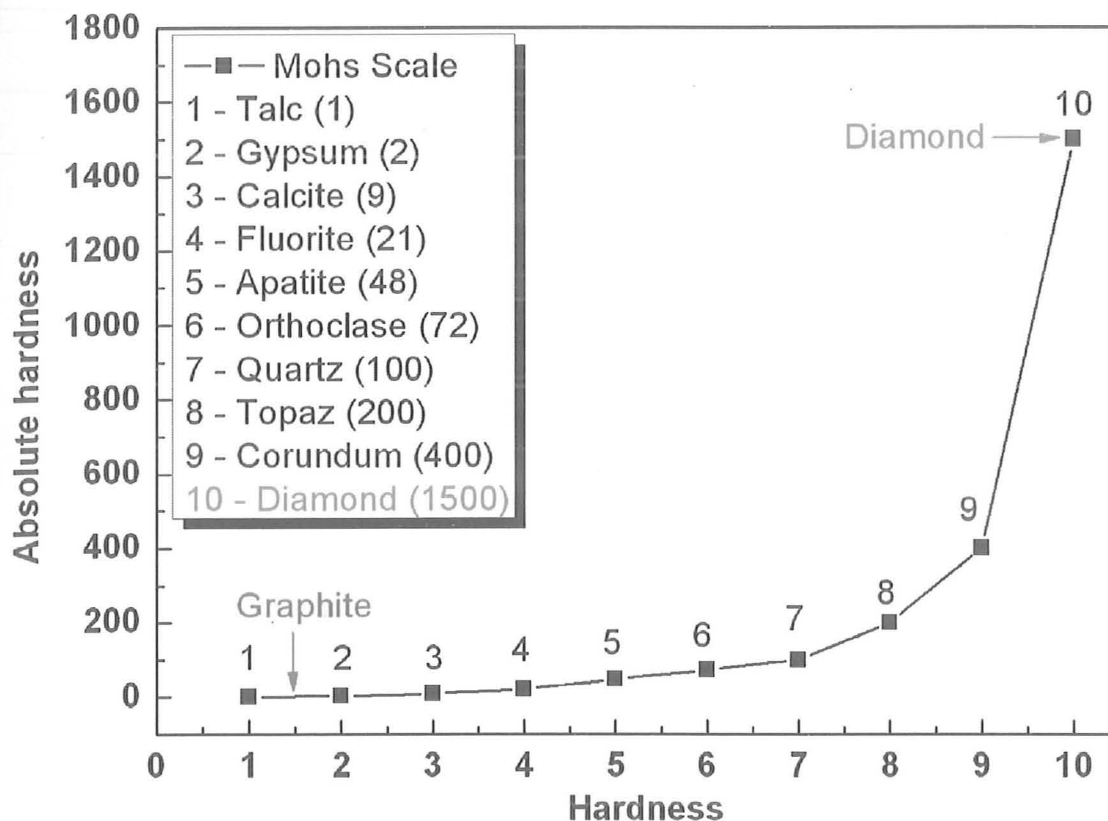

Fig. 2.2 – Mohs scale of mineral hardness
The absolute hardness of each material is mentioned between brackets,
in the legend of the figure

By simply rearranging the carbon atoms in the lattice, one can obtain graphite, a material much softer than diamond (ranks between 1 and 2 on Mohs scale). In graphite [18], each carbon atom uses three of its electrons to form simple bonds to its three close neighbours (**Fig. 2.3**). That leaves a fourth electron in the bonding level, which becomes delocalised over the whole of the sheet of atoms in one layer, and is free to wander throughout the whole sheet. There is, however, no direct contact between the delocalised electrons in one sheet and those in the neighbouring sheets. The sheets themselves are extremely strong, as in the case of diamond. The distance between atoms in the same sheet is 1.42Å, even lower than in diamond, but the distance between successive sheets is much higher (3.41Å).

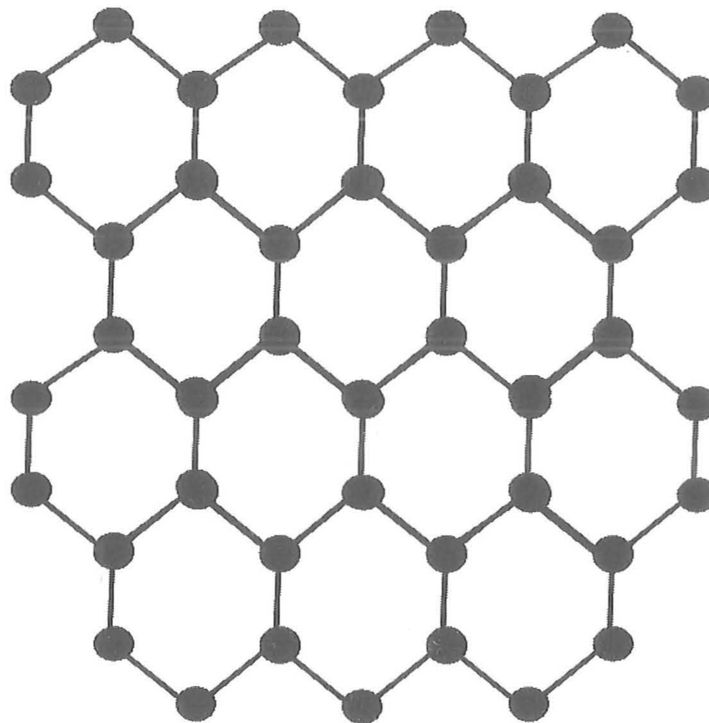

Fig. 2.3 – Sheet structure in graphite crystal

The softness of the material is in fact due to the weak bonds that link the sheets one to another. As a delocalised electron moves throughout a sheet, it creates very large temporary dipoles within the sheet, which, in turn, induce opposite dipoles in the sheets above and below. These dipoles keep the graphite sheets together through what is generally called van der Waals dispersion forces. However, this dispersion forces are much weaker than the covalent bonds, therefore, in the direction perpendicular to the sheets, graphite is much softer than diamond.

Apart from being the hardest material, diamond has also other extreme properties due to the extremely strong covalent bonds between its atoms. It is indeed the least compressible and stiffest substance known. Its melting and boiling points are extremely high (3550^0C and 4827^0C, respectively) and is also insoluble in water and organic solvents [19]. It is important to notice that graphite itself has an outstanding melting point (around 3600^0C). In order to melt graphite, not only the rather loose bonds between difference sheets have to be destroyed, but also the strong covalent bonds between carbon

atoms within the same sheet. Due to its symmetric atomic structure, diamond is optically isotropic and because its electrons are very tightly held they cannot be excited by light with wavelength in the visible range, therefore the material is highly transparent [20]. Synthetic diamond only reacts to light waves with wavelength lower than 0.225μm, which yields photon energy (E_{ph}) in excess to the material's band gap (5.47eV) [21]. This property makes synthetic diamond suitable for UV detector applications, as discussed in **Section 2.4** of this chapter.

Another important property of diamond is related to its thermal conductivity [22]. Thermal conductivity refers to material's ability of conducting heat through its crystalline structure. Due to its symmetric crystalline structure, diamond excellently conducts heat in the same way in all directions (thermal conductivity: 24W/cmK), while graphite has a good thermal conductivity along its parallel layers (19.6W/cmK), but a poor one along the direction perpendicular to the layers (0.0573W/cmK). This is again due to the lack of bonding between the layers, which is also responsible for the much lower hardness of graphite compared to diamond.

With respect to the level of impurities, natural diamonds can be classified into four categories [23]:

- type Ia diamond: the most spread, contains up to 0.3% nitrogen
- type Ib diamond: very rare, contains nitrogen concentrations of up to 500 ppm
- type IIa diamond: even more rare, has nitrogen concentrations which cannot be detected by means of IR (infra-red) or UV (ultra-violet) measurements
- type IIb diamond: extremely rare, has nitrogen concentration lower than type IIa

The synthetic diamond which is now used in industry and which will be discussed in this thesis is of type Ib. Synthetic diamond shares with natural diamond all the physical properties presented so far and it has lots of attractive electrical features which are introduced in **Section 2.2.2**.

2.2.2 Electrical properties

Diamond devices have been subject to extensive research in the last 10-15 years. They are meant to become serious competitors to Si, GaN or SiC devices in the near

future. This hope is mainly nourished by the excellent electrical properties of diamond [24]. A comparison between the main properties of diamond and its potential competitors is provided in **Table 2.1**.

	Si	4H-SiC	GaN	Diamond
Band gap (eV)	1.1	3.2	3.44	5.47
Intrinsic carrier concentration at 300K (cm^{-3})	$1.5*10^{10}$	$8.2*10^{-9}$	$2.25*10^{-10}$	$1.1*10^{-27}$
Breakdown field (MV/cm)	0.3	2.4	5	10
Hole mobility (cm^2/Vs)	480	120	200	3800
Electron mobility (cm^2/Vs)	1450	900	2000	4500
Saturated hole mobility (cm/s)	0.9	2.0	2.5	2.0
Relative electric permittivity	11.8	9.7	5.35	5.7
Thermal conductivity (W/cmK)	1.5	4.9	1.3	24

Table 2.1 – Comparison between the electrical properties and thermal conductivities of Si, 4H-SiC, GaN and synthetic diamond (T=300K)

Diamond has the largest band gap among semiconductors (5.47eV). This high value yields an extremely low level of the intrinsic carrier concentration (n_i). In a semiconductor, n_i is given by the following formula:

$$n_i = (N_C N_V)^{1/2} \exp\left(-\frac{E_G}{2kT}\right) \tag{2.1}$$

E_G is the band gap (5.47eV for diamond), N_C the density of states in the conduction band ($5*10^{18}cm^{-3}$ for diamond, at 300K), N_V the density of states in the valence band ($1.8*10^{19}cm^{-3}$ for diamond, at 300K), and k is Boltzmann's constant ($1.38066*10^{-23}$J/K) [25]. At 300K, the intrinsic concentration of diamond is $1.1*10^{-27}cm^{-3}$, with 17 orders of magnitude lower than in SiC and with 37 orders of magnitude lower

than in Si. This low value gives diamond significant advantages compared to the other materials used in the power device industry.

Diamond devices are, theoretically, capable of operating at much higher temperatures compared to their competitors [26]. As it can be noticed from **equation 2.1**, n_i has a severe increase with temperature. Thus, for silicon devices operated at 600K for example, the intrinsic concentration is around $10^{15}cm^{-3}$. This value is fatal for a power device which typically has a drift doping level close, or even lower, than $10^{15}cm^{-3}$ (see **Chapter 4, Section 4.2**, for more details). Therefore, silicon power devices cannot be operated at 600K or larger temperatures. In the case of diamond, at 600K, the intrinsic concentration is around $10^{-5}cm^{-3}$, well below the typical doping levels of the drift layer.

Another advantage induced by the value of the intrinsic concentration in diamond is the low values of the leakage currents exhibited by diamond devices. For a p-n junction, the leakage current is given by **equation 2.2**:

$$I = qAWn_i / \tau \tag{2.2}$$

q is the electron charge, A is the area of the p-n junction, W is the width of the depletion region and τ is the generation time in the same region. It can be easily noticed that the smaller the intrinsic carrier concentration, the smaller the leakage current.

In terms of breakdown electric field, diamond has the largest value among semiconductors. This offers the advantage of designing diamond devices with thin drift regions capable of blocking high breakdown voltages. For a power device having the drift layer depleted at breakdown, Baliga has proposed the following relationship between the on-state resistance (R_{ON}), the breakdown voltage (BV) and the breakdown (critical) electric field ($E_{CRITICAL}$):

$$R_{ON} = \frac{4BV^2}{\varepsilon \mu E_{CRITICAL}^3} \tag{2.3}$$

For a given BV and a common device design, diamond's critical electric field, twice larger than in GaN, four times larger than in SiC and more than 30 times larger than in Si, yields a much lower on-state resistance. Therefore, the diamond device has significantly lower losses.

At the same time, diamond has a relative electric permittivity (ε_r) twice lower compared to Si and SiC, and of the lowest among semiconductors [27]. According to Gauss' law, the product between ε_r and the normal electric field of two materials has to be constant at their interface. Since diamond has such a large critical electric field, there is a considerable risk of premature dielectric breakdown when operating a diamond power device at high reverse voltages. The reduced value of its relative permittivity lowers this risk [28]. More considerations about this issue are to be found in **Chapter 6, Section 6.6**.

Diamond also exhibits both the highest electron and hole mobilities at room temperature of any wide band gap semiconductor. Mobilities of 4500cm^2/Vs, for electrons, and 3800cm^2/Vs, for holes, have been measured in intrinsic single crystal synthetic diamond, at 300K [12]. The corresponding values for Si, SiC or GaN are significantly lower, as shown in **Table 2.1**. However, diamond mobility decreases abruptly with both impurity doping level and temperature [29, 30]. A more detailed study regarding this issue is inserted in **Chapter 3**.

Overall, with respect to its physical and electrical properties, diamond looks as a very promising material. Its high band gap and critical electric field makes it suitable for both high voltage, and high temperature applications [31, 32]. The high thermal conductivity provides reliable operation even at high temperatures. The high critical electric field also allows the design of diamond devices with rather thin drift layers, which reduces the occupied area and induces a decrease of the on-state resistance. In the same time, since the cut-off frequency of a power device is proportional with the breakdown field and the saturation velocity, diamond qualifies as well as material suitable for devices operating at high frequencies [33, 34]. This means fast turn-on and turn-off cycles, which, together with the reduced on-state resistance, leads to lower general losses of a diamond power device compared to the silicon, silicon carbide or gallium nitride ones. Considering the physical properties presented in **Section 2.2.1**, diamond has also the ability of operating in harsh environments. Due to the material's atomic structure, extreme hardness and high melting and boiling points, diamond devices are to be considered for applications prone to high radiation levels in extreme conditions [35, 36].

Diamond has, however, a significant disadvantage compared to other semiconductors. Due to its extremely well organized atomic structure, it cannot easily incorporate dopants. The shallowest known dopant is boron (B) [37], which has an activation energy of 0.37eV. The same donor has 0.045eV activation energy in silicon, for example. Due to this large activation energy, not all the dopant atoms will be ionized at room temperature. This has to be taken into consideration when designing diamond devices. The situation regarding the potential acceptors is even worse. The shallowest is phophorus (P), with an activation energy of 0.59eV (0.045eV in silicon) [38]. This prohibits the design of devices with n-type region, since reasonable electron concentrations available for conduction are not to be expected, unless the device is operated at high temperature. As a comparison, in 4H-SiC, the most used donor, nitrogen (N), has an activation energy of 0.059eV, while the shallowest acceptor is aluminium (Al), with 0.19eV.

2.2.3 Figures of merit

In order to further confirm the potential of diamond power devices, several figures of merit (FM) have been calculated and are presented in this section. In 1965, Johnson proposed a figure of merit (*JFM*) which sets the limit of the device performance of a typical JFET (Junction Field Effect Transistor) [39]. *JFM* has the following expression, in which v_{SAT} is the electron drift saturation velocity:

$$JFM = \frac{E_{CRITICAL} v_{SAT}}{2\pi} \tag{2.4}$$

Few years later, Keyes proposed a FM (*KFM*) in which the switching speed of transistors used in integrated circuits and their thermal limitation are considered [40]:

$$KFM = \lambda \left(\frac{c v_{SAT}}{4 \varepsilon_r \pi} \right)^{0.5} \tag{2.5}$$

λ is the thermal conductivity and c the speed of light ($3*10^8$m/s). Finally, in 1982, Baliga derived its own figure of merit (*BFM*) to define the material parameters for minimizing conduction losses [41]:

$$BFM = \mu\varepsilon_r E^3_{CRITICAL} \tag{2.6}$$

The values of all these figures of merit are listed in **Table 2.2**, for Si, SiC, GaN, and synthetic diamond. The values for each material are normalized with respect to the ones corresponding to silicon.

	Si	4H-SiC	GaN	Diamond
JFM	1	17.7	46.3	74
KFM	1	5.3	2.1	34.3
BFM for holes	1	105	875	141635

Table 2.2 – Several figures of merit for Si, GaN, 4H-SiC and synthetic diamond

The material properties of diamond lead to outstanding figures of merit. If in the case of *JFM* and *KFM* the improvement, although significant, is not impressive, the real potential of diamond can be seen when comparing Baliga's figure of merit. *BFM* predicts an improvement of three orders of magnitude for FETs fabricated on diamond over their SiC counterparts. Owing to its outstanding critical electric field, diamond devices seem well equipped for applications requiring high switching speed, since its *BFM* is with three orders of magnitude larger than in Si and SiC devices.

However, caution is required when considering the values of these figures of merit for diamond, since there are based on the performance of conventional high voltage FETs, where it is assumed that the dopants are fully activated at room temperature. This is not the case for dopants in diamond, as shown in **Chapter 3**. To fully exploit these remarkable figures of merit, alternative device designs need to be explored.

CAMBRIDGE UNIVERSITY LIBRARY

2.3 Process and fabrication issues

2.3.1 Synthesis of diamond

The first synthesis of diamond produced in 1954 was based on a process called High Pressure High Temperature (HPHT) synthesis [15]. During this process, graphite is put into a huge hydraulic press at high pressure and high temperature, and, after the addition of a metallic catalyst, it converts to diamond over a period of few hours. The process is still utilized, but the obtained diamond crystal has not the quality required by an electronic device. Instead, is used as hard edge for cutting tools and drill bits.

In September 2002, Element Six reported in Science the fabrication of single crystal (SC) diamond samples which exhibited 4500cm^2/Vs electron mobility and 3800cm^2/Vs hole mobility at room temperature, by far the largest mobilities ever reported for a wide band gap semiconductor [12]. The samples were obtained using a chemical vapour deposition (CVD) process. The synthesis required a microwave plasma-assisted CVD reactor operating at 2.45GHz. The epitaxial growth required a total gas flow of 700cm^3/minute, consisting of hydrogen with 5.5% methane and 10% argon. The pressure was more than 15kPa. The intrinsic layer was deposited on a specially prepared HPHT-grown substrate, heated at 830^{0}C. After synthesis, the high purity CVD grown layer was separated from the HPHT substrate via laser cutting. Intrinsic layers with thicknesses varying from 390 and 690μm were obtained in an experiment reported by Element Six, and since then the technique is commonly used to fabricate high purity diamond layers [12].

To produce highly boron doped diamond layers, a similar technique is employed. The main difference consists in adding diborane (B_2H_6) in the gas composition flowing within the CVD reactor. Layers with boron concentrations in excess of 10^{21}cm^{-3} and thicknesses up to 800μm were obtained this way [12].

In order to obtain the M-i-P diamond structure introduced in **Chapter 4**, an i-P junction needs to be produced. This is generally done by first creating the highly-boron doped layer via the CVD technique described before. After growing the p++ doped

diamond layer, the HPHT-grown diamond substrate is removed via laser cutting and the highly doped layer is polished to get parallel sides. Then, this layer acts as substrate during the CVD growth of the intrinsic layer. Subsequent to this new deposition, P-i structures are obtained, consisting of an i-layer grown on top of a p++ region [42].

2.3.2 Ohmic and Schottky contacts

Forming good quality ohmic contacts on wide band gap semiconductors is not an easy task. However, in diamond, this might be less difficult than in other materials due to the low, even negative, electron affinity of the material. With respect to the type of passivation used, diamond exhibits affinities from (-1.5eV) [43], when hydrogen-terminated, up to (+1.3eV), when oxygen-terminated [44]. In this thesis, we study only oxygen-terminated samples, therefore the electron affinity is considered (+1.3eV).

On a typical i-P structure such the one presented in the M-i-P diode, the ohmic contact is formed on the p-side of the sample by first implanting boron ions ($\sim 5*10^{16}cm^{-3}$ concentration) at 37keV, and then performing an annealing at 1100^0C. Any graphite which might occur due to the carbon atoms in diamond is etched-off, and then the ohmic contact, which generally consists of three (Ti-Al-Au) or two (Ti-Al) metal layers, is formed using physical vapour deposition (PVD). A final annealing is performed at 600^0C [42].

The formation of Schottky contact is more difficult. An excellent crystalline quality as well as a smooth surface is required for the diamond intrinsic layer. After being oxygen-terminated using low pressure oxygen plasma, either gold or aluminium is deposited via the same PVD technique. Annealing at $400\text{-}450^0C$ is generally performed after the deposition. Although serious advances have been done in the recent years, the quality of Schottky contacts on diamond is still not at the expected level. This leads to large concentrations of defects at the metal-semiconductor interface, to non-uniform Schottky barriers, and to others effects which seriously affect the performance of the electrical devices.

2.4 Diamond devices

2.4.1 Introduction

As already mentioned in this thesis, diamond has an atomic structure in which the insertion of dopant atoms is a difficult task. Due to the small distance between two carbon atoms, any dopant leads to severe distortion of the lattice and therefore is hard to incorporate. Until now, only three elements have been successfully incorporated in diamond: one acceptor (boron, activation energy = 0.37eV), and two donors (phosphorus, activation energy = 0.59eV; and nitrogen, activation energy = 1.7eV). Due to the large values of their activation energies, all of them are incompletely ionized at room temperature [45]. There is however an exception to this rule. At high doping levels (in excess of $10^{20}cm^{-3}$), due to the overlapping between the valence band and the acceptor band, all boron atoms within a diamond layer are ionized at room temperature [29]. Since experimentally it was possible to obtain diamond layers with boron concentrations up to $10^{21}cm^{-3}$ (as shown in **Section 2.3.1**), and since layers with large concentrations of nitrogen or phosphorus were not reported until now, the research has mainly focused on devices with unipolar, p-type conduction. Taken into consideration all the physical and electrical properties of diamond, two large categories of diamond devices are currently investigated: Schottky diodes and field effect transistors [46].

2.4.2 Schottky diodes

Following the significant success of silicon carbon power rectifiers, which, after becoming commercially available in 2001, evolved as a serious competitor to silicon P-i-N structures, the research in the field of diamond diodes was dedicated to high voltage Schottky diodes. With a critical electric field fours times larger and a thermal conductivity five times larger, diamond Schottky barrier diodes (SBD) have far better off-state capabilities than their SiC counterparts. A drift layer with a given thickness can theoretically withstand significantly larger breakdown voltage in diamond than in SiC.

However, due to the high activation energy of boron atoms in diamond, low hole concentrations at room temperature are expected, therefore a much higher on-state resistance is exhibited by diamond SBDs in comparison with the SiC SBDs. The solution for this problem is to decrease as much as possible the drift doping level, thus approaching the hole mobility level measured in intrinsic diamond layers. After Element Six proved, in 2002, its ability of growing high-purity layers on top of highly boron doped regions [12], the diamond M-i-P Schottky structure introduced in **Fig. 2.4** has been subject to intensive research. Physical analysis, design, and electrical behaviour of this device are given in **Chapters 4, 5 and 6**. At this stage, it is important to mention that breakdown voltages up to 4.1kV [47] have been obtained on this structure, in the absence of any edge termination, and on-state currents densities of 100A/cm^2 at 5V forward voltage bias have been measured [48].

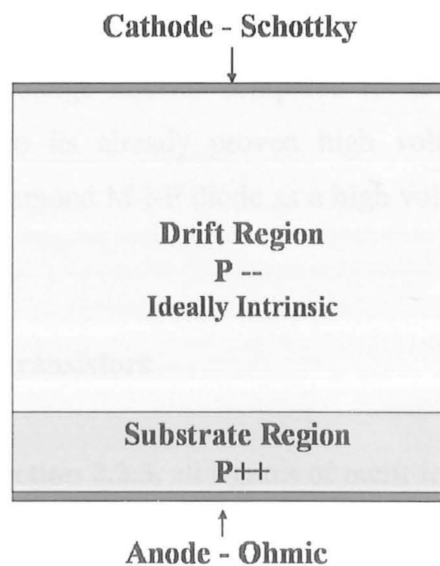

Fig. 2.4 – Diamond M-i-P Schottky diodes

If high-temperature operation is preferred to high-voltage capability, then significantly higher doped drift layers can be employed. With a drift doping concentration of approximately 10^{16}cm^{-3}, a diamond SBD was shown to successfully operate at 1000^0C, while being able to block 50V and exhibiting significant leakage currents [49]. A special

Schottky contact was used in this case: first a highly doped silicon-interfacial layer was deposited on top of the diamond drift region, then a silicon-tungsten (Si-W) alloy was added, and, finally, an Au layer came on top.

Ultra-violet (UV) photodetector is another possible role for diamond SBDs. Structures lacking the intrinsic drift layer, but with thick, CVD grown single-crystal diamond substrates, were shown to have visible/UV rejection ratios of six orders of magnitude [50]. Good signal to noise ratios, stability and reproducibility of the device response were also obtained [51]. The photodetection capability of CVD single crystal diamond in extreme UV spectral region looks indeed extremely encouraging.

Finally, theoretical studies and numerical simulations triggered hopes for using the diamond M-i-P Schottky structure as an optically-addressed switch in the UV region [52]. Such a diamond device can be switched on by applying a beam of light with wavelength lower than 225nm (corresponding to a photon energy superior to diamond's band gap) at a reverse voltage inferior compared to its dark breakdown voltage. By combining this feature to its already proven high voltage blocking capability, the possibility of using the diamond M-i-P diode as a high voltage light-triggered switch are extremely high.

2.4.3 Field effect transistors

As presented in **Section 2.2.3**, all figures of merit for power field effect transistors (FET) have the highest values for diamond. However, in order for these values to be translated in reality, issues like overcoming the incomplete ionization of dopants at room temperature need to be addressed.

One of the special features of diamond is that a p-type 2DHG-like conductive surface channel can be obtained if the diamond surface is hydrogen-passivated [53]. 2DHG refers to a gas of holes free to move in two dimensions, but tightly confined in the third. The holes appear to be a 2-D sheet in a 3-D device. Such a sheet appears, for example, in a MOSFET with p-type doped drain and source regions, when operated in the inversion mode. In diamond, such a sheet is obtained, if hydrogen-terminated, without

any extrinsic doping, the nature of the internal doping still being under debate in the scientific world.

Field effect transistors on such hydrogen-terminated diamond layers have been produced under the label of Surface Channel FETs (SC-FETs), and can be either Metal Semiconductor FETs (MESFETs) or Metal Insulator Semiconductor FETs (MISFETs) [54]. The structure of a diamond MESFET is presented in **Fig. 2.5** [55]. The channel has full room temperature activation, a sheet charge density of $5*10^{12}$-$10^{13}cm^{-2}$ and a hole mobility of approximately $150cm^2/Vs$. Typically, a CVD undoped layer in grown on top of a HTHP diamond substrate. The intrinsic layer has a thickness of around 1μm. The conducting active device areas are hydrogen-passivated (the dangling bonds on the surface of the atoms are terminated with H atoms), while the surrounding passive areas are oxygen-passivated, in order to isolate the active areas. The source and and drain electrodes form ohmic contacts with the diamond layer, while the gate (typically Al) forms a Schottky contact. The typical gate-drain and gate-source gap is of 0.5μm.

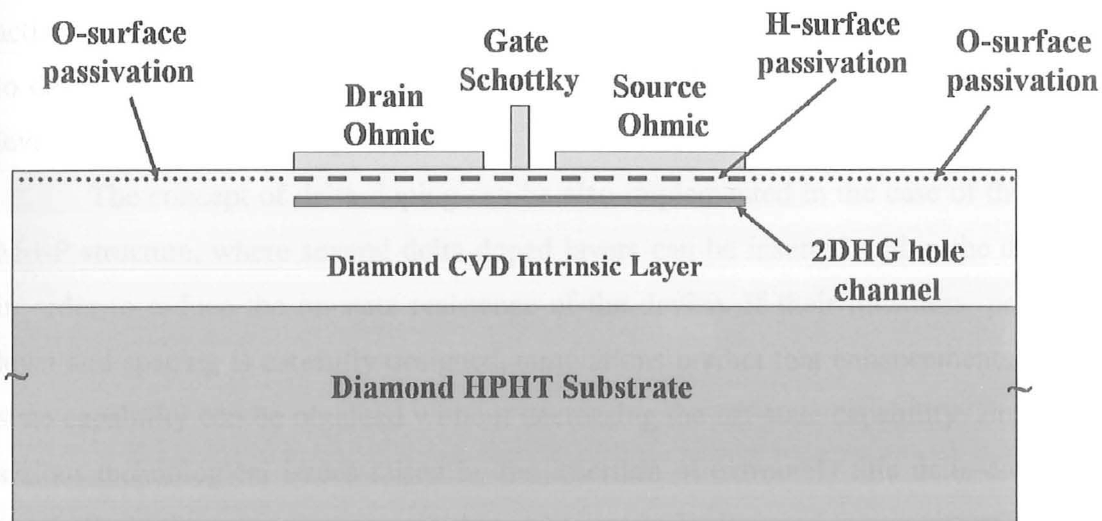

Fig. 2.5 – Diamond MESFET with 2DHG hole channel obtained without extrinsic doping due to the hydrogen passivation

Such a diamond MESFET structure was shown to have outstanding RF performance. Kubovic et al. reported a transition frequency (f_T) of 25GHz and a

maximum oscillation frequency (f_{MAX}) of 63GHz for 0.2μm gate length [56]. f_T refers to the maximum frequency at which the device can operate in a digital circuit, while f_{MAX} represents the maximum operating frequency in analog amplification [57]. A similar MESFET transistor built on poly-crystalline diamond exhibited even higher cut-off frequencies: f_T = 45GHz and f_{MAX} = 120GHz for a gate length of 0.1μm [55]. On single crystal diamond, Hirama et al. reported f_T up to 30GHz for a MISFET [58]. The main difference between a MESFET and a MISFET resides in the thin gate dielectric (typically Al_2O_3) which is deposited between the gate electrode and the diamond surface. For the quoted MISFET structure, the dielectric was 8nm thick.

Higher cut-off frequencies are expected to be obtained if the hole channel mobility is improved. This might require the move from the 2DHG-like conductive surface channel obtained when passivating with the diamond surface hydrogen to a better controllable channel configuration based on boron delta doping [59]. Such delta-doped layers require a peak doping concentration above $10^{20}cm^{-3}$ in order to yield full dopant activation at room temperature. The layers should be made as thin as possible in order not to degrade the carrier mobility which in diamond drastically decreases with the doping level (as described in **Chapter 3**).

The concept of delta-doping can be also implemented in the case of the diamond M-i-P structure, where several delta-doped layers can be inserted within the drift region in order to reduce the on-state resistance of the device. If their thickness, peak doping level and spacing is carefully designed, simulations predict that enhancements in the on-state capability can be obtained without decreasing the off-state capability. However, the serious technological issues raised by the insertion of extremely thin delta-doped layers (typically in the nm range, or even thinner) in intrinsic diamond region has prohibited, so far, the fabrication of delta-doped diamond FETs or M-i-P diodes with good electric performance.

Chapter 3

Models used in numerical simulations

CHAPTER 3

Models used in numerical simulations

3.1 Introduction

In the last two decades, numerical simulations have become an essential tool for designing competitive electronic devices. Evaluating the electrical or thermal behaviour of such devices require the use of powerful simulators, able to compute in parallel a large number of equations. One of the most popular simulators is the ISE-TCAD (Integrate Systems Engineering – Technology Computer Aided Systems), which has now reached version 10.0 [60].

For the purpose of this thesis, only the tools of device creation and simulation were of interest. MDRAW is a tool which offers a friendly graphical interface for defining the 2D device boundaries, together with its doping and refinement specifications. The simulation is run with the aid of DESSIS, "a multidimensional, electro-thermal, mixed-mode device and circuit simulator for one-, two-, and three-dimensional semiconductor devices". The simulation results presented in the next chapter were performed on two-dimensional devices and required only the electro-thermal features of the software. Finally, for viewing the results, two other tools, INSPECT and Tecplot-ISE, were used.

The electrical simulations were mainly based on computing in parallel the continuity and the Poisson equations. The continuity equations for electrons and holes take into consideration the overall effect when drift, diffusion, generation and recombination occur simultaneously in a semiconductor. The rate of electrons located in an infinitesimal portion of space with thickness dx located at x (**Fig. 3.1**) is given by the of electrons flowing in the slice at x, by the electron concentration flowing out at $(x + dx)$, by the rate at which the electrons are generated and by the rate at which the recombine with holes within the slice.

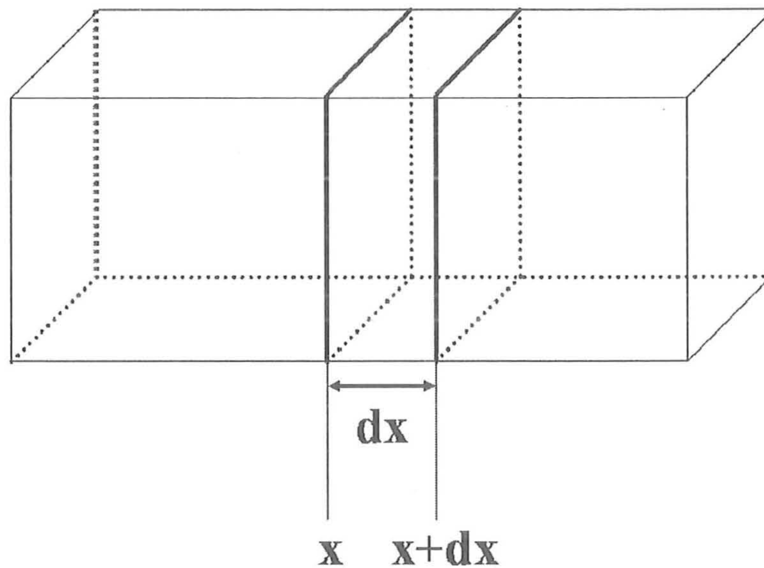

Fig. 3.1 – Infinitesimal slice of thickness *dx*

The continuity equation for electrons has the following expression:

$$\frac{\delta n}{\delta t} = \frac{1}{q}\frac{\delta J_n}{\delta x} + (G_n - R_n) \tag{3.1}$$

n is the concentration of electrons, q the elementary charge ($1.6*10^{-19}$C), J_n the density of electron current, G_n the electron generation rate and R_n and the recombination electron rate. Similarly, the hole concentration is given by the hole continuity equations:

$$\frac{\delta p}{\delta t} = -\frac{1}{q}\frac{\delta J_p}{\delta x} + (G_p - R_p) \tag{3.2}$$

Together with the continuity equation, Poisson's equation has also to be satisfied:

$$\frac{\delta E}{\delta x} = \frac{\rho}{\varepsilon_S} \tag{3.3}$$

E is the electric field, ε_S is the permittivity of the semiconductor and ρ is the charge density, given by the algebraic sum of the charge carrier density and of the ionized impurities charge (N_D^+ - concentration of ionized donor atoms; N_A^- - concentration of ionized acceptor atoms):

$$\rho = q(p - n + N_D^+ - N_A^-) \tag{3.4}$$

One of the main challenges when trying to run reliable simulations is to have proper material parameters. ISE-TCAD has a large library of predefined materials, including wide band gap materials such as SiC and GaN. However, due to its relative short history as a material suitable for electronic devices, diamond is not included in this library. Hence, we had to define it as a new material. The main features of this new material are presented in the following sections of this chapter. The full listing of the diamond parameters is included in **Appendix A**, at the end of this thesis.

3.2 Incomplete ionization

As mentioned in **Chapter 2**, due to the material's atomic structure, dopants which can be incorporated by diamond are not completely ionized at room temperature. Even the shallowest dopant, boron, which is extensively used in the simulations presented in this thesis, has a rather high activation energy: 0.37eV. Therefore, an incomplete ionization model has to be taken into consideration when running simulations [61]. The concentration of ionized acceptor atoms, N_A^-, obeys the following formula:

$$N_A^- = \frac{N_A}{1 + g_A \dfrac{p}{p_1}} \tag{3.5}$$

N_A is the doping concentration of acceptor atoms, g_A is the degeneracy factor for the impurity level (we consider this to be 4 for boron, in diamond), p in the hole concentration and p_1 is given by the expression (3.6) for $N_A < N_{A,crit}$:

$$p_1 = N_V \exp\left(-\frac{E_A - E_V}{kT}\right) \tag{3.6}$$

E_A is the acceptor activation energy, E_V is the valence energy level, N_V is the density of states in the valence band ($1.8*10^{19}cm^{-3}$ at 300K, for diamond) and $N_{A,crit}$ is the critical doping level above which all the dopants are ionized ($10^{20}cm^{-3}$ for diamond). If

we consider the diamond M-i-P Schottky structure introduced in **Chapter 2** and extensively analysed in the next chapters, then we can plot in parallel the doping and hole concentration (**Figs. 3.2 and 3.3**). We have considered a constant drift doping level of $10^{11}cm^{-3}$ boron atoms, which well approximates the behaviour of the intrinsic diamond layer obtained experimentally. All the simulation results presented in this chapter and in the rest of the thesis will consider the doping level of the intrinsic layer to be $10^{11}cm^{-3}$ boron atoms, value which is low enough to satisfactorily reproduce the behaviour of the real intrinsic layer, but also high enough to avoid computational errors normally associated with such low doping levels. It is important to note that by "intrinsic diamond layer" we actually refer to a quasi-intrinsic region (a relatively lowly doped region), since a perfectly intrinsic layer cannot be produced experimentally.

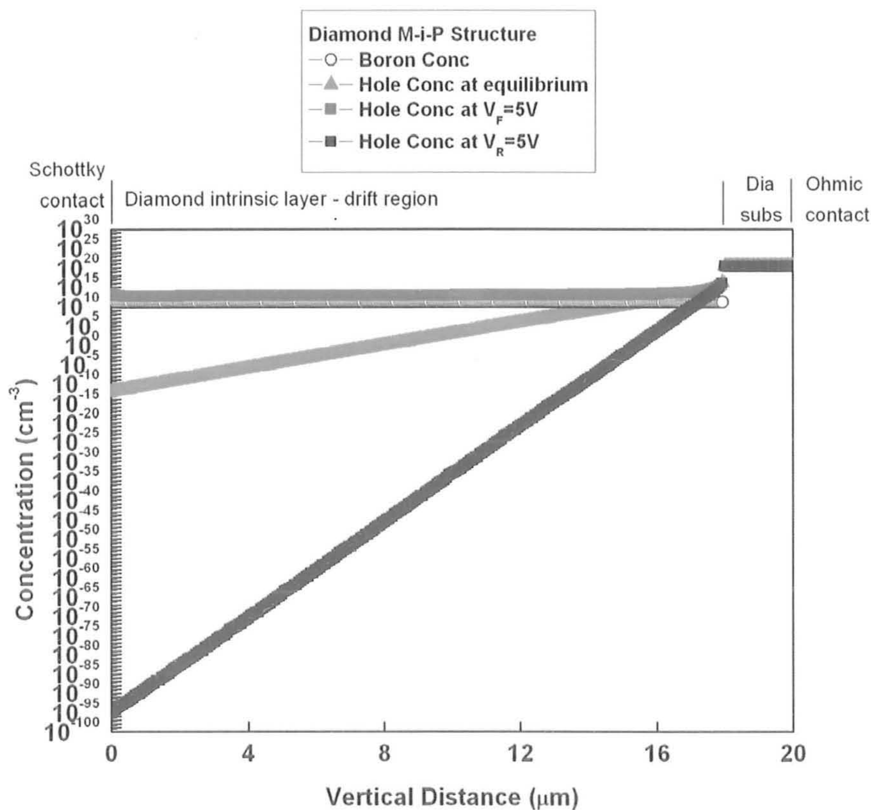

Fig. 3.2 – Boron and hole concentration through the device in three cases: at thermal equilibrium, when the device is forward biased (V_F) with 5V and reverse biased (V_R) with 5V

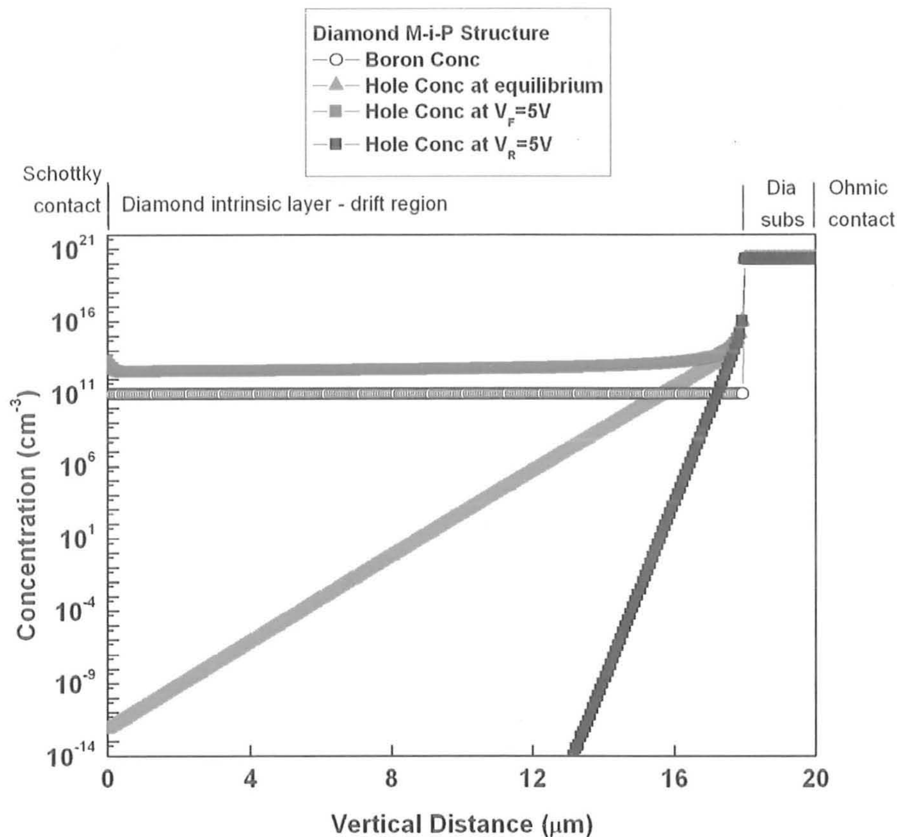

Fig. 3.3 – Boron and hole concentration through the device in three cases: at thermal equilibrium, when the device is forward biased (V_F) with 5V and reverse biased (V_R) with 5V - ZOOM

The drift region is 18μm thick, while the substrate is 2μm thick and has a boron concentration of $2*10^{20}cm^{-3}$. At thermal equilibrium, the hole concentration varies from extremely low values ($10^{-13}cm^{-3}$) next to the Schottky contact, up to $10^{16}cm^{-3}$ next to the junction between the intrinsic diamond layer and the highly doped diamond substrate, as presented in **Fig. 3.3**. This distribution is due to the incomplete ionization of boron dopants at room temperature and to the built-in depletion region induced by the Schottky contact at the metal-diamond interface. The latter phenomenon is detailed in **Section 4.3**. When biased with a forward voltage (V_F = 5V), the device exhibits a nearly constant distribution of the hole concentration through the drift layer, due to the large amount of carrier injected by the substrate. When the structure is biased with a reverse voltage of 5V

(V_R = 5V), the hole concentration decreases dramatically, as the holes are attracted by the ohmic contact and the depletion region expands towards the substrate (**Fig. 3.2**).

As expected, in the substrate, for all the cases considered, the hole concentration is equal with the boron one, meaning that all the acceptors are ionized. In diamond, at high boron concentration (typically larger than $10^{20}cm^{-3}$), the activation energy reduces to zero due to the overlapping of the acceptor energy level with the valence energy. Thus, at these high doping levels, diamond exhibits a metallic-like conducting mechanism.

3.3 Mobility versus doping

The highest mobilities ever reported for a wide band gap semiconductor were measured by Isberg in intrinsic diamond: $3800cm^2/Vs$ for holes and $4500cm^2/Vs$ for electrons [12]. However, as the diamond layer gets doped with impurities, the mobility starts to significantly decrease. Nebel measured the hole mobility in samples with boron doping in excess of $10^{14}cm^{-3}$ and the results he obtained confirm the descendent trend [29]. In order to implement these experimental data in the simulator, we have put them together in an empirical model, which we called CONMOB fitting curve (the blue line in **Fig. 3.4**) [62]. The orange point represents the hole mobility in undoped diamond (as mentioned before, the intrinsic concentration was considered in simulations to be $10^{11}cm^{-3}$), while the red dots correspond to the Nebel data. The CONMOB model unifies these two sets of data. In order to implement this model into the simulator, dummy points (the full blue rectangles) were considered along the CONMOB curve. In this way, a table look-up model was obtained.

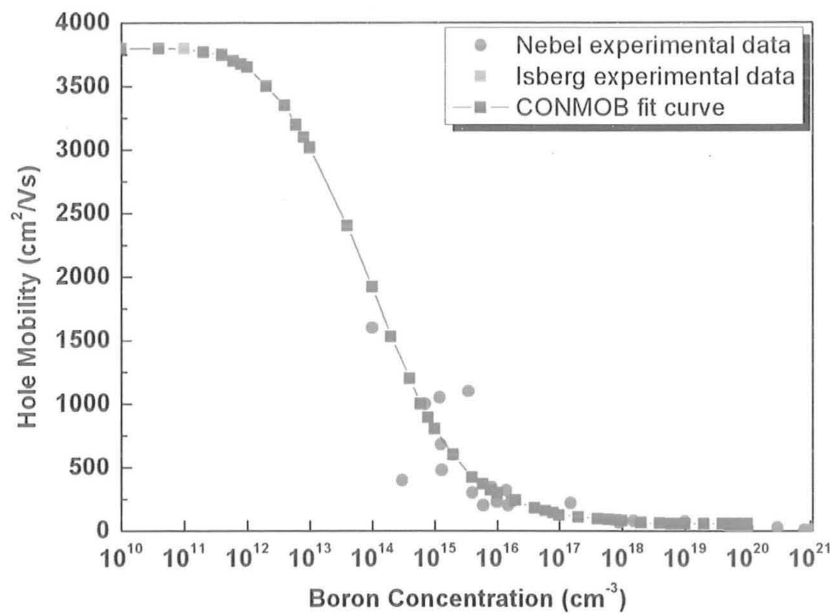

Fig. 3.4 – Hole Mobility vs Boron Concentration
Experimental Data and the empirical CONMOB model

The next step was the attempt of finding the equation which describes the CONMOB curve. Several models were taken into consideration and an excellent approximation was found with the Masetti model [63]. The Masetti bulk mobility model takes into account the scattering of the carriers by charged impurity ions, phenomenon which leads to a degradation of the carrier mobility (ionized impurity scattering). This temperature independent model is described by the following equation:

$$\mu_{Hole} = \mu_{\min 1} \exp\left(-\frac{P_C}{N_A}\right) + \frac{\mu_{CONST} - \mu_{\min 2}}{1 + \left(\frac{N_A}{C_r}\right)^{\alpha}} - \frac{\mu_1}{1 + \left(\frac{C_S}{N_A}\right)^{\beta}} \tag{3.7}$$

The values for the nine parameters of this model are available for Si and 6H-SiC and are implemented in ISE-TCAD. By suitably choosing the parameters, **equation 3.7** proves to be an excellent approximation for p-type diamond, too. The values corresponding to diamond, as well to Si and SiC, are given in **Table 3.1**.

Parameter	Si	6H-SiC	**Diamond**	Unit
μ_{CONST}	470.5	70	**3800**	cm^2/Vs
μ_{min1}	44.9	5	**103**	cm^2/Vs
μ_{min2}	0	0	**70**	cm^2/Vs
μ_1	29	0	**48.5**	cm^2/Vs
P_C	$9.23*10^6$	0	**0**	cm^{-3}
C_r	$2.23*10^{17}$	10^{19}	$\mathbf{10^{14}}$	cm^{-3}
C_S	$6.1*10^{20}$	-	$\mathbf{5.6*10^{14}}$	cm^{-3}
α	0.719	0.5	**0.57**	1
β	2	-	**10**	1

Table 3.1 – Masetti parameters for hole mobility corresponding to Si, 6H-SiC (already implemented in ISE-TCAD) and diamond (corresponding to CONMOB curve)

The Masetti equation has the following expression for diamond:

$$\mu_{Hole} = 103 + \frac{3800 - 70}{1 + \left(\frac{N_A}{10^{14}}\right)^{0.57}} - \frac{48.5}{1 + \left(\frac{5.6 * 10^{14}}{N_A}\right)^{10}} \qquad (3.8)$$

The excellent match between the graph generated by this equation and the CONMOB curve can be observed in **Figs. 3.5 and 3.6**. The maximum relative error is 10.5%. For drift doping levels lower than $10^{12}cm^{-3}$, which correspond to the drift doping in an M-i-P Schottky structure, the relative errors are lower than 2%, proving even more the realibility of the proposed model. **Equation 3.8** was implemented in the simulator to model the hole mobility versus doping variation.

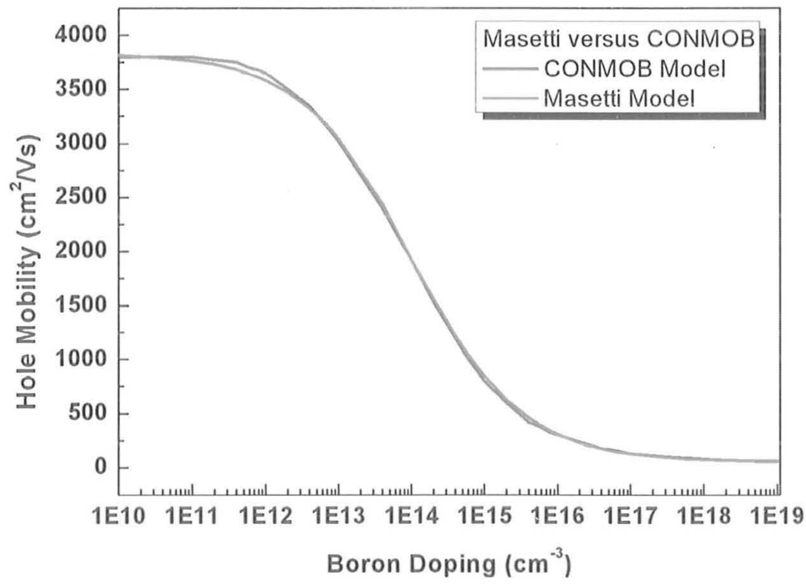

Fig. 3.5 – Masetti model versus CONMOB curve for diamond

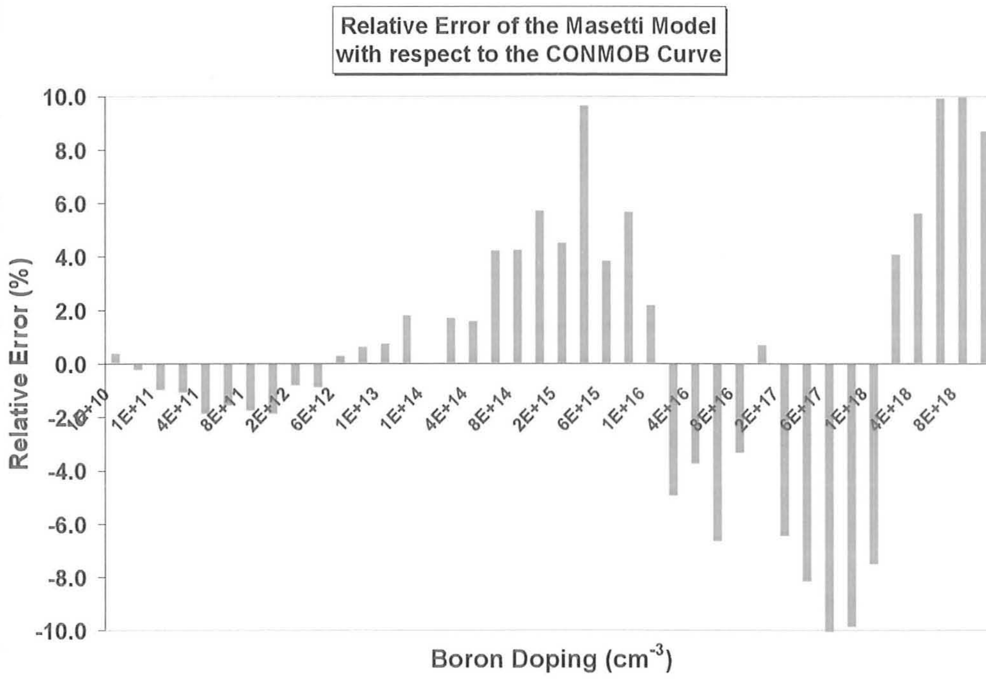

Fig. 3.6 – Relative error distribution of the Masetti model with respect to the CONMOB curve

3.4 Mobility versus temperature

In diamond, the hole mobility (μ_{Hole}) has a significant variation not only with the impurity concentration level, but also with the temperature [64]. Measurements carried out by Isberg [30] show that for temperatures lower than 325K the hole mobility is proportional with $T^{-1.5}$, while for larger temperature it varies with $T^{-3.2}$ (**Fig. 3.7**). The acoustic phonon scattering is the main phenomenon responsible for this behaviour.

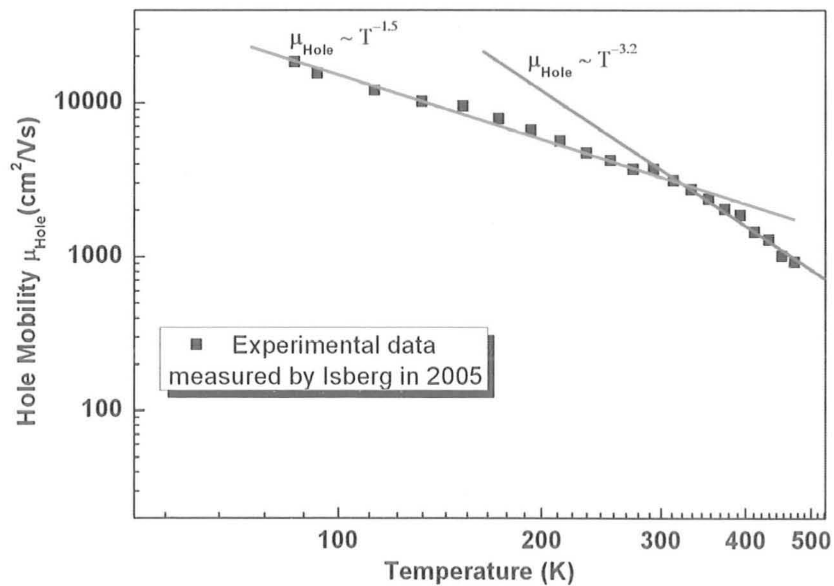

Fig. 3.7 – Experimental mobility versus temperature data and two approximated trends of variation

In order to implement these experimental trends in the simulator, a simple exponential model, with three parameters (α_1, α_2 and $\mu_{Hole\text{-}MAX}$), was taken into consideration:

$$\mu_{Hole} = \frac{\mu_{Hole-MAX} * \left(\frac{T}{300}\right)^{\alpha_1}}{1+\left(\frac{T}{300}\right)^{\alpha_2}} \tag{3.9}$$

A single set of parameters able to model the whole range of temperatures with reasonable errors cannot be established. In turn, if we consider two temperature intervals, then good approximations of the experimental data are obtained. For T ε (86K–393K), a good agreement (maximum relative error 13%) is obtained with:

$$\mu_{Hole} = \frac{6200 * \left(\frac{T}{300}\right)^{-1.79}}{1+\left(\frac{T}{300}\right)^{-0.55}} \tag{3.10}$$

For larger temperatures, an acceptable match (maximum relative error 22%) can be obtained with:

$$\mu_{Hole} = \frac{5500 * \left(\frac{T}{300}\right)^{-2.4}}{1+\left(\frac{T}{300}\right)^{-0.6}} \tag{3.11}$$

Since all the simulations were performed at constant temperature, the simulator was using either **equation 3.10** or **3.11**. However, in order to perform more complex simulations, with variable temperature, a unified model has to be obtained.

3.5 Ionization coefficients

One of the main advantages of diamond is that due to its large band gap, Schottky contacts with large barrier potentials can be deposited. For example, if deposited on an oxygen-passivated diamond layer, gold yields a Schottky barrier of 1.87eV. These large values induce extremely low leakage currents in diamond Schottky diodes, for example,

which, in turn, lead to reduced off-state losses. However, from the point of value of numerical simulations, there is a downside. The severely low leakage current levels add complexity to the calculus, which can cause errors. Therefore, when running the off-state simulations extensively presented in **Chapter 6**, we have taken into consideration as sole condition for determining the breakdown voltage the condition regarding the ionization integrals. The ionization integrals corresponding to electrons (I_n) and holes (I_p) for a p-n junction are given by the following formulas [65]:

$$I_n = \int_0^W \alpha_n(x) e^{-\int_x^W (\alpha_n(x') - \alpha_p(x'))dx'} dx \tag{3.12}$$

$$I_p = \int_0^W \alpha_p(x) e^{-\int_0^x (\alpha_p(x') - \alpha_n(x'))dx'} dx \tag{3.13}$$

W is the width of the depletion region of the junction and α_n and α_p are the ionization coefficients. The two integrals are calculated along field lines through the depletion zone. Breakdown occurs if one of the ionization integrals equals one. For the ionization coefficients, the model proposed by Van Overstraeten and De Mann considers [65]:

$$\alpha_{n,p} = A_{n,p} \exp\left(-\frac{B_{n,p}}{E}\right)^{C_{n,p}} \tag{3.14}$$

E is the electric field through the device, while $A_{n,p}$, $B_{n,p}$ and $C_{n,p}$ are fitting parameters. No information on the values of these coefficients in diamond is available in the literature. In order to implement this model in the simulator, estimated values were obtained via extrapolation from silicon and silicon carbide, based on the band gaps of the three materials. **Table 3.2** presents these values. This method of calculating the ionization coefficients introduces errors in determining the breakdown voltage. Their experimental determination in the future is essential for better simulation-experiment fitting.

Material	Si	4H-SiC	**Diamond**
Band gap (eV)	1.12	3.26	**5.47**
A_n (cm^{-1})	$7.030*10^5$	$4.5*10^5$	**$1.89*10^5$**
A_p (cm^{-1})	$1.582*10^6$	$3.5*10^6$	**$5.48*10^6$**
B_n (V/cm)	$1.231*10^6$	$9*10^6$	**$1.7*10^7$**
B_p (V/cm)	$2.036*10^6$	$8*10^6$	**$1.42*10^7$**
C_n	1.0	1.0	**1.0**
C_p	1.0	1.0	**1.0**

Table 3.2 – Ionization coefficients for Si and 4H-SiC (measured) and for diamond (extrapolated based on band gap)

Chapter 4

Schottky rectifiers

CHAPTER 4

Schottky rectifiers

4.1 Schottky contact essentials

In 1938, the German physicist Walter Schottky published a study that explained the rectifying behaviour of the metal-semiconductor contact [66]. He analysed the spontaneous formation of a potential barrier when a metal and a semiconductor are brought together and he identified that barrier, which was lately called the Schottky barrier, as the main cause of the phenomenon occurring at the metal-semiconductor interface. The metal semiconductor diodes built later on the basis of this theory were called Schottky Barrier Diodes (SBD).

Let us consider an n-type semiconductor with work function $q\Phi_S$ and a metal with work function $q\Phi_M$. We define the metal work function, $q\Phi_M$, as the work needed to extract an electron from the metal, the electron affinity, $q\chi$, as the width of the semiconductor conduction band, and the semiconductor work function, $q\Phi_S$, as the work needed to extract an electron from the semiconductor, E_F, and the vacuum level [67]:

$$q\Phi_M = E_{VACUUM} - E_{FM} \tag{4.1}$$

$$q\chi = E_{VACUUM} - E_C \tag{4.2}$$

$$q\Phi_S = E_{VACUUM} - E_{FS} \tag{4.3}$$

If $q\Phi_M > q\Phi_S$, then the electrons in the metal have lower absolute potential energy than the electrons in the semiconductor and the Fermi level, E_{FM}, in the metal is lower compared to the one in the semiconductor, E_{FS} (**Fig. 4.1**). When the two materials are brought together, electrons start flowing in both directions [68]. Due to their higher electrostatic potential energy, a significantly larger concentration of semiconductor electrons flow into the metal compared to the amount of electrons which move in

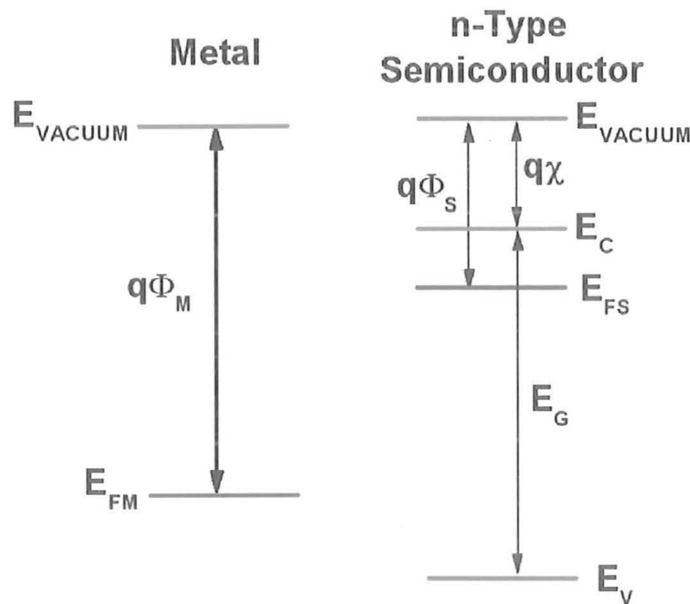

Fig. 4.1 – Band diagrams for a metal and an n-type semiconductor, before the contact is established

the reverse direction. Therefore, the metal gets negatively charged and a depletion region is created within the semiconductor, next to the interface with the metal. The width of this space charge region is W. The depletion region is filled with uncompensated ionized donor atoms, which are positively charged. This depleted area expands as the concentration of carriers migrating from the semiconductor into the metal increases, thus creating an electrostatic potential barrier (also called built-in potential barrier), which opposes the flow of carriers.

At the same time, E_{FS} lowers towards E_{FM}. After a sufficient amount of electrons is transferred into the metal, the electrostatic potential of the semiconductor is lowered enough for the two Fermi levels to get aligned. At this point, the potential barrier is large enough so that the flux of electrons flowing from the semiconductor to the metal is equal to the opposite flux, therefore the thermal equilibrium is reached (**Fig. 4.2**).

The potential barrier at which the equilibrium is obtained is called the equilibrium contact potential or the built-in potential ($V_{0\text{-}N}$). $V_{0\text{-}N}$ defines the barrier which prevents electron diffusion from the semiconductor conduction band into the metal and is equal to

the electrostatic potential lost by the semiconductor so that the Fermi energies in the two materials get at the same level.

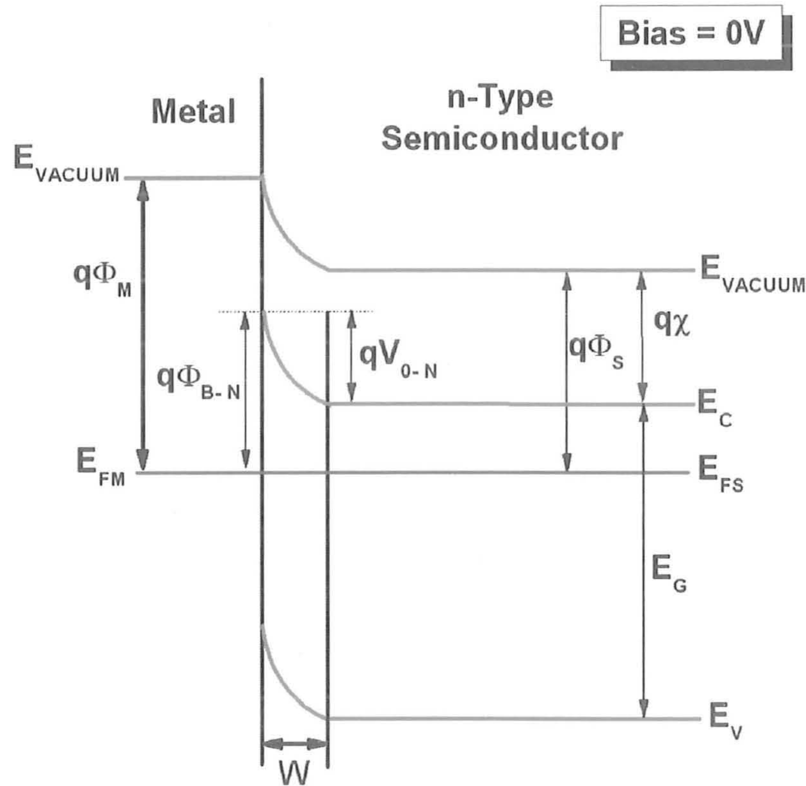

Fig. 4.2 – Band diagram for a metal - n-type semiconductor contact, at thermal equilibrium

When no interaction between the two materials is established, the vacuum level is constant and has the same value for both materials, as shown in **Fig. 4.1**. The distance between the metal Fermi level and the vacuum level is $q\Phi_M$, while, in the case of the semiconductor, the similar distance is $q\Phi_S$. When the metal-semiconductor contact is created, because the Fermi levels need to get aligned, the vacuum level remains constant in the metal, but starts decreasing as it advances within the semiconductor, from its surface towards its bulk (**Fig. 4.2**). The decrease ends at the edge of the depletion region. Same trend of variation is followed by E_C and E_V. In the bulk region, the semiconductor has the same band energy diagram as in the case when it is isolated from the metal.

If we consider the case of an electron migrating from the semiconductor (S) into the metal (M) after the equilibrium is established, we have to assume that the electron is positioned at a distance larger than W from the M-S interface. Otherwise, the electron would be in the space charge region, which we consider depleted of carriers. In order to get into the metal, this electron would have to overcome the potential built in the structure (V_{O-N}) as the conduction level drops from its initial position (when the materials were separated) to its current, bulk level. But this drop is equal to the drop suffered by E_{FS} and, further on, equal to the difference between $q\Phi_M$ and $q\Phi_S$. Therefore, V_{0-N} obeys the following formula:

$$qV_{0-N} = q(\Phi_M - \Phi_S) \qquad (4.4)$$

The built-in potential can be lowered or raised by biasing the diode. The bias introduces a gap between the Fermi levels in the metal and in the bulk of the semiconductor, gap which is proportional with the bias.

The barrier which prevents the flow of electrons in the reverse direction, from the metal to the semiconductor, is called the Schottky barrier, Φ_{B-N}. If an electron in the metal elevates its energy level from E_{FM} to the E_C level in the semiconductor, then it can migrate from the metal into the semiconductor. Since the distance between E_{FM} and the vacuum level is $q\Phi_M$, and the one between E_C and the vacuum is $q\chi$, by following a similar reasoning as for calculating V_{O-N} the Schottky barrier corresponding to an n-type semiconductor is given by:

$$q\Phi_{B-N} = q(\Phi_M - \chi) \qquad (4.5)$$

When the Schottky contact is forward biased with a voltage V_F, a negative potential is applied on the n-type semiconductor, therefore the absolute potential energy of its electrons is elevated with qV_F. For an n-type semiconductor, the energy is reversely proportional with the potential, the proportionately factor being the electron charge which is negative ($-q$, where q = $1.6*10^{19}$C). The barrier between the semiconductor and the metal lowers and the built-in potential decreases from V_{0-N} to ($V_{0-N} - V_F$) (**Fig. 4.3**). The conduction, Fermi and valence levels of the semiconductor are lifted with qV_F. The electrons are attracted by the positively biased metal and start migrating from the semiconductor into the metal, creating a forward current through the diode.

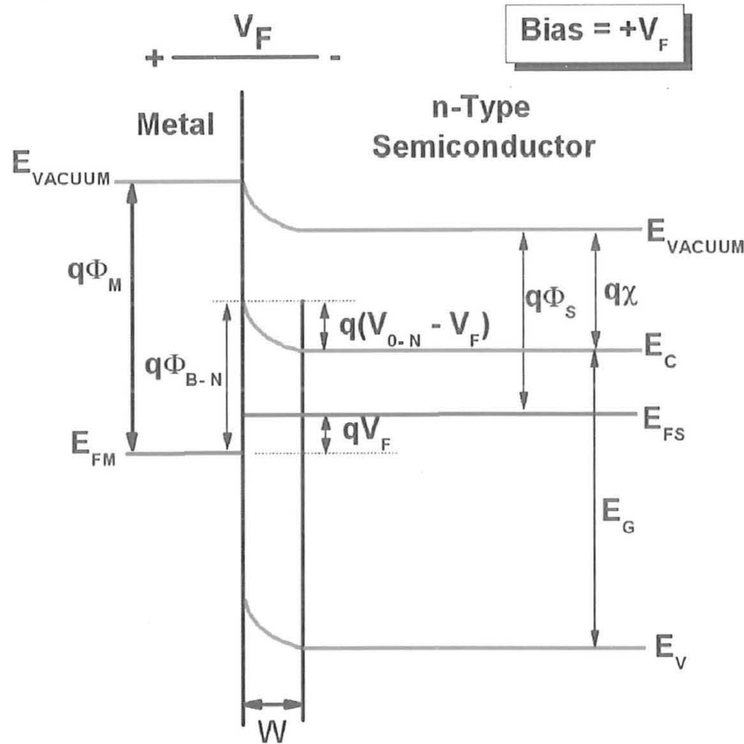

Fig. 4.3 – Band diagram for a metal - n-type semiconductor contact, when forward biased with V_F

On the other hand, when a reverse-bias voltage, V_R, is applied to the contact, the built-in potential becomes ($V_{0\text{-}N} + V_R$), the conduction, Fermi and valence levels of the semiconductor are lowered with qV_R, the barrier which needs to be overcome by electrons migrating from the semiconductor to the metal rises and very few carrier migrate from the semiconductor to the metal. Therefore, only a small, leakage current passes through the diode and this is mainly given by the carrier flowing from the metal into the semiconductor over the Schottky barrier (**Fig. 4.4**).

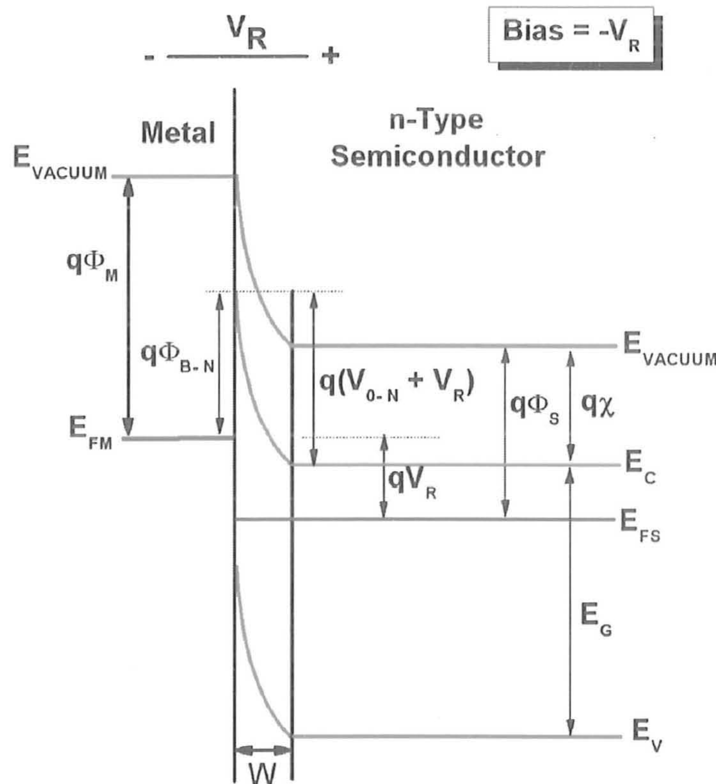

Fig. 4.4 – Band diagram for a metal - n-type semiconductor contact, when reverse biased with V_R

Similar phenomena occur when a p-type semiconductor is considered for a metal-semiconductor contact and $q\Phi_M < q\Phi_S$ **(Fig. 4.5)**. It is important to note that for the p-type semiconductor we shall consider E_V as the lowest hole energy level within the valence band and that the energy drops while moving from E_V towards E_C. In order to produce a model perfectly similar to the one presented for the n-type semiconductor, we should have defined a vacuum level for holes and a hole affinity. However, we preferred not to, as these concepts would not have any physical background.

Since $E_V > E_C$, it means that the holes here have higher absolute potential energy than the ones in the metal. Therefore, when the materials are brought together, the holes start migrating towards the metal. They create a positive charge within the metal, and, by leaving back uncompensated ionized acceptor atoms, they also contribute to the appearance of negatively charged depletion region in the semiconductor. As in the case of

the n-type semiconductor, the depletion region, which expands as the holes migration from the semiconductor to the metal becomes more significant, is accompanied by an electrostatic potential barrier which opposes the holes flow.

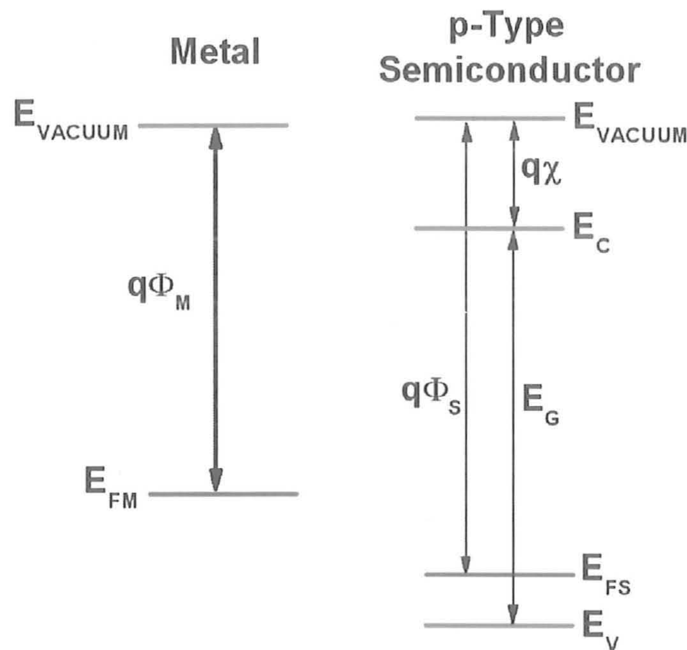

Fig. 4.5 – Band diagrams for a metal and a p-type semiconductor, when the materials are separated

The thermal equilibrium is reached when the flow of holes from the semiconductor to the metal is equal to the opposite one, from the metal towards the semiconductor (**Fig. 4.6**). The built-in potential, V_{0-P}, which represents the equilibrium contact potential that prevents the hole diffusion from the semiconductor to the metal, is now given by the difference between the semiconductor work function and the metal one:

$$qV_{0-P} = q(\Phi_S - \Phi_M) \qquad (4.6)$$

This is because, initially, when the materials are separated, the Fermi level of the p-type semiconductor is higher than that of the metal. Therefore, as the materials are brought together, E_{FS} and the bulk levels of E_V and E_C (the levels at a distance larger than W from the M-S interface) are all lowered with exactly $[q(\Phi_S - \Phi_M)]$eV. As in the case of

the n-type semiconductor, V_{0-P} can be increased or decreased by applying a positive or a negative voltage across the diode.

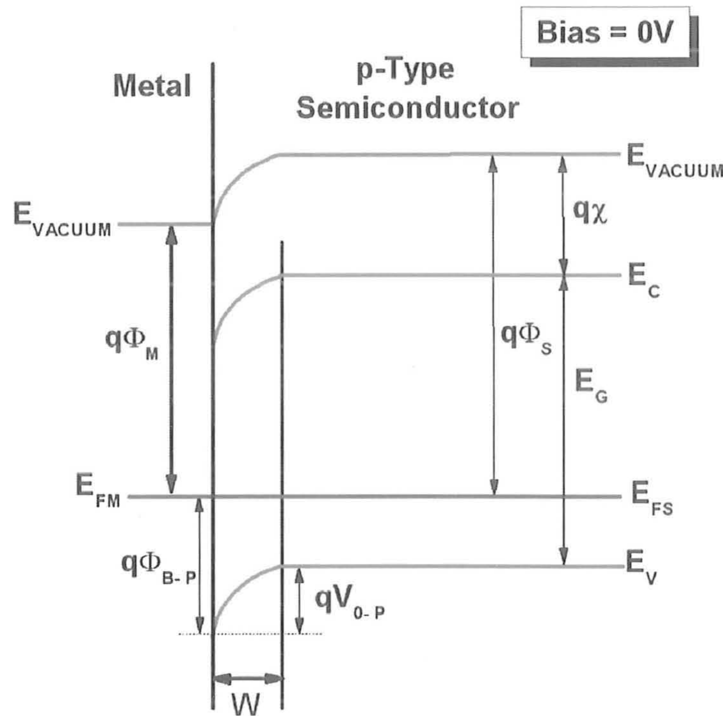

Fig. 4.6 – Band diagram for a metal - p-type semiconductor contact, at thermal equilibrium

As expected, in this case, the Schottky barrier (Φ_{B-P}) is the barrier that prevents the flow of holes from the metal into the semiconductor. If a hole in the metal increases its energy level from E_{FM} to E_V, then it can migrate from the metal into the semiconductor. With respect to the vacuum level, E_{FM} is placed at a distance equal with $q\Phi_M$, while E_V is at a distance equal with ($q\chi + E_G$), where E_G is the band gap of the semiconductor. Thus, the Schottky barrier corresponding to a p-type semiconductor is given by:

$$q\Phi_{B-P} = E_G + q\chi - q\Phi_M = E_G - q(\Phi_M - \chi) \qquad (4.7)$$

By combining **equations 4.5 and 4.7**, we obtain:

$$q\Phi_{B-P} + q\Phi_{B-N} = E_G \tag{4.8}$$

For the p-type semiconductor, when the Schottky contact is forward biased with a voltage V_F, a positive potential is applied to the semiconductor, therefore the absolute potential energy of its holes is elevated with qV_F. This happens because, for a p-type semiconductor, the energy is directly proportional with the potential, the proportionately factor being the hole charge, which is positive ($+q$, where $q = 1.6*10^{19}C$). Since we consider $E_V > E_C$, when the absolute energy of holes is elevated with qV_F it actually gets closer to E_V. The hole barrier between the semiconductor and the metal lowers and the built-in potential decreases from V_{0-P} to $(V_{0-P} - V_F)$ (**Fig. 4.7**). The conduction, Fermi and valence levels of the semiconductor are shifted with qV_F, and the holes start migrating from the semiconductor into the metal, creating a forward current through the diode.

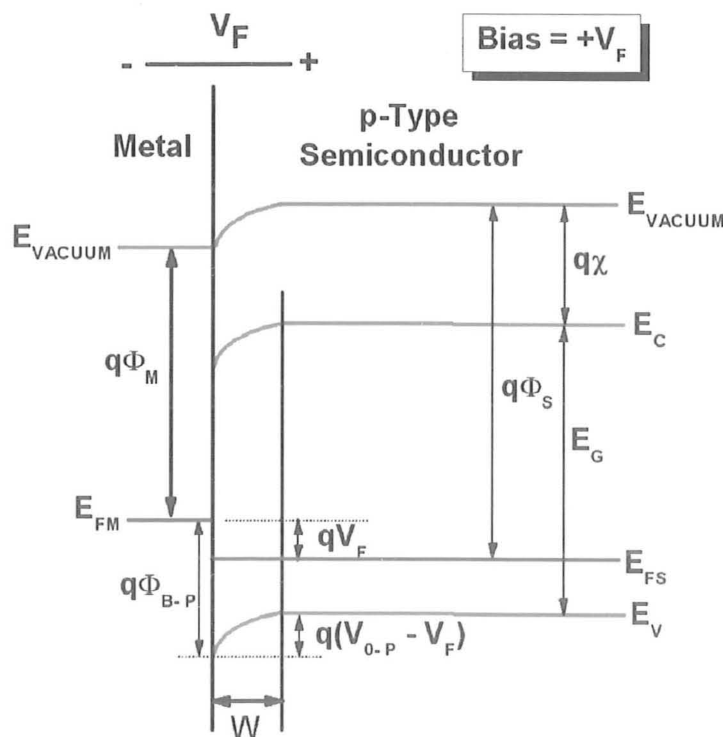

Fig. 4.7 – Band diagram for a metal - p-type semiconductor contact, when forward biased with V_F

When the structure is reversed biased with V_R, the negative potential on the semiconductor induces the increase of $qV_{O\text{-}P}$ with qV_R. Thus, the built-in potential rises at $(V_{0\text{-}P} + V_R)$. As in the previous case, only a small, leakage current passes through the diode at this stage (**Fig. 4.8**).

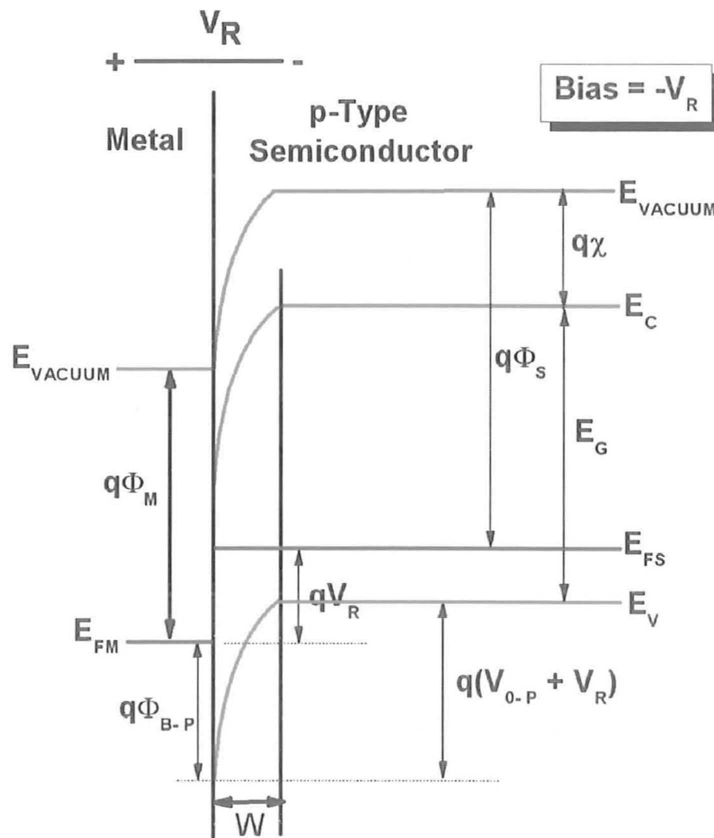

Fig. 4.8 – Band diagram for a metal - p-type semiconductor contact, when reverse biased with V_R

For both cases analyzed in this section, n-type and p-type semiconductor, when a contact is established with a metal then, then if the structure is forward biased a significant current is passing through it, and if the structure is reverse biased a small current is allowed. The only condition for this to happen is to have $q\Phi_M > q\Phi_S$ for the n-type semiconductor, and $q\Phi_M < q\Phi_S$ for the p-type semiconductor. We call this type of structure a Schottky barrier diode (SBD). Its electrical behaviour, which allows flow of

current in one direction and prohibits it in the reverse, is a typical rectifying behaviour. Therefore, SBDs are generally used as rectifying devices in electrical circuits. As described before, the conduction is mainly unipolar in Schottky diodes and is due to the injection of majority carriers (electrons for n-type semiconductor, holes for p-type) from the semiconductor into the metal. Injection in reverse direction, above the Schottky barrier, together with minority carrier injection, does exist, but their influence in the total current level is not significant. Therefore, SBDs are considered to be unipolar devices.

4.2 Power rectifiers

4.2.1 Silicon power rectifiers

The research in power discrete devices used in power electronic systems is focused on two main categories: power rectifiers and power switches. While the largest amount of effort has been dedicated to the power switches development, enhancements in power rectifiers have been subject to increased interest in the last decade. Historically, the first diode used as power rectifier was the silicon power Schottky barrier diode (Si SBD) [69]. Such a structure consists of a thin, lowly or moderately doped, drift layer and a much thicker, highly doped substrate (**Fig. 4.9**).

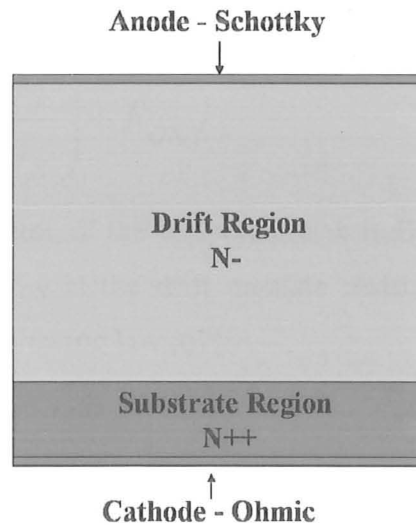

Fig. 4.9 – Ideal structure of a planar n-type Schottky barrier diode

A Schottky metal is deposited on top of the drift layer, while an ohmic contact is formed on the substrate. In order to increase the off-state capability of the device, the drift layer needs to be designed as lowly doped and as thick as possible. On the other hand, for reducing the on-state resistance, the drift region should be thin and highly doped. For a power device having the drift layer fully depleted at breakdown, the relationship between the on-state resistance (R_{ON}) of the drift region and the breakdown voltage is, according to Baliga, given by the following formula [5, 41, 70]:

$$R_{ON} = \frac{4BV^2}{\varepsilon\mu E_{CRITICAL}^3} \tag{4.9}$$

ε is the material permittivity, μ is the carrier mobility and $E_{CRITICAL}$ is the critical electric field of the material. Cooper and Agarwal suggested a very similar formula, in which the proportionality factor is 3.375, instead of 4 [6].

Another way of reducing the on-state resistance is to use metals with low Schottky barrier. This solution would lead to lower turn-on voltages, thus increasing the on-state capability, but would also significantly increase the leakage current, raising the off-state losses. The forward voltage drop, V_F, in a power Schottky diode is given by the following formula [67]:

$$V_F = \frac{nkT}{q}\ln\left(\frac{J_F}{J_S}\right) + R_{ON}J_F \qquad (4.10)$$

n is the ideality factor, T the temperature, k is Boltzmann's constant, J_F is the forward current density, R_{ON} is the drift on-state resistance, and J_S is the saturation current, which obeys the following law [67]:

$$J_S = A^* T^2 \exp\left(-\frac{q\Phi_B}{kT}\right) \qquad (4.11)$$

A^* is the effective Richardson constant, and Φ_B is the Schottky barrier. From **equations (4.10) and (4.11)**, the forward voltage drop is proportional with Φ_B. When the diode is reverse-biased, the current is mainly given by carriers which migrate over the Schottky barrier, from the metal into the semiconductor. This current is modelled by J_S. Taken into account **equation 4.11**, a small decrease of the Schottky barrier would induce a significant, exponential increase of the reverse, leakage current. Therefore, trying to solve the high breakdown voltage – low on-state resistance trade-off by simply using Schottky metals with low Φ_B might not be a recommendable solution. The attempt of optimizing this trade-off has led to the use of Si SBDs in applications which generally require breakdown voltages (*BV*) lower than 100V [69].

If larger *BVs* are needed, then Si SBDs cease to be a high-quality solution for power rectifiers. P-i-n diodes are used instead **(Fig. 4.10)** [4]. A Si p-i-n structure with the same breakdown voltage as a Si SBD has far better on-state capability due to its bipolar conduction. The conductivity modulation induced by the bipolar conduction allows the lowering of the drift layer doping level and its increase in thickness, meant to improve the off-state capability, without significantly compromising the on-state resistance.

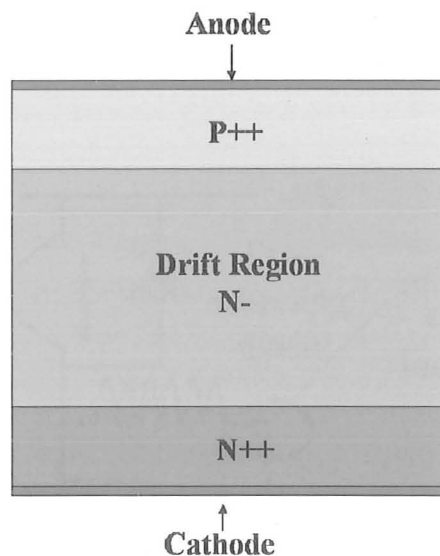

Fig. 4.10 – Cross section of a p-i-n diode

However, the bipolar conduction has a drawback: because a large amount of charge needs to be swept out from the drift region when the device turns-off, the switching time and the energy losses are significantly larger compared to those of the SBDs. Even though progress has been made by altering the structure of the p-i-n diode in order to reduce the switching time, this still remains the main problem of the structure. Therefore, Si power rectifiers able to block more than 500V and to operate at high frequencies (larger than 50kHz) cannot be produced [69].

4.2.2 Silicon carbide power rectifiers

Power rectifiers rated at more than 500V and able to operate at high frequencies are, however, required. A typical application for rectifying diodes with these parameters is as freewheeling diode in power circuits, such as the inverter in **Fig. 4.11** [71]. From the moment electrical power is supplied to the gate of the IGBT (Insulated Gate Bipolar Transistor), the inductive load accumulates stored energy. If an attempt is made to turn-off the IGBT, this energy will arc across its contacts, and could cause damage to the circuit components. The freewheeling diode is placed across the inductive load to provide

a path for the release of energy stored in the load when the load voltage drops to zero [71].

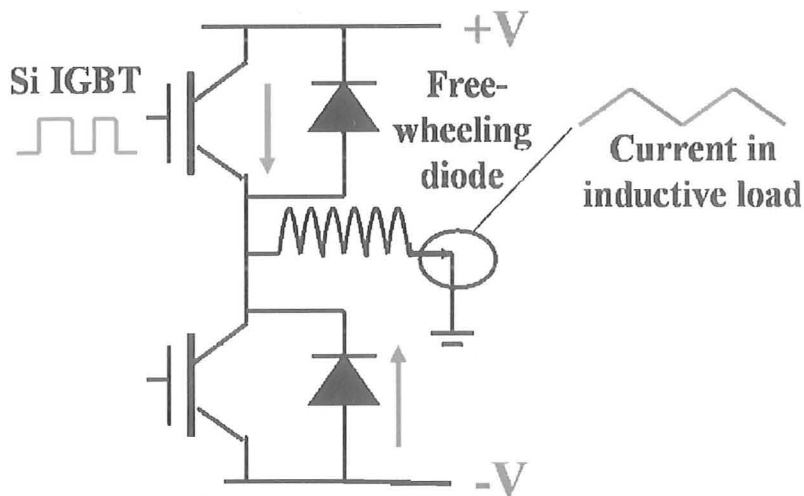

Fig. 4.11 – Power inverter circuit

The solution was the fabrication of Schottky barrier diode on silicon carbide (SiC). Due to the material high critical electric field (3MV/cm, compared to 0.41MV/cm in Si), SiC SBDs can withstand large breakdown voltages with thin drift layers. By keeping the drift layer thin, the on-state resistance remains low, therefore the main disadvantage of Si SBDs is eliminated. The first SiC SBD was successfully produced in 1992 and was able to block 400V [72], while the first device with a high-quality termination was experimentally demonstrated two years later [73]. However, it was only in 2001 when Infineon launched the first SiC SBD commercially available [9]. The SDP04S60 was able to block 600V and had a forward current capability of 4A.

Currently, Infineon is in production with its second-generation of SiC diodes, the ThinQ!2G series [9]. The rectifier has a merged p-i-n / Schottky structure, where small p-n juctions are interleaved within the rectifying metal-SiC contact (**Fig. 4.12**). This structure is most commonly known as JBS rectifier (Junction Barrier Schottky) [69].

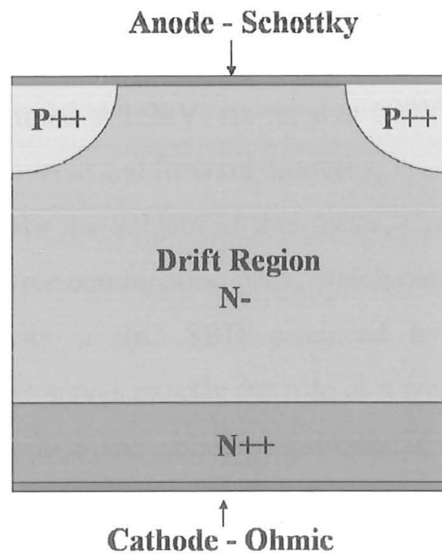

Fig. 4.12 – Cross section of a Junction Barrier Structure (JBS) diode

The device is designed such as, when forward-biased with low voltages, the pn junctions are basically inactive and only the unipolar conduction dictated by the Schottky contact gives the forward current. In this way, the device takes advantage of the small turn-on voltage of the Schottky diodes compared to the p-n junctions and also of the small turn-off time of the SBDs. If, however, large currents are required, then the forward voltage is increased to the point where the p-n junctions start conducting and current becomes bipolar. When reverse-biased, the JBS has smaller leakage currents compared to the SBD due to the potential barrier generated beyond the metal-semiconductor interface by the p-n junctions.

The other major producer of SiC devices, Cree, has recently reported (9th of February 2007), the new CPW2-1200-S050B, "a 50A Zero Recovery® Schottky rectifier operating at 1200 volts" [74]. According to the official statement of the company, "Compared with traditional silicon-based diodes, Cree's SiC-based Zero Recovery rectifiers can: simplify Power Factor Correction Boost design by eliminating the need for snubbers and reducing component count, reduce power losses, leading to cooler operating temperatures, produce significantly less electromagnetic interference (EMI), better support new design objectives for efficiency set forth by the EPA, California Electric

Commission and other agencies" [74]. In their current commercial offer, Cree have four other SiC SBD structures rated at 1.2kV, six rated at 600V and two at 300V [75]. All of these products have zero reverse and forward recovery.

More importantly for the subject of this thesis, Cree has announced in 2006 the availability of a power device combination pack, which combines a Si IGBT produced by International Rectifier with a SiC SBD produced by Cree [76]. In this circuit (CID150660), the SiC SBD serves exactly the role of a freewheeling diode, connected in anti-parallel across the emitter and collector contacts of the IGBT, introduced by the scheme in **Fig. 4.11**. The pack is rated at 600V breakdown voltage. While the diode has zero reverse recovery losses, the switching losses of the IGBT and, therefore, of the whole pack, are also significantly reduced compared to the ones of a IGBT-SBD package built completely on silicon.

4.3 Diamond M-i-P Schottky diodes

Compared to SiC, diamond has a critical electric field more than 3 times larger (10MV/cm for diamond, 3MV/cm for SiC). In terms of thermal conductivity, the superiority of diamond is even more evident (24W/cmK, compared to 5W/cmK for SiC), while the saturation velocity is the same for both wide band gap materials ($2.0\text{x}10^7$cm/s). These values enable the hope that, if carefully designed, diamond SBD structures could not only compete with SiC SBDs in terms of high-frequency operation, but could also overtake them in terms of high temperature and high voltage performance [47].

While the off-state performance is expected to be superior to that of SiC, the high on-state resistivity, due to the depth of boron acceptor level in diamond leading to a low room temperature concentration of free charge carriers available for conduction, might seriously affect the overall performance of diamond diodes. In order to overcome this problem, we propose the use of an M-i-P (Metal-intrinsic semiconductor-P++ doped semiconductor) structure (**Fig. 4.13**) [42].

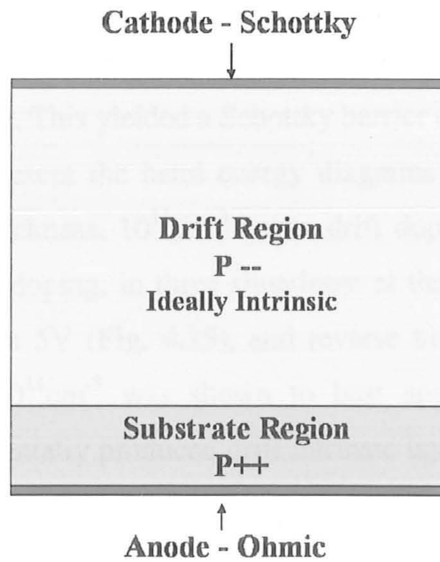

Fig. 4.13 – Cross section of an ideal, plane-parallel, diamond M-i-P Schottky structure

The main difference between the M-i-P structure and the typical power SBD rectifier is that the drift region of the former is extremely lightly doped (ideally intrinsic), while the latter is only lowly-doped. The extremely high hole mobility in the intrinsic diamond layer (4 times larger than the electron mobility in SiC) can compensate for the lack of carriers to yield an acceptable conductivity. In diamond, increasing the boron concentration leads to metallic, rather than semiconductor behaviour. For doping concentrations larger than $10^{20}cm^{-3}$, all the impurity ions are ionized at room temperature and the semiconductor becomes metallic. In the M-i-P structure, a highly doped substrate layer (10^{19}–$10^{20}cm^{-3}$ boron concentration) is used as the free carrier source from which current is injected into the intrinsic layer under forward bias [77].

In order to fully understand the operation of the diamond M-i-P diode, drawing the band energy diagrams is an essential requirement. Using both numerical simulations and theoretical considerations, we managed to draw these diagrams for several applied voltages, drift doping profiles and drift thicknesses. Gold was chosen to form the Schottky contact (work function = $q\Phi_M = 4.9eV$), diamond band gap was considered E_G

= 5.47eV, while the electron affinity in diamond was $q\chi_{DIA}$ = 1.3eV, corresponding to an oxygen-terminated surface. This yielded a Schottky barrier of 1.87eV.

Figs. 4.14-4.16 present the band energy diagrams for a p-type M-i-P Schottky diode with 18μm drift thickness, $10^{11}cm^{-3}$ boron drift doping, 2μm substrate thickness, and $2*10^{20}cm^{-3}$ substrate doping, in three situations: at thermal equilibrium (**Fig. 4.14**), when forward biased with 5V (**Fig. 4.15**), and reverse biased with 5V (**Fig. 4.16**). As shown in **Chapter 2**, $10^{11}cm^{-3}$ was shown to best approximate in simulations the behaviour of the experimentally produced drift intrinsic layer. Even low compared to the typical levels of doping in classical power Schottky diodes, the drift doping in the M-i-P structure is still with many orders of magnitude higher than the intrinsic concentration of diamond ($1.1*10^{-27}$ cm^{-3}). This is the reason why, for all the band diagrams presented below, E_F is significantly closer to E_V than to E_C. On the other hand, due to the high doping level of the substrate, the valence level within the substrate is at the same level as the Fermi one. Therefore, at equilibrium, $\Phi_{B-P} = V_{O-P}$. The vacuum level (E_{VACUUM}) is a continuous function all the way from the Schottky metal towards the substrate.

Before they are emitted over the barrier into the metal, the holes must first be transported from the interior of the semiconductor to the interface. Their motion towards the metal-semiconductor interface is governed by the two mechanisms: diffusion and drift in the electric field of the barrier. The emission of holes from the semiconductor to the metal over the top of the barrier is modelled by the thermionic emission theory, while the current due to diffusion and drift within the semiconductor is modelled by the diffusion theory.

The diffusion and drift processes occur simultaneously with the thermionic emission, therefore the current is given by whichever causes the more significant flow of holes. In equilibrium, when the M-i-P Schottky structure is not biased, the current is mainly given by the holes overcoming the semiconductor-metal barrier, therefore it obeys the thermionic-emission theory. According to this theory, the Fermi level is flat within the semiconductor, and, at equilibrium, is at the same level as the Fermi level within the metal ($E_{F-M} = E_{F-S}$, **Fig. 4.14**). The thermionic-emission theory was also the one taken into consideration in first section of this chapter, when presenting the band diagrams for the metal-semiconductor contact.

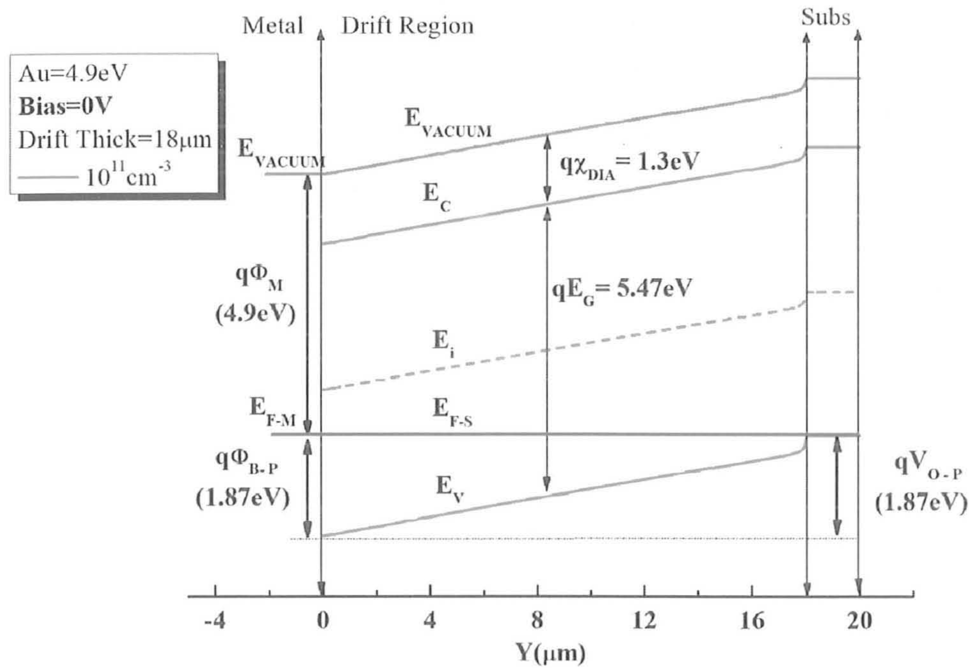

Fig. 4.14 – Band energy diagram for an ideal M-i-P structure at thermal equilibrium

When the device is forward biased with 5V (V_F = 5V), the highly doped diamond substrate injects a high concentration of holes in the intrinsic layer, which form an excess carrier concentration. The current is now mainly due to the diffusion of carriers through the diamond drift layer. The Fermi level concept used until now is meaningful only when no excess carriers are present. Instead, two quasi-Fermi levels, one for electrons ($E_{F\text{-}n}$) and one for holes ($E_{F\text{-}p}$), are introduced to describe the behaviour of electrons and holes, respectively, under non-equilibrium conditions. These levels have the property of correctly predicting the concentration of electrons in the conduction band and of holes in the valence band, respectively, if the carriers are assumed to be in thermal equilibrium at the lattice temperature and if the quasi-Fermi levels are used in the Fermi-Dirac distribution function in place of the equilibrium Fermi level. Thus, the concentration of electrons, n, and holes, p, are given by the following equations:

$$n = n_i \exp\left[\frac{1}{kT}\left(E_{F-n} - E_i\right)\right] \quad (4.12)$$

$$p = n_i \exp\left[\frac{1}{kT}\left(E_i - E_{F-p}\right)\right] \tag{4.13}$$

E_i is the semiconductor intrinsic energy level and is always placed in the middle of the band gap.

For the case of the M-i-P diode, according to the diffusion theory, the hole quasi-Fermi level is not required to be flat throughout the whole semiconductor. As presented in **Chapter 3**, the hole concentration at V_F = 5V is significantly higher the drift boron concentration (therefore, we have excess hole concentration within the drift layer injected by the substrate) and is nearly constant from the metal-semiconductor interface till near the drift-substrate junction (**Fig. 4.17**). As a consequence, the hole quasi-Fermi level follows the shape of E_i up to Y = 16.5μm (**Fig. 4.15**). For the rest of the drift layer, the distance between the two energy levels slightly increases. In the substrate, all the boron atoms are ionized are room temperature due to their large concentration ($2*10^{20}cm^{-3}$), therefore the hole quasi-Fermi level is at the same level with the E_V.

When the structure is reverse-biased with V_R = 5V, the drift hole concentration decreases dramatically (**Fig. 4.16**). The current is mainly given by the thermionic emission and the hole quasi-Fermi level is constant within the whole drift layer. For $Y < 11\mu m$, the hole concentration is lower than the intrinsic concentration in diamond (n_i = $1.1*10^{27}cm^{-3}$ – **Fig. 4.17**), therefore the hole quasi-Fermi level is higher than E_i.

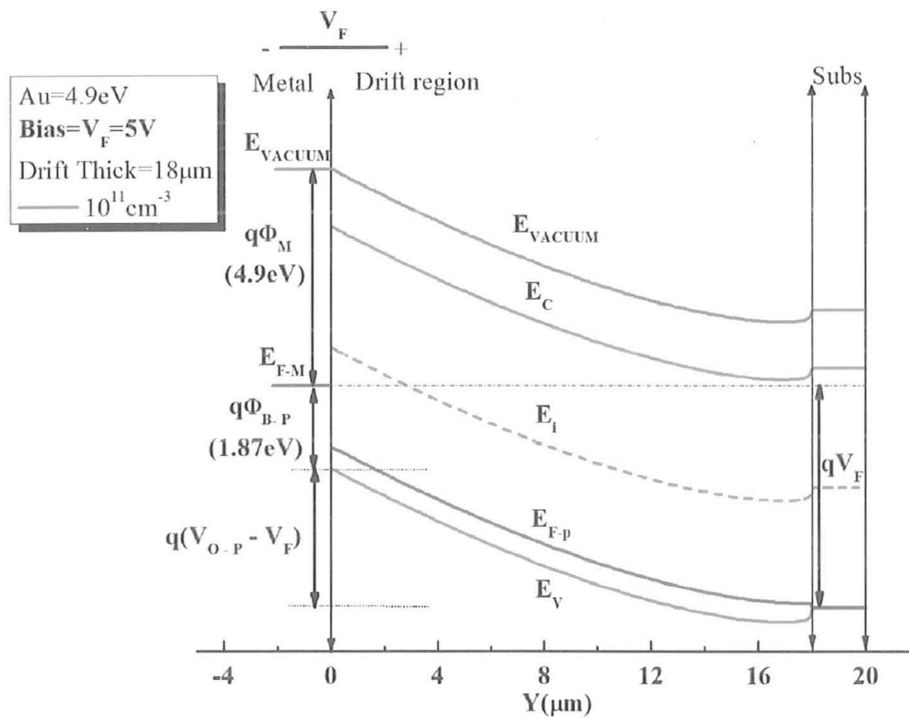

Fig. 4.15 – Band energy diagram for an ideal M-i-P structure when forward biased with $V_F = 5V$

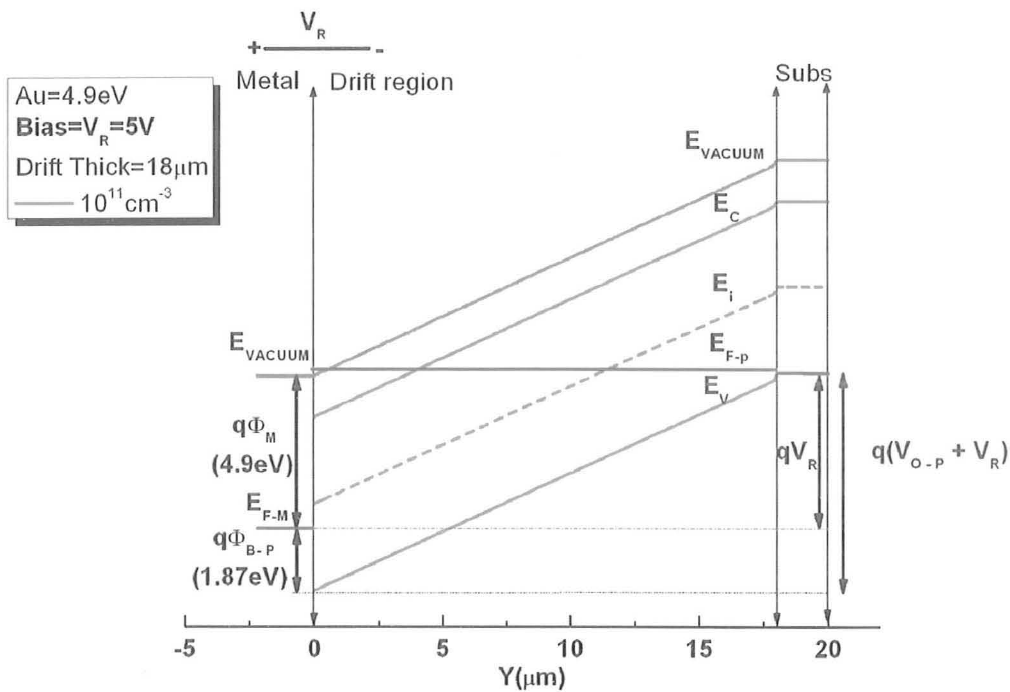

Fig. 4.16 – Band energy diagram for an ideal M-i-P structure when reverse biased with $V_R = 5V$

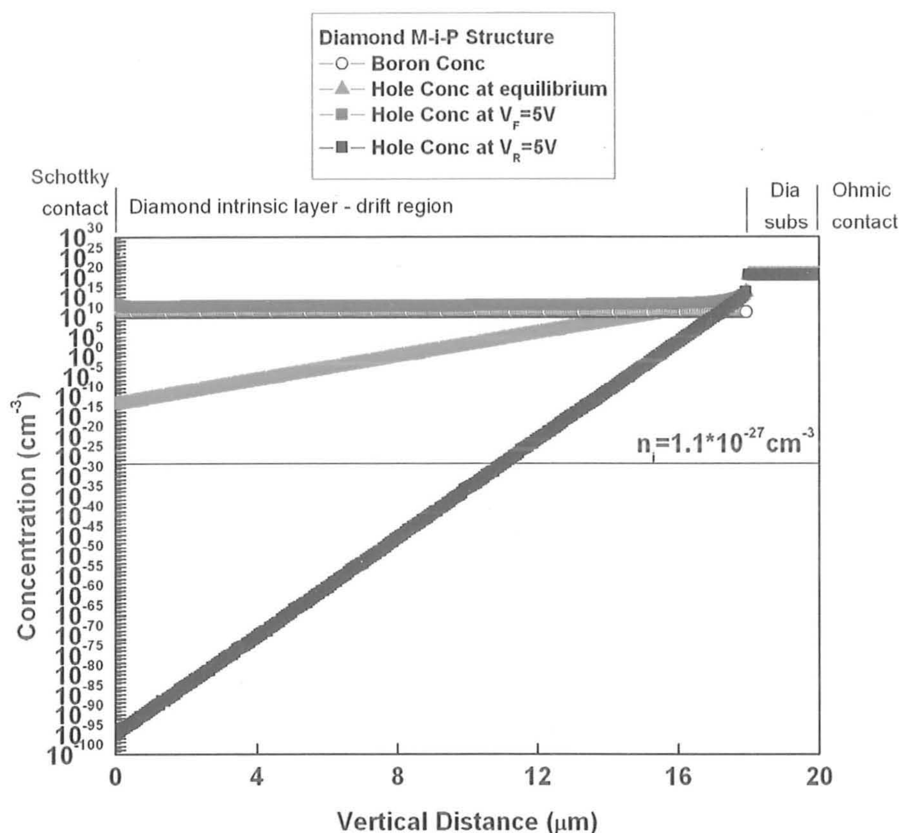

Fig. 4.17 – Boron and hole concentration through the device in three cases: at thermal equilibrium, for V_F = 5V and for V_R = 5V

For larger levels of doping **(Fig. 4.18)**, the drift region is only partially depleted at equilibrium, therefore the energy levels are constant in the vicinity of the drift-substrate interface and the band diagrams look very much alike those shown in **Section 4.1**, for p-type semiconductor. The depletion region is approximately 11μm long for 10^{13}cm^{-3} drift doping level and 1μm for 10^{15}cm^{-3} drift doping concentration. In terms of variation with the drift layer thickness, no significant differences can be noticed for the diamond M-i-P diode **(Fig. 4.19)**. Even at a thickness of 50μm, the drift layer is still completely depleted at equilibrium due to its extremely low doping.

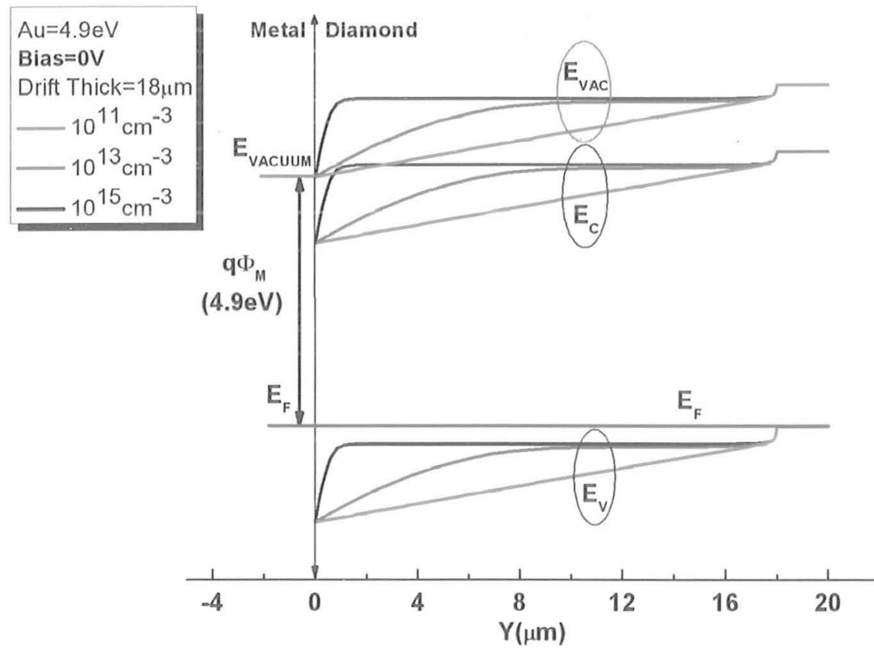

Fig. 4.18 – Band energy diagram for diamond power Schottky diodes with different drift doping levels, at equilibrium

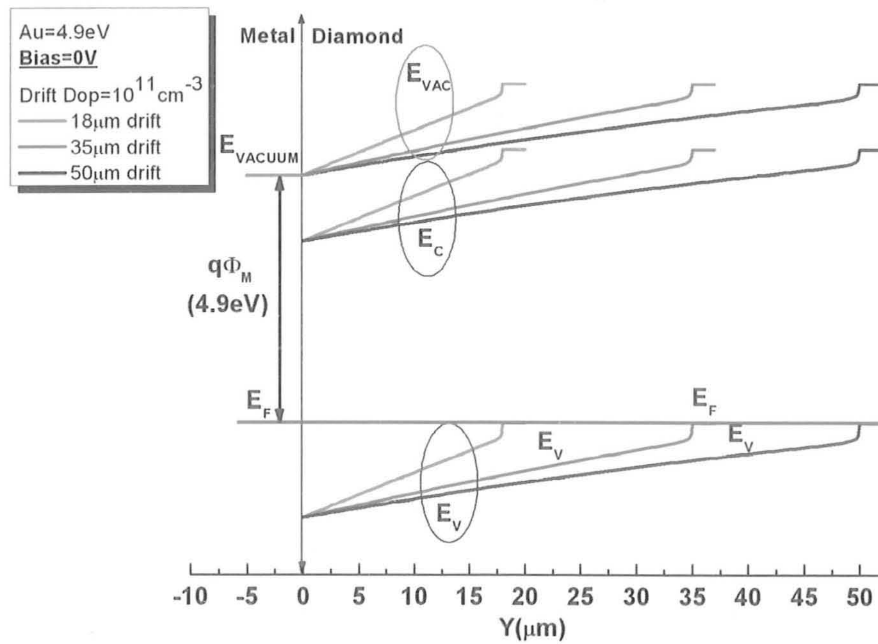

Fig. 4.19 – Band energy diagram for a diamond M-i-P Schottky structure with different drift thicknesses, at equilibrium

Chapter 5

The on-state behaviour of the diamond M-i-P structure

CHAPTER 5
The on-state behaviour of the diamond M-i-P structure

5.1 The shape of the forward characteristic

When a diamond M-i-P diode is positively biased with V_F (high voltage on the p++ substrate, low voltage on the i-layer), holes are injected from the highly p++ doped substrate into the thin, extremely lowly doped (ideally 'intrinsic'), drift layer. As shown in **Chapter 4**, the absolute potential energy of the holes in the drift region is elevated with qV_F, the Fermi level in the semiconductor with qV_F with respect to the Fermi level in the metal, therefore the barrier that holes need to overcome to diffuse into the Schottky metal is lowered and the probability of having a hole current flowing from diamond into the metal increases. However, the flux of holes transported from the metal towards diamond remains the same, as the barrier seen by the carriers (also called the Schottky barrier, $\Phi_{B\text{-}P}$) is practically unaffected by the biasing voltage. In conclusion, when a positive voltage is applied on the anode (ohmic contact), a hole current starts flowing from the substrate, via the drift region, towards the cathode (Schottky contact). A typical experimental on-state characteristic of the diamond M-i-P structure which is the subject of this study exhibits three regions of variation of the forward current density, J_F, with the forward voltage, V_F and is inserted in **Fig. 5.1** (in logarithmic scale) and in **Fig. 5.2** (in linear scale). In the first region, the current has an exponential increase with the voltage, then in turns to a superlinear dependence, while for large V_F it has an ohmic behaviour.

For low voltage, the current is best described by the thermionic emission theory. This phenomenon was for the first time reported in 1873 by Professor Fredrick Guthrie [78], who noticed that a red-hot iron sphere with a negative charge would lose its charge into vacuum. Seven years later, Thomas Edison rediscovered the same effect, when he

measured an electric current between a positively charged foil and an incandescent filament within a bulb.

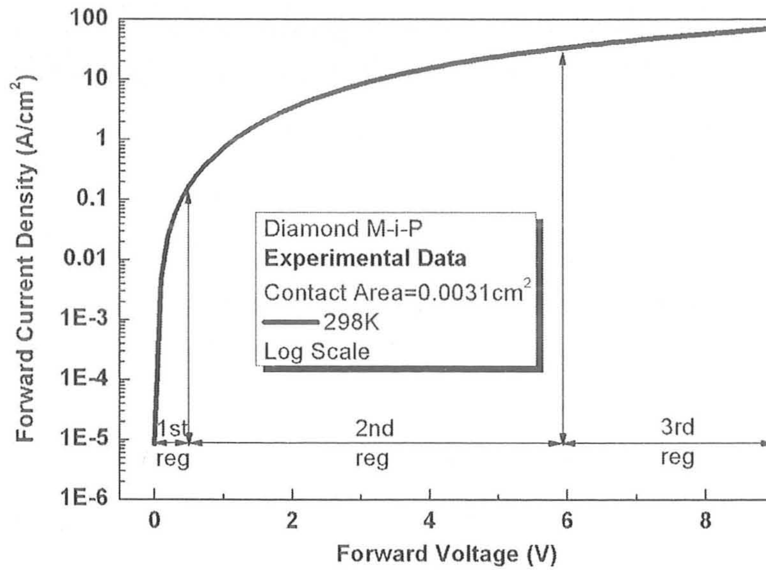

Fig. 5.1 – Typical on-state characteristic of a diamond M-i-P diode

Logarithmic scale

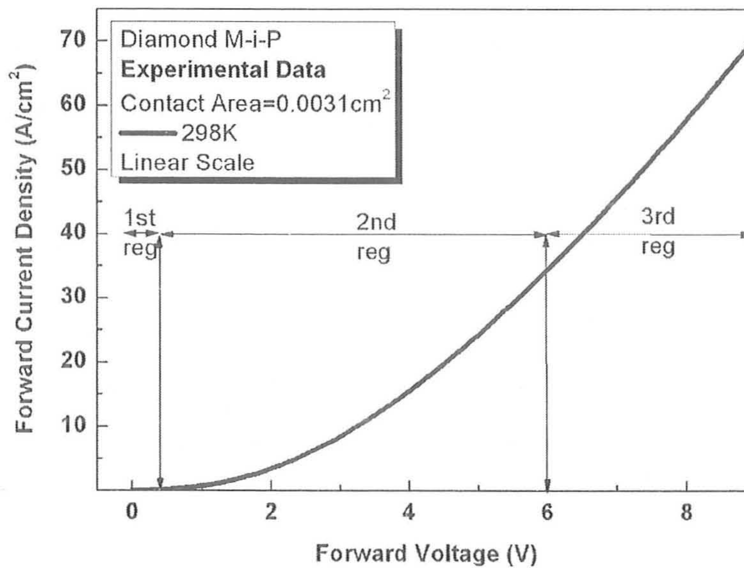

Fig. 5.2 – Typical on-state characteristic of a diamond M-i-P diode

Linear scale

The current was determined by the flow of electrons from the filament, caused by thermal vibrational energy overcoming the electrostatic forces holding electrons to the surface. He found that the current increased rapidly with the temperature of the filament and that enough current would pass in order to operate a telegraph. Therefore, he filed a patent application in which he described the effect (also called the Edison effect), which became the first patent for an electronic device [79]. Later, it was discovered that, although significant at large temperatures (1000K-3000K), the effect is present at any temperature above absolute zero [78]. The science dealing with this phenomenon was called thermionics and the charged particles are known as thermions.

In 1901, Owen Richardson published the first equation which aimed to model the thermionic emission process. He proved that the current generated by a heated metal varies exponentially with the temperature (*T*) of the metal and can be increased by decreasing the work function of the metal (*W*)

$$J = AT^2 \exp\left(-\frac{W}{kT}\right) \tag{5.1}$$

A is Richardon's constant, while *k* is Boltzmann's constant. The law for which Richardson was awarded the Nobel Prize, was first announced by him in a paper read before the Cambridge Philosophical Society on the 25th November, 1901, in the following words, as recorded in the published Proceedings: "If then the negative radiation is due to the corpuscles coming out of the metal, the saturation current should obey the law $s = AT^{1/2}e^{-w/kT}$. This law is fully confirmed by the experiments to be described." [80]. A decade later, Richardson refined his initial formula: "In 1911, as a result of pursuing some difficulties in connection with the thermodynamic theory of electron emission, I came to the conclusion that $i = AT^2e^{-w/kT}$ was a theoretically preferable form of the temperature emission equation to the one presented in 1901, with, of course, different values of the constants *A* and *w* from those used in the previous equation. It is impossible to distinguish between these two equations by experimenting. The effect of T^2 or $T^{1/2}$ is so small compared to the exponential factor that a small change in *A* or *w* will entirely conceal it." [78, 81, 82].

In 1942, four years after Walter Schottky explained the rectifying behaviour of the metal-semiconductor contact as dependent on the barrier potential which appears at the

interface between the two materials [66], the German physicist Hans Bethe proved that the current flowing in a metal-semiconductor barrier is given by the emission of the majority carriers from the semiconductor into the metal [83]. Bethe claimed that, when the rectifying metal-semiconductor contact (later called Schottky contact) was forward biased, the carriers (electrons for an n-type semiconductor, holes for a p-type) would migrate from the semiconductor over the potential barrier (also known as built-in potential) to the metal, in a similar manner to the thermionic emission of electrons from a metal into vacuum. The only condition for the thermionic theory to be applicable to the Schottky contact would be that the carrier mean free path must be larger than the distance in which the Schottky barrier falls by kT from its maximum value. This is similar with assuming that the Schottky barrier is significant larger than kT. For a Maxwellian distribution of the carrier velocity, the current density is given by the following formula [67]:

$$J_F = J_S\left[\exp\left(\frac{qV_F}{nkT}\right)-1\right] \tag{5.2}$$

where V_F is the forward voltage, n is the ideality factor (ideally it should be equal to 1) and J_S is the saturation current, which obeys **equation 5.3** [67].

$$J_S = A^* T^2 \exp\left(-\frac{q\Phi_B}{kT}\right) \tag{5.3}$$

A^* is the effective Richardson constant, while Φ_B is the Schottky barrier.

In conclusion, for low forward voltages, the current has an exponential increase (**Fig. 5.1** – 1st reg) with the voltage, thus obeying the thermionic emission theory and, therefore, **equation 5.2**. As the voltage increases and more and more holes are injected from the substrate into the drift layer, J_F ceases to vary exponentially with V_F (**Fig. 5.1**). This phenomenon is related to the extremely low doping level of the drift region. Due to this, the increased concentration of injected carrier, cannot be charged-balanced, thus the conduction is space-charge limited.

The space-charge concept is directly related to the thermionic (Edison) effect. When an incandescent filament starts emitting a current towards the positively charged foil, the emission current is many times larger than the current normally collected by the

foil. Most of the electrons emitted by the filament are driven back by the repulsion of the cloud of electrons in its neighbourhood. This is called the space charge effect.

At the beginning of the second decade of the 20th century, Child and Langmuir have demonstrated that in a plane-parallel diode in vacuum, the space-charge limited current is proportional with $V^{3/2}/d^2$, where V is the applied voltage and d is the distance separating the cathode and the anode [84, 85]. In 1940, Mott and Gurney developed a similar law for unipolar current through insulators or extremely lowly doped semiconductors [86]. According to the Mott-Gurney law, the current is proportional with V^2/d^3. The difference between the Child and the Mott-Gurney equations comes from the fact that, in semiconductors and dielectrics, electrons travel with constant velocity, while in vacuum they travel with constant acceleration. In both cases, the current does not depend on the amount of excess carriers in the vacuum or in the insulator or in the extremely lowly doped semiconductor, as long as there is an excess.

In the case of the diamond M-i-P structure, after the turn-on of the device (**Fig. 5.2**), the holes injected in the drift region form a cloud, and thereby a positive space-charge. The holes are attracted by the un-biased cathode (the Schottky contact), which has a smaller potential compared to the positively doped anode (the ohmic contact). The result of this attraction is a space-charge limited current, meaning a current limited by the repelling force between injected holes. This current obeys the Mott-Gurney law:

$$J_F = \frac{9}{8}\varepsilon_D \mu_p \left(\frac{V_F^{\ 2}}{L_i^{\ m}} \right) \tag{5.4}$$

where ε_D is the relative permittivity of diamond (5.7), μ_p the hole mobility, L_i the thickness of the drift layer and m is a constant between 2.3 and 3. The superlinear increase of current with forward voltage is confirmed by experimental data (**Fig. 5.2** – 2nd region).

At this point, one might raise the following question: Why, for small V_F (1st region), the current obeys the thermionic theory, while for larger voltage drops (2nd region) it follows the space-charge limited Mott-Gurney equation? The explanation resides in the imperfect quality of the i-layer, as detailed below.

The diamond M-i-P structure which is the subject of this investigation has a substrate which acts as a reservoir of carriers ready to enter the i-layer when a positive voltage is applied at the ohmic contact. In order for the space-charge theory to be valid, the hole concentration injected into the drift layer needs to be in excess of the hole concentration within this layer at equilibrium (this hole concentration balances the static doping charge). In reality, the diamond i-layer is not perfectly intrinsic. Therefore, for low V_F, the injected concentration of holes is insufficient to overcome the drift layer carrier concentration. Thus, the structure behaves like a typical power Schottky diode and the current is given mainly by the thermionic emission. However, due to the low levels of carrier concentration, the currents are extremely small. As V_F increases, the injected hole concentration becomes significant, hence it overcomes the drift layer concentration and therefore the current becomes space-charge limited.

It can be shown that the cross-over forward voltage at which the current shifts from the thermionic behaviour to the space-charge limited one is the voltage at which the hole transit time becomes equal to the relaxation time [87]. The transit time is the time required by a hole injected from the substrate to flow through the whole of the drift layer and to be collected by the cathode. Meanwhile, the relaxation time refers to the time required by a material, in our case the diamond intrinsic layer, to compensate an injected charge. If free charge is injected into a material, then this charge must be neutralized by mobile carrier from the material boundary. This process, called dielectric relaxation, occurs within a finite period of time, called the relaxation time. Initially, for small V_F, this time is significantly smaller than the transit time. When increasing V_F, the transit time gets smaller and smaller. When it becomes lower than the relaxation time, it means that some of the holes injected in the drift cannot be compensated, and, thus, the current becomes space-charge limited.

Finally, a third trend of variation of the forward characteristics occurs for large V_F (**Fig. 5.2** – 3rd region). In this case, the current ceases to be space-charge limited and has a linear increase. This behaviour indicates that the voltage drop on the internal drift and substrate resistances becomes predominant. The contribution of the internal resistances to the total forward voltage drop of the structure is negligible in the first and second region

of the on-state characteristic. However, as the current increases, this contribution becomes more and more significant.

In the 2nd and 3rd region of variation, a complete equation regarding the total voltage drop should consider not only the contribution of the space-charge limited current, but also the one of the internal resistances ($R_{INTERNAL}$):

$$V_F = \sqrt{\frac{8L_i^{\;m}}{9\varepsilon_D \mu_p} I_F} + R_{INTERNAL} I_F \qquad (5.5)$$

For large currents (I_F), the second term in (5.5) becomes significantly larger than the first one and therefore the current shifts from the space-charge limited behaviour to an ohmic one.

5.2 The dispersion of the on-state characteristic

Experimental measurements show that the extremely high intrinsic hole mobility in diamond (3800cm^2/Vs) can partly compensate for the lack of carriers in the drift region and on-state current densities up to 100A/cm^2 at 5V are measured with limited area Schottky contacts (area of approximately 10^{-5}cm^{-2}) (**Fig. 5.3**). However, these results cannot be reproduced for deposited Schottky contacts with larger area. At 5V, a current density three times lower (33A/cm^2) is measured when a circular gold layer with an area of 0.03cm^2 is used to form the Schottky contact (**Fig. 5.4**). This phenomenon might be due to the non-uniformity of the drift diamond layer surface, which can seriously affect the quality of the Schottky contact. For large contacts, the active area of the contact that enables conduction can be significantly lower than the nominal one.

Even now, five years after Element Six reported the synthesis of high-quality diamond layers, there are still uncertainties regarding the quality of the grown semiconductor. Although the methods for producing synthetic single-crystal diamond have improved dramatically in the last few years, there is still room for improvement in crystal quality for enhanced electronic performance. To this end, an extensive study

regarding the type and concentration of defects which affect device performance in diamond is under way.

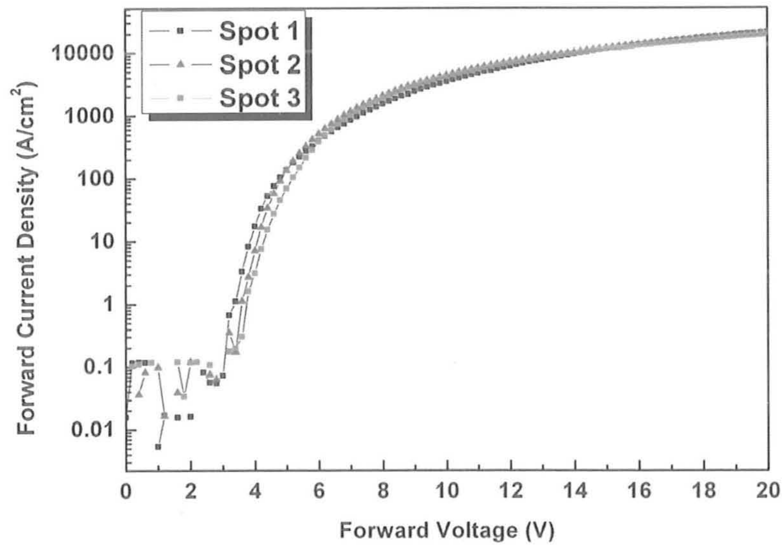

Fig. 5.3 - On-state characteristics of three M-i-P diodes fabricated on the same diamond sample, with limited area Schottky (gold) contacts

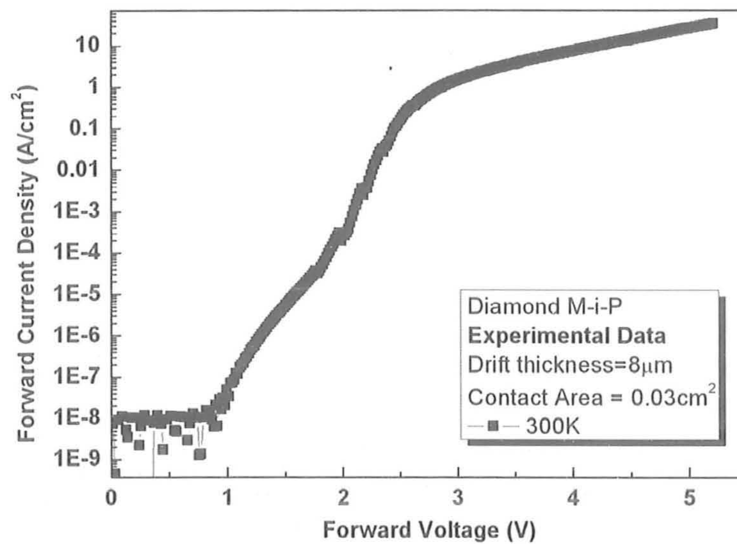

Fig.5.4 – Measured on-state curve of a diamond M-i-P structure with 0.03cm^2 Schottky area contact

Apart from vertical dislocations and traps which occur within the bulk of the material, surface non-uniformities might seriously decrease the on-state capability when using large Schottky contacts. SEM images (**Figs. 5.5** and **5.6**) show that, although polished, diamond samples still exhibit a rather non-smooth surface. If a large area contact is deposited on such a surface, the effective interface between the semiconductor and the metal comprises only the pits of the diamond surface. Only these pits, which are higher than the rest of the diamond surface, make the contact with the metal. Thus, a Schottky contact with an effective area significantly lower than its nominal area is obtained. This is a possible explanation for the degradation of the forward current density for large area contacts.

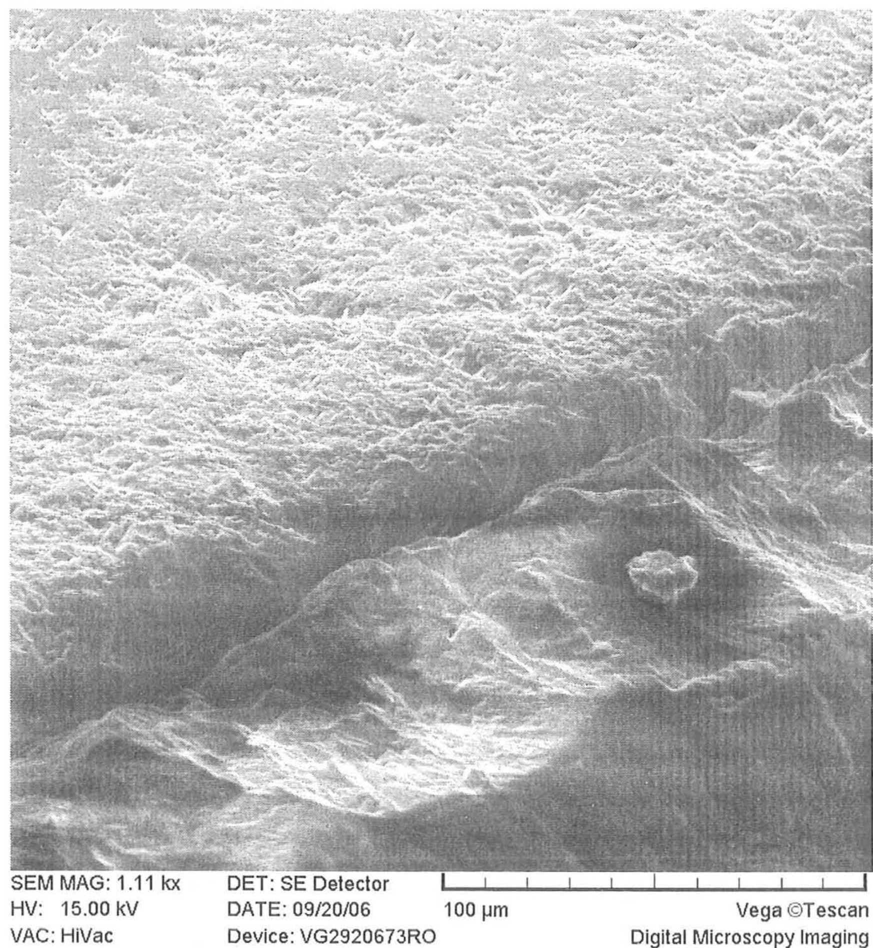

Fig.5.5 – SEM image of the surface of the diamond drift layer

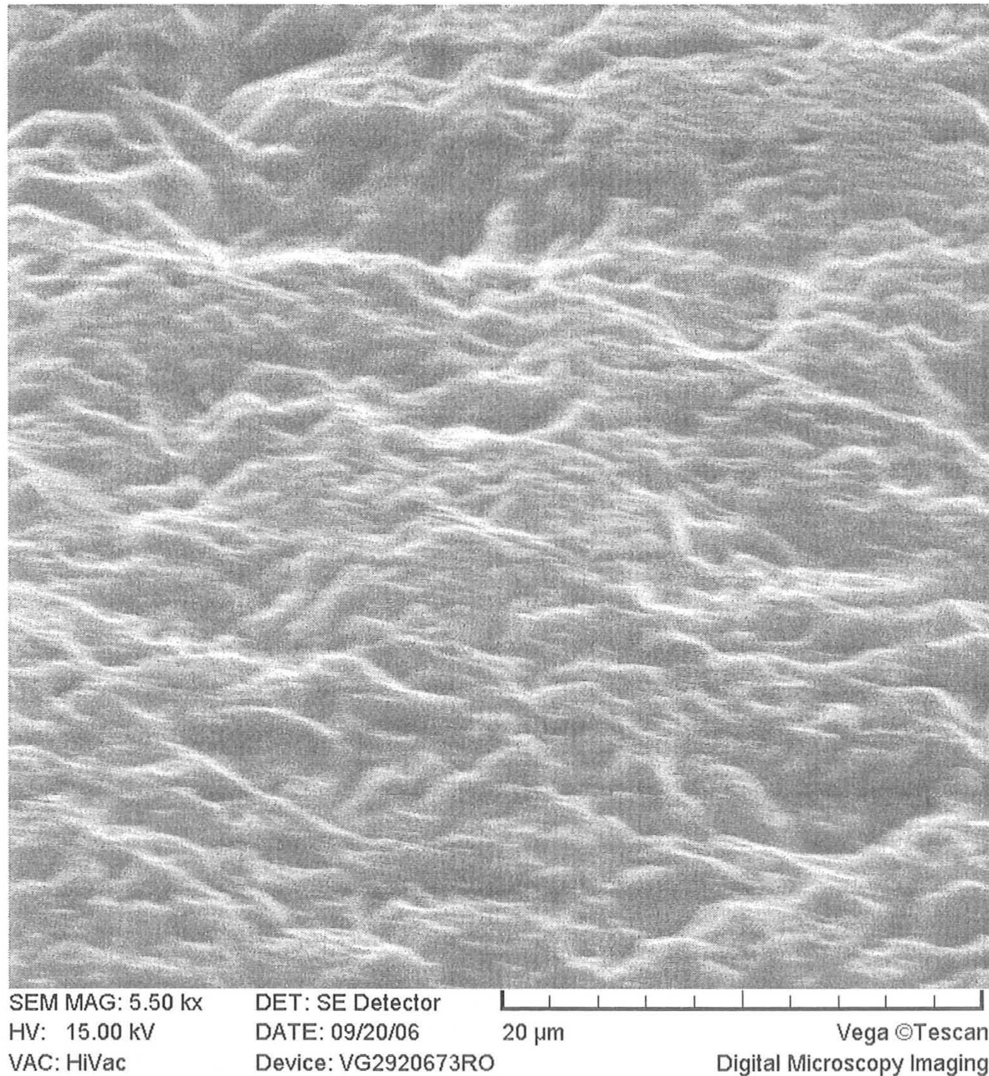

Fig.5.6 – SEM image of the surface of the diamond drift layer, showing the numerous non-uniformities of the surface

Another reason for the non-scalability of the on-state performance of the diamond M-i-P Schottky structure when increasing the area of the Schottky contact is related to the possible non-uniformities of the contact. The deposition of large contacts might induce, via mechanical stress, the deformation of the contact, which can bend upwards near its edges. Thus, the effective area of the contact is again lower the nominal one. Aluminium and gold were proven to form good Schottky contact on diamond. However, a study

whether the performance can be reproduced for large contact area has not been performed yet.

To further confirm that there is still place for improvement in growing high quality diamond layers and depositing uniform Schottky contacts on diamond, one can consider nearly any set of forward characteristics measured on a diamond M-i-P samples. In **Fig. 5.7**, the on-state curves of five M-i-P diodes created on the same diamond sample are inserted. Although all the Schottky contacts have the same area (approx. 0.002cm^2) and were obtained by evaporating the same metal (aluminium), the on-state current density varies with up to 30% from one diode to the other. This dispersion needs to be seriously reduced in order to fabricate reliable diamond M-i-P Schottky diodes.

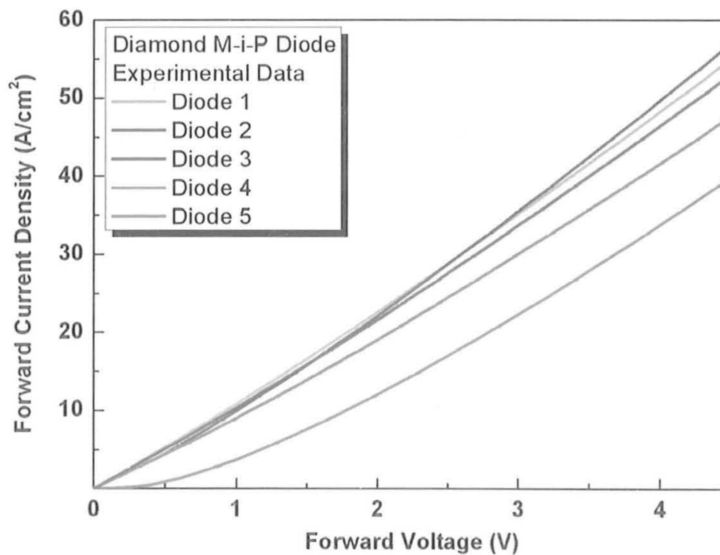

Fig. 5.7 – On-state characteristics
for five M-i-P diodes created on the same diamond sample

5.3 Temperature variation

5.3.1 M-i-P structures

Figures 5.8 and 5.9 show experimental I-V characteristics at three temperatures, for a diamond M-i-P diode with large Schottky contacts. The curves emphasize the way the forward characteristics of the diamond M-i-P structure vary with temperature. For V_F close to the turn-on voltage, the forward voltage drop decreases with temperature. For larger V_F, the opposite trend is observed.

In **Section 5.1**, the typical on-state characteristics of diamond M-i-P diodes was divided in three regions. In the first region, the current obeys the thermionic emission theory, in the second is space-charge limited, while in the third it has an ohmic behaviour.

As shown in **Fig. 5.8**, in the first region of the characteristic, the current increases significantly with temperature for a given V_F. This is mainly due to the severe dependence of the saturation current, J_S, on temperature (**equation 5.3**), which, in turn, becomes the leading effect when it comes to the variation of J_F with T (**equation 5.2**). This leads to lower turn-on voltages and larger currents with increasing T.

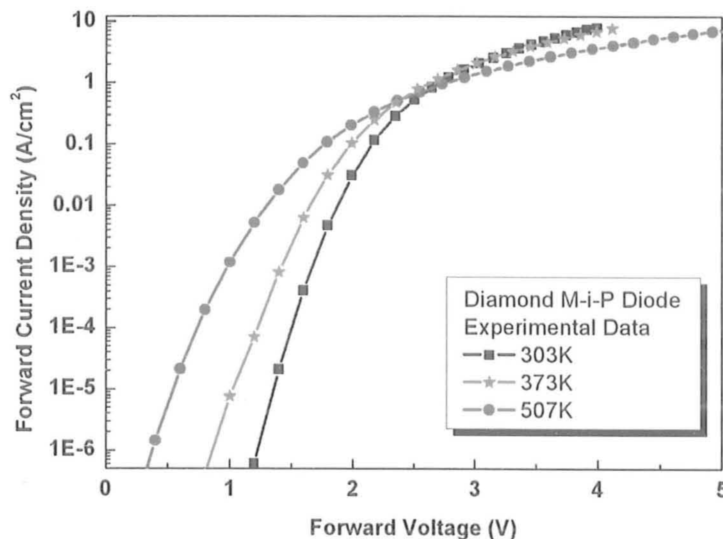

Fig. 5.8 – Measured forward characteristics

for a diamond M-i-P diode at different temperatures – logarithmic scale

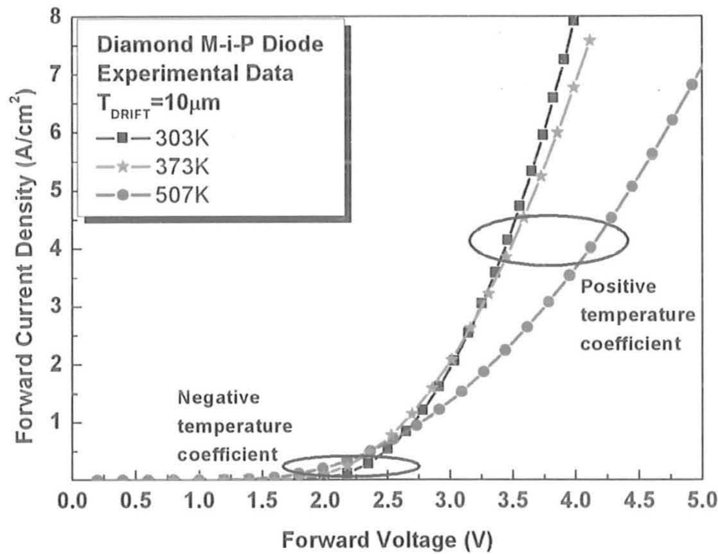

Fig. 5.9 - Measured on-state curves
of a diamond M-i-P diode at different temperatures – linear scale

In the second region of the forward curve, J_F shifts from an exponential variation with V_F to a superlinear one, obeying the Mott-Gurney equation. In the first part of this space-charge limited region, the diode continues to exhibit the negative temperature coefficient observed in the thermionic region. This trend of variation with temperature continues for V_F up to 2.5V.

Recent measurements have proven that at high temperatures, due to various scattering mechanisms, the hole mobility in single crystal diamond decreases significantly. The mobility was shown to be proportional with $T^{-1.5}$ for temperatures below 350K and with $T^{-3.4}$ for higher temperatures [30]. At the same time, as temperature rises, the ionization rate of doping atoms is higher. These two contradictory effects determine the temperature behaviour of the diamond M-i-P on-state characteristic after the device turns on.

Since the drift doping level is extremely low, the increased ionization rate obtained at high temperature has low influence of the current forward level. On the other hand, as J_F rises, the degradation of mobility with temperature plays a more significant role. Therefore, for a V_F with approximately 1V in excess than the turn-on voltage, the

negative temperature coefficient turns into a positive one (**Fig. 5.9**). This is the voltage range where, for a given J_F, V_F increases with temperature.

As the forward characteristic enters the third region, as defined in **Section 5.1**, the current shifts from the space-charge limited behaviour to the linear one. In this region, the positive temperature coefficient is even clearer. The lowered mobility increases significantly the resistivity of both the drift layer and substrate. Thus, the internal resistances rise and the forward current for a given V_F are drastically lowered at high temperatures (**equation 5.5**).

5.3.2 Experiment-simulation matching

Extensive measurements and simulations were performed for an 18 μm thick diamond SBD sample, with circular Schottky contact (200 μm diameter). Gold was used for the Schottky contact (work function = 4.9eV), while a sandwich of Ti and Al provided a good ohmic contact. On-state measurements were performed at seven different temperatures in the range 313K-573K and the characteristics are shown in **Figure 5.10**. A current limit was set at 10μA (0.03185A/cm^2), therefore only the region in which the forward voltage drop decreases as the temperature is increased can be noticed.

As expected, the turn-on voltage reduces for larger temperatures. When trying to match the simulated data with the experimental results, a significant offset of the turn-on voltage could be observed (**Fig. 5.11**). In order to match this parameter, the work function of gold (Φ_{AU}) was increased from 4.9eV to 5.1eV in simulations, which corresponds to decreasing the Schottky barrier from 1.87eV to 1.67eV (**Fig. 5.12**). This is a reasonable approximation, since it has been shown that gold work function varies when evaporated on different semiconductors and 5.1eV corresponds to the gold work function on diamond reported in the literature [88].

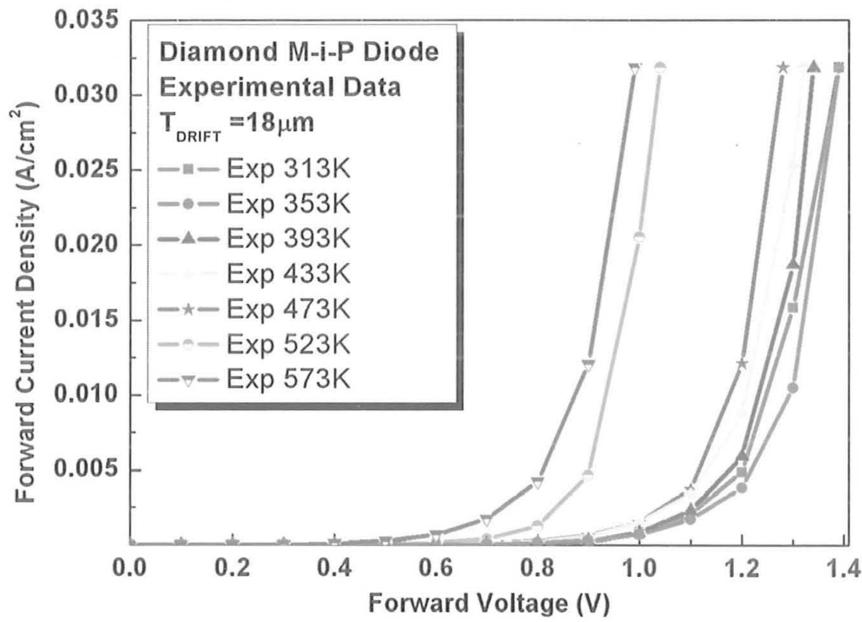

Fig. 5.10 - Experimental forward characteristics, at low voltage, for a diamond M-i-P sample with 18μm drift thickness

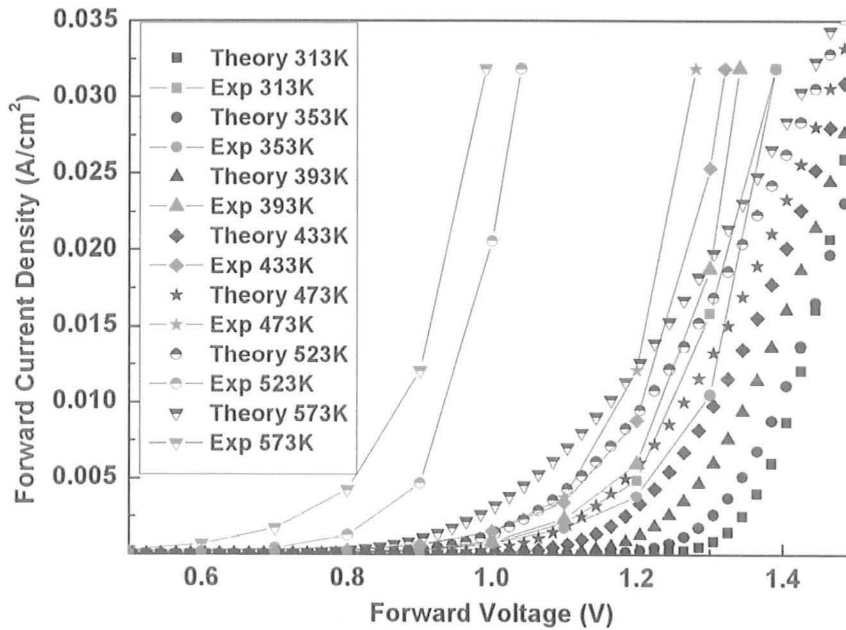

Fig. 5.11 - Significant offset between measured and simulated on-state characteristics when considering, in simulations, the work function of gold to be 4.9eV

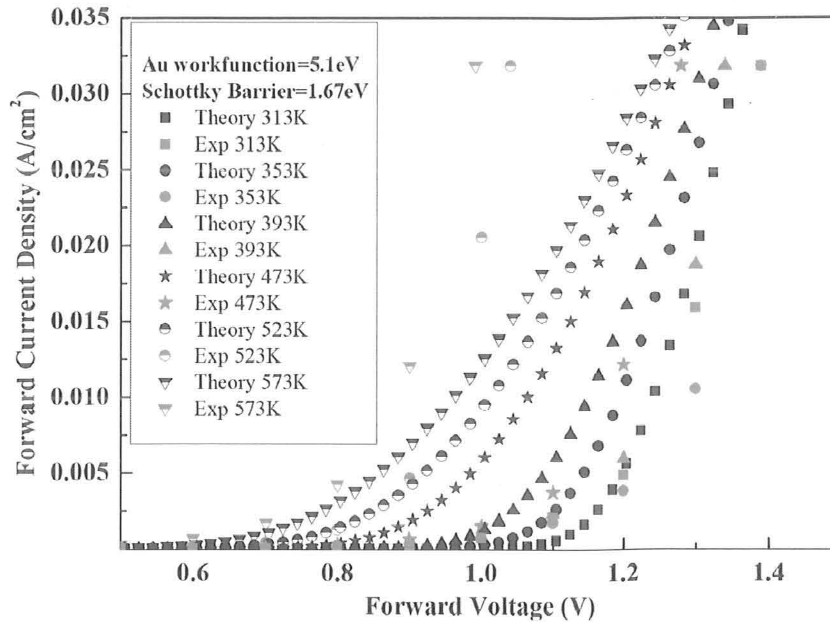

Fig. 5.12 - Acceptable agreement between measured and simulated on-state characteristics when considering, in simulations, the work function of gold to be 5.1eV

With this adjustment, good simulation-experiment agreements were obtained for 313K (**Fig. 5.13**), 353K, 393K and 473K. For temperatures larger than 523K, the estimated current was significantly smaller than the measured one (**Fig. 5.14**).

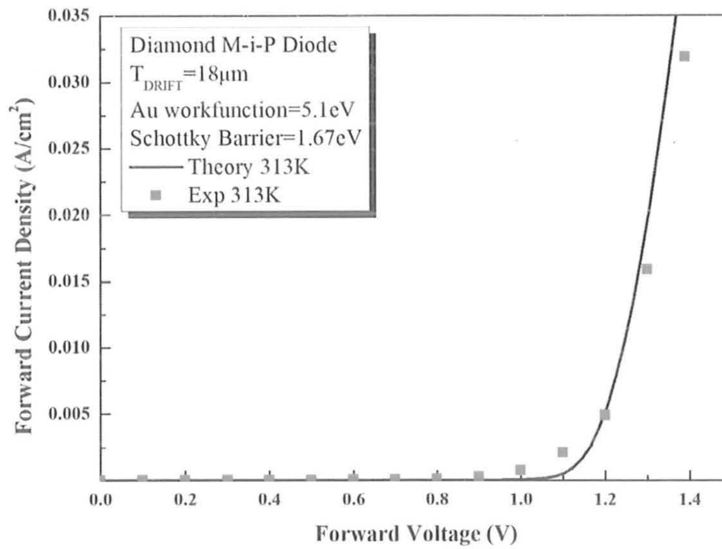

Fig. 5.13 - Good experiment-simulation matching at 313K

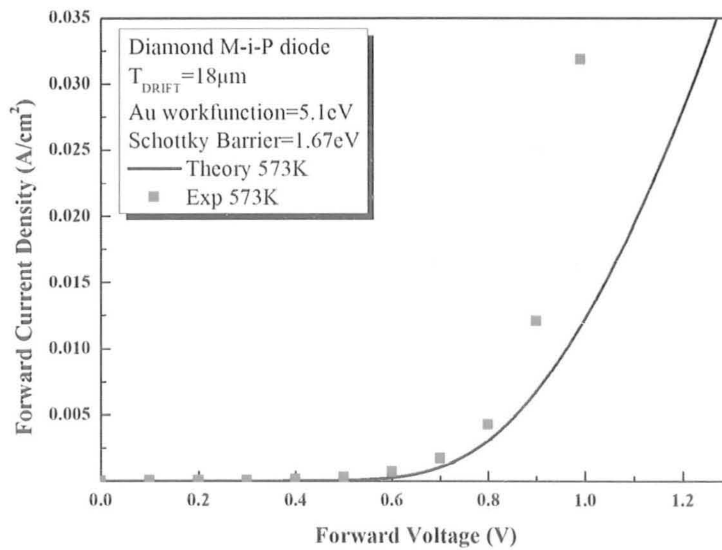

Fig. 5.14 - Poor experiment-simulation matching at 573K

5.3.3 Non M-i-P structures

Obtaining extremely lowly doped drift layers is not an easy task. During the growth of the so-called intrinsic layer, contamination with boron atoms from the substrate

is possible and higher drift doping levels than expected are obtained. Taking this into account, we investigated whether an increased doping concentration of the drift layer would have a significant impact of the on-state behaviour of the diamond power Schottky structures. For a constant concentration profile of approximately $10^{16}cm^{-3}$ boron atoms in the drift region, experimental data suggest that the second trend of variation with temperature disappears (**Fig. 5.15**). The curves still exhibit the space-charge limited and the resistive regions, but no change in the temperature coefficient is obtained. For the whole range of V_F values, the diamond Schottky diodes with medium drift doping have a negative temperature coefficient.

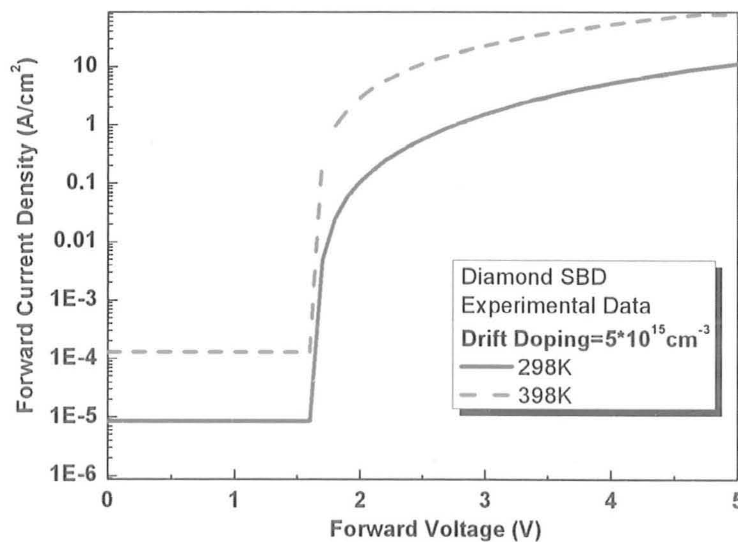

Fig. 5.15 – Experimental on-state characteristic for a diamond SBD with $10^{16}cm^{-3}$ drift doping

In order to confirm this result and to further investigate its justification, we also performed numerical simulations on a diamond SBD, for two different doping levels: $10^{11}cm^{-3}$ and $10^{16}cm^{-3}$. $10^{11}cm^{-3}$ was shown to be the impurity concentration which best approximates in simulations the behaviour of intrinsic layers obtained experimentally, while $10^{16}cm^{-3}$ is a typical drift doping for a classical structure of a power SBD [61]. The on-state characteristics for the two doping profiles, at 298K and 398K, are shown in **Fig. 5.16**. While the curves for the lowly doped structure confirm the experimental data

corresponding to the M-i-P structure, the ones for a significantly higher drift doping show only one trend: an increase of the forward current with temperature for a given voltage drop, no matter the value of V_F. This result indicates that the behaviour of the forward characteristics with temperature is indeed significantly influenced by the drift doping level. If the impurities concentration exceeds a certain level, then the second trend of variation of the on-state curve with temperature (decrease of current with temperature for a given voltage drop) disappears.

The important role played by the drift doping in the temperature behaviour of the diamond power Schottky diodes is mainly due to the high activation energy of boron and all other dopants in diamond. The high activation energies (0.37eV for boron) induce incomplete ionization at room temperature. Still, this phenomenon has different effects on the behaviour of the device, with respect to the drift doping level.

As temperature rises, the dopants ionization rate increases. However, for drift boron concentrations of around $10^{11}cm^{-3}$, which corresponds to $3*10^{10}cm^{-3}$ carrier concentration at room temperature, the influence of this increase on the on-state characteristic is not important, due to the extremely low level of the doping. This is the reason why, for forward voltages in excess with approximately 1V to the turn-on voltage, the current starts decreasing with temperature at a given V_F, as the degradation of mobility with temperature becomes the dominant effect. For drift boron concentrations larger than a certain level (which simulations predict to be around $5*10^{13}cm^{-3}$ for 18μm drift thickness), the increase of the dopant atoms ionization rate with temperature becomes the leading effect that influences the forward current behaviour. For example, for a drift boron doping of $10^{16}cm^{-3}$, the increase in carrier concentration from $10^{14}cm^{-3}$ (at room temperature) to $2*10^{15}cm^{-3}$ (at 398K) has an important impact on the current. At the same time, for a boron concentration of $10^{16}cm^{-3}$, the hole mobility ($300cm^2/Vs$) is significantly lower than the one in intrinsic diamond ($3800cm^2/Vs$) even at room temperature. Therefore, the decrease in mobility with temperature, although still exponential, has less impact compared to the case of an extremely lowly doped drift layer. These two facts enable the conclusion that for medium doped drift layers the current variation with temperature is mainly given by the increased concentration of

dopant atoms ionized at elevated temperatures, therefore the current increases with temperature for a given V_F, no matter the value of V_F.

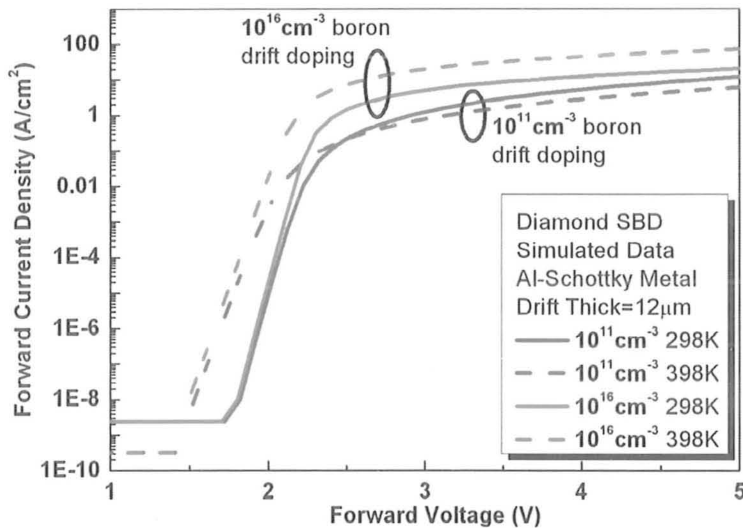

Fig. 5.16 – Simulated on-state characteristics for two drift doping levels and two temperatures

In order to obtain a confirmation of this theory, we have performed simulations at 298K and 398K for the drift doping levels discussed above, without enabling the incomplete ionization model. For a drift boron doping of $10^{16}cm^{-3}$, the on-state curves, included in **Figure 5.17**, show that if all the atoms would be ionized at room temperature, then the on-state characteristics of the diamond SBD would exhibit a negative temperature coefficient for low V_F and a positive one for forward voltages in excess with, on average, 1V than the turn-on voltage. But in real devices incomplete ionization does occur, hence the difference caused to the temperature behaviour by the drift layer doping. For $10^{11}cm^{-3}$ drift boron doping, the simulated forward characteristics obtained without enabling the incomplete ionization model **(Fig. 5.18)** look very much alike the ones obtained when taking into consideration this model and exhibit only the negative temperature coefficient.

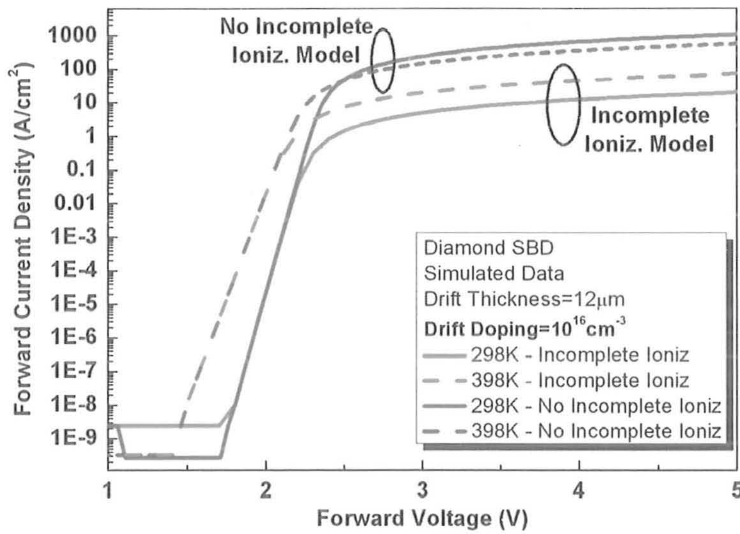

Fig. 5.17 – On-state behaviour of diamond SBD with 10^{16}cm^{-3} drift doping, with and without the incomplete ionization model

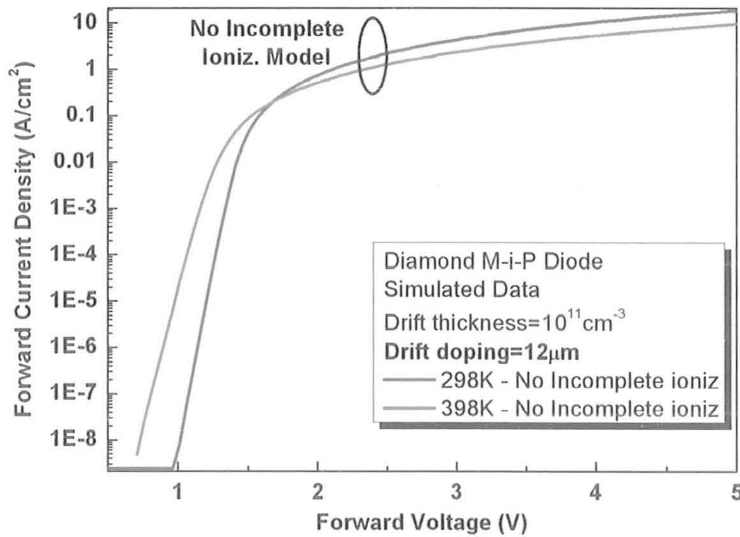

Fig.5.18 – On-state behaviour of diamond SBD with 10^{11}cm^{-3} drift doping, without the incomplete ionization model

5.4 Zero temperature coefficient point on the forward characteristic

Apart from gold, aluminium and nickel are also commonly used to form Schottky contacts on diamond devices. The variation with temperature of the on-state characteristics of diamond M-i-P diodes obtained when using gold as Schottky metal was presented in 5.3.1. In order to further confirm this behaviour, we have replaced gold with nickel (work function = 4.5eV) and aluminium (work function = 4.1eV) and performed simulations for the same drift thickness (T_{DRIFT} = 18μm). For all the analysed metals, the two trends of variation with temperature can be clearly noticed (**Figs. 5.19-5.21**). At the same time, for each of the Schottky metals considered, the transition between the two trends of variation with temperature occurs within a very narrow range of values of the forward voltage. We can approximate this narrow range to be a single point on the on-state characteristic, which we call the zero temperature coefficient (*ZTC*) point [48]. The V_F corresponding to *ZTC* varies, with respect to the Schottky metal work function, from 1.55V for Au to 2.4V for Al (**Table 5.1**). A larger metal work function corresponds to a smaller Schottky barrier, which determines a smaller turn-on voltage and a smaller $V_F - ZTC$. Therefore, the zero temperature coefficient point can be controlled via the metal chosen for the Schottky contact.

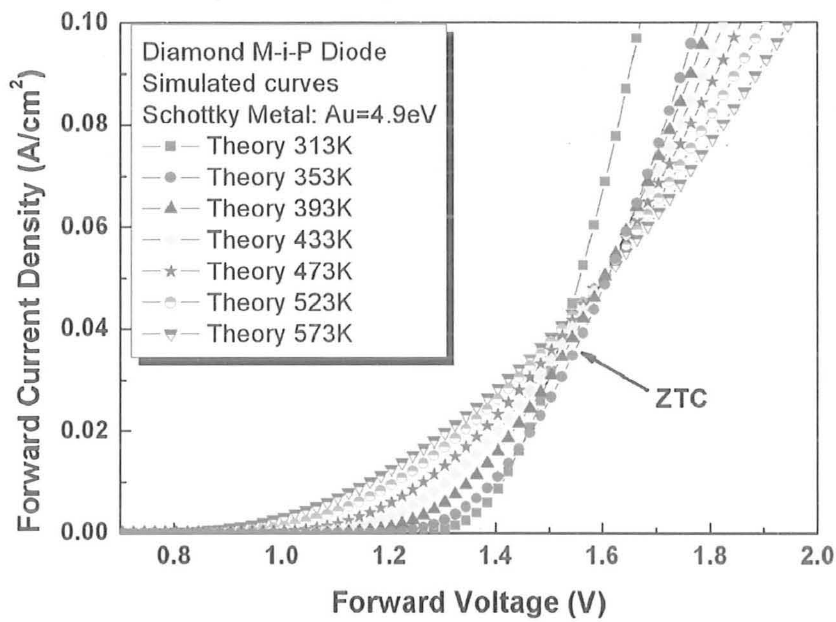

Fig.5.19 - On-state simulated curves for diamond M-i-P diodes with gold as Schottky metal and T_{DRIFT} = 18μm

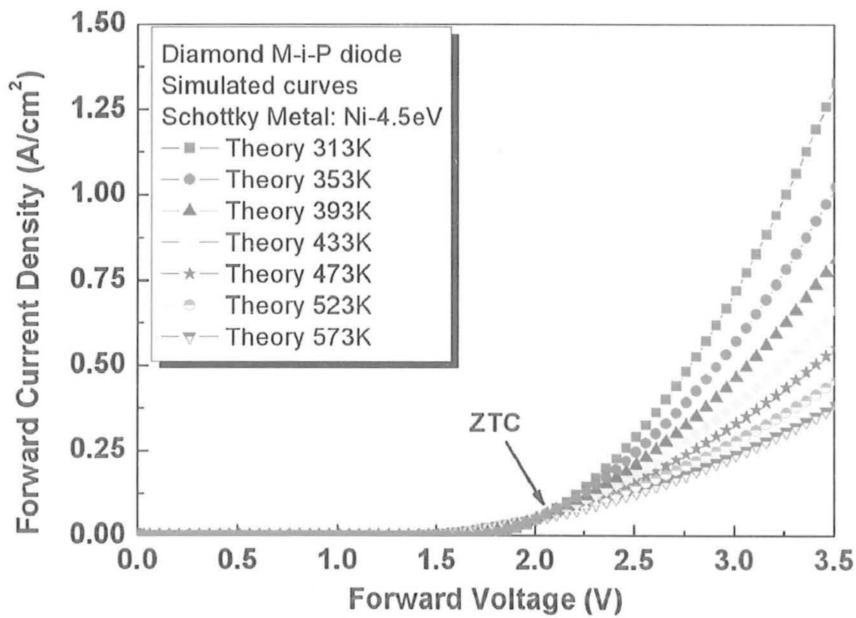

Fig.5.20 - On-state simulated curves for diamond M-i-P diodes with nickel as Schottky metal and T_{DRIFT} = 18μm

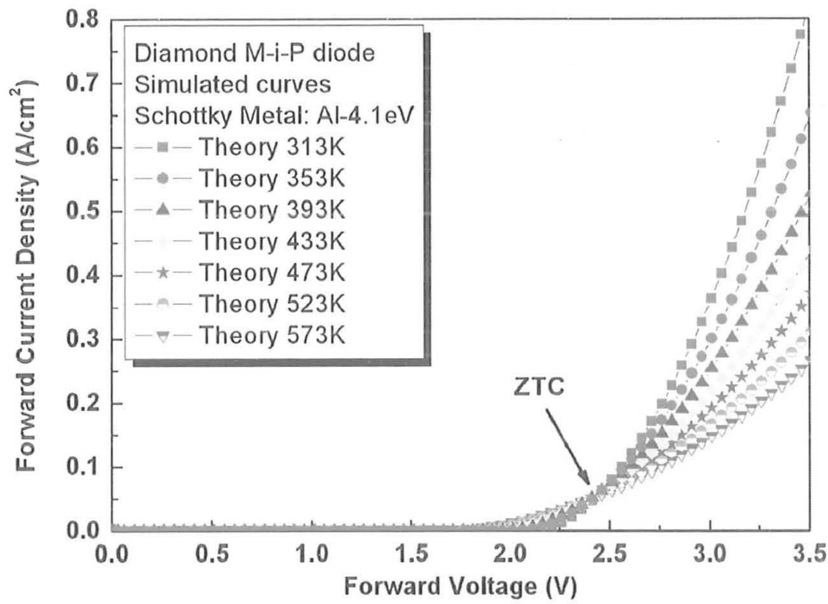

Fig.5.21 - On-state simulated curves for diamond M-i-P diodes with aluminium as Schottky metal and $T_{DRIFT} = 18\mu m$

Metal	Work function (eV)	Schottky Barrier (eV)	Turn-on Voltage (V)	ZTC – V_F (V)	ZTC – J_F (A/cm^2)
Al	4.1	2.67	1.6 – 2.1	2.4	0.06
Ni	4.5	2.27	1.2 – 1.6	2.1	0.05
Au	4.9	1.87	0.8-1.3	1.55	0.04

Table 5.1 - Simulated V_F corresponding to the *ZTC* point for three different Schottky metals

Chapter 6

Termination structures suitable for diamond M-i-P diodes

Chapter 6

Termination structures suitable for diamond M-i-P diodes

CHAPTER 6
Termination structures suitable for diamond M-i-P diodes

6.1 Introduction

Power Schottky devices on wide band gap semiconductors are the main subject of this thesis. These devices are expected to operate at large voltages, typically beyond 600V. Up to this point in the study, in order to estimate the on-state behaviour of the analysed power devices, only ideal, plane-parallel, structures were considered (**Chapter 5**). For this type of structures, no edge effects occur. In the case of ideal diamond M-i-P diodes, for example, the Schottky metal which forms the cathode fully covers the top surface of the drift region (**Fig. 6.1**). For a structure with T_{DRIFT} = 18μm, T_{SUBS} = 2μm, $10^{11}cm^{-3}$ drift boron doping and $2*10^{19}cm^{-3}$ boron substrate doping, simulation predict a breakdown voltage (*BV*) of 3171V. At breakdown, all the potential lines are parallel with the cathode (**Fig. 6.2**) and the electric field has a virtually uniform distribution within the drift region (**Fig. 6.3**).

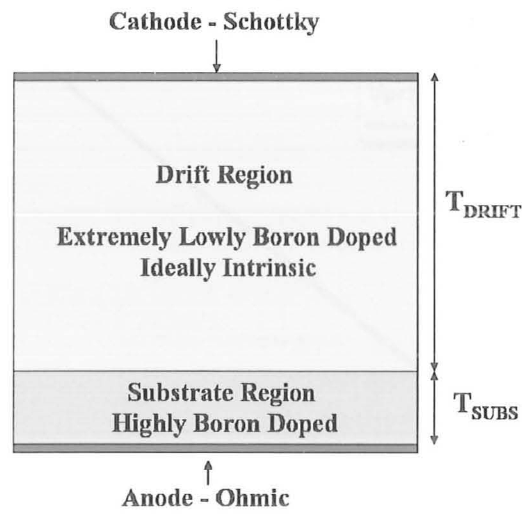

Fig. 6.1 – Cross-section of an ideal, plane parallel, diamond M-i-P diode, used for on-state simulations

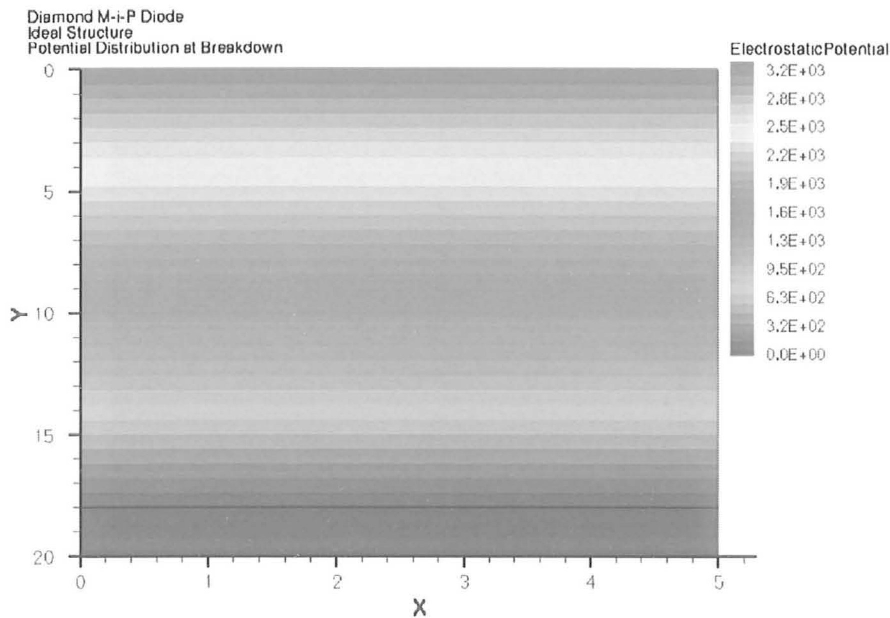

Fig. 6.2 a) – Potential distribution of an ideal diamond M-i-P diode, at breakdown (BV=3171V for T_{DRIFT} = 18μm)

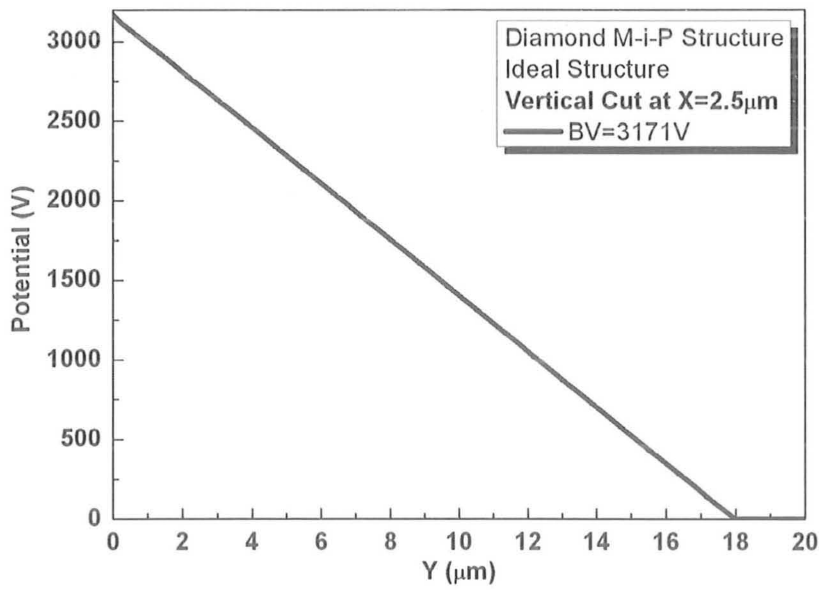

Fig. 6.2 b) – Vertical cut through the potential distribution at X=2.5μm

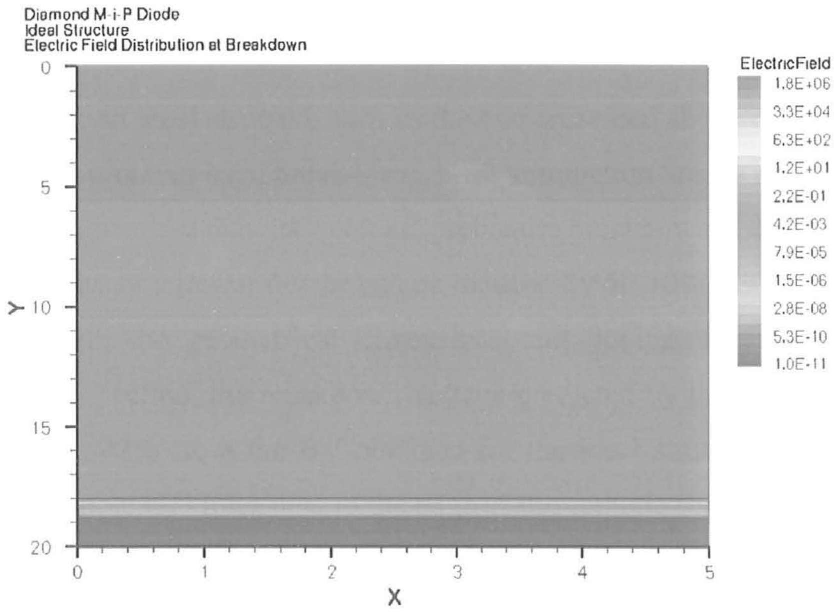

Fig. 6.3 a) – Electric field distribution of an ideal diamond M-i-P diode, at breakdown (T_{DRIFT} = 18μm)

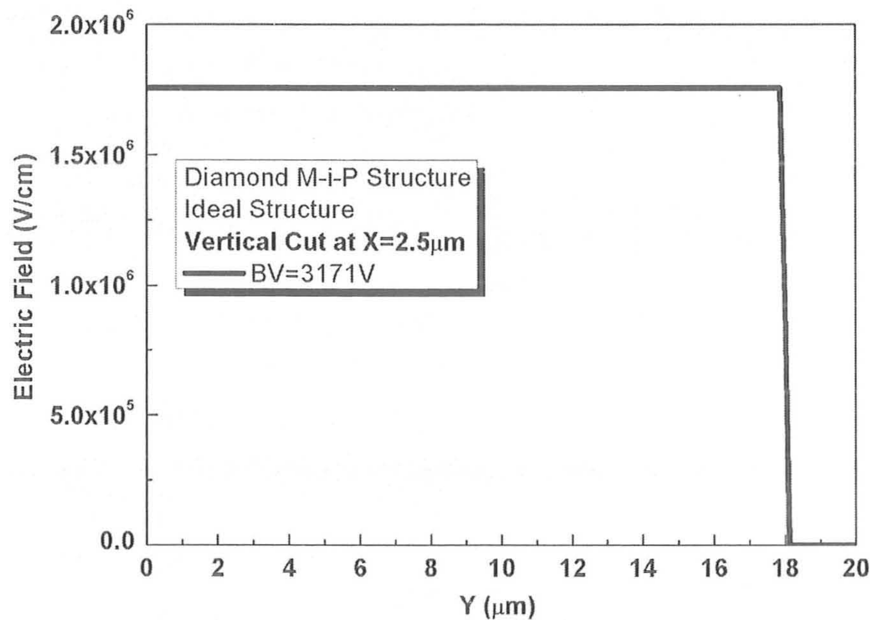

Fig. 6.3 b) – Vertical cut through the electric field distribution at X=2.5μm

However, an ideal structure such as the one presented above cannot be fabricated. Real devices are prone to edge breakdown. If no termination area is employed (**Fig. 6.4**), then at the margins of the Schottky contact premature breakdown is due to occur, and the off-state capability of a power device can be reduced by 50-70% [89]. For a diamond M-i-P structure with the geometrical dimensions and doping levels mentioned at the beginning of this section, the breakdown voltage predicted by the simulations is 1331V, which represents 42% from the BV obtained for the ideal structure. This is due to the crowding of the potential lines next to the edge of the cathode (**Fig. 6.5**), which leads to a peak of the electric field distribution (**Fig. 6.6**) that induces premature diamond breakdown.

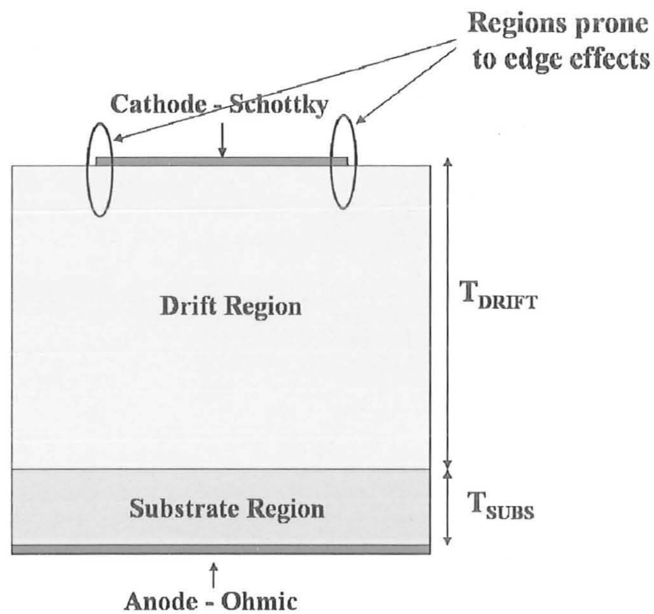

Fig. 6.4 – Cross section of a diamond M-i-P diode, with no termination structure

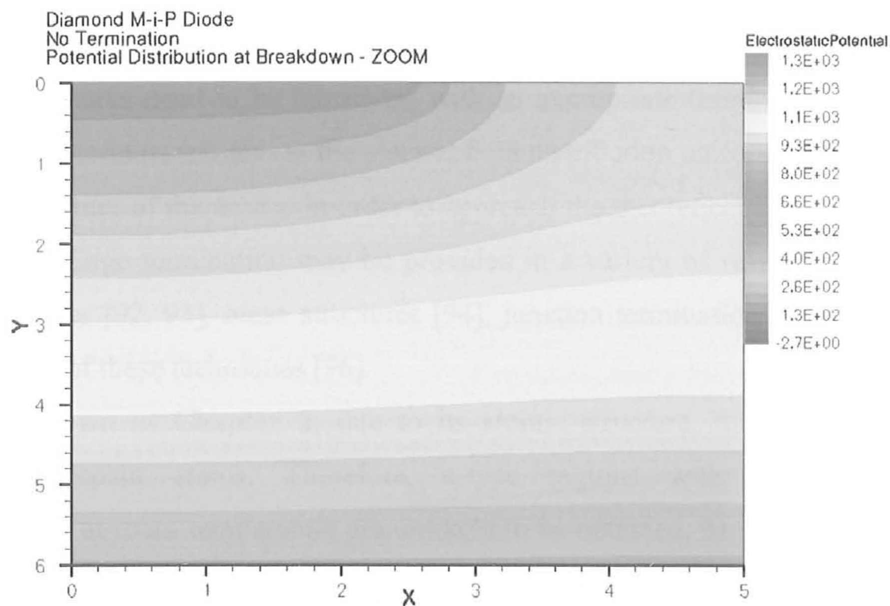

Fig. 6.5 – Potential distribution for a diamond M-i-P diode with no termination, at breakdown (BV=1331V) – ZOOM at the edge of the Schottky contact

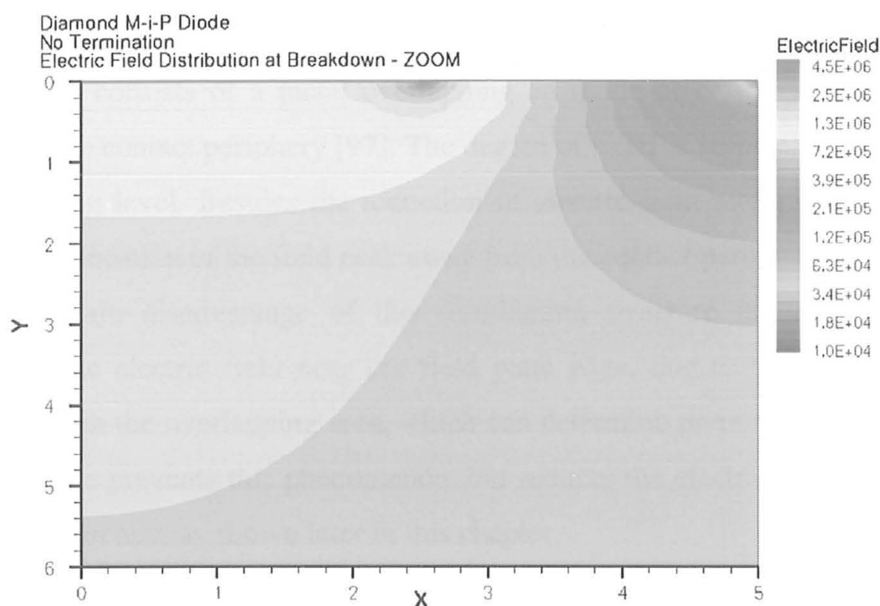

Fig. 6.6 – Field distribution for a diamond M-i-P diode with no termination, at breakdown – ZOOM at the edge of the Schottky contact

In order to avoid this severe degradation of the off-state capability, diamond Schottky structures need to be fabricated with an appropriate termination structure. An effective edge termination makes the electric field distribution uniform in the bulk and at the cathode corner of the device in order to approach the theoretical limit of the ideal M-i-P structure. Edge termination may be provided in a variety of ways: guard rings [90, 91], field plates [92, 93], mesa structures [94], junction termination extensions [95], or combinations of these techniques [96].

As shown in **Chapter 2**, due to its atomic structure, diamond cannot easily incorporate dopant atoms. Therefore, n-type regions with acceptable electron concentrations at room temperature are unlikely to be obtained. This prohibits the use of conventional termination techniques, such as field rings or junction termination extensions, which require both p-type and n-type regions. This is the reason why research has mainly focused on the field plate concept, as a concept based mainly on depositing several insulators layers and extended metallization, rather than on floating p-n junctions within the semiconductor.

The field plate technique is probably the simplest and easiest to implement edge termination. It consists of a metal overlapping an oxide layer which relieves the field crowding at the contact periphery [97]. The degree of relief is reversely proportional with the drift doping level. Besides the reduction of electric field maximum, the field plate also shifts the location of the field peak away from the contact periphery.

The main disadvantage of this termination structure is that it suffers from enhanced oxide electric field near the field plate edge, due to the reduction in oxide thickness within the overlapping area, which can determine premature oxide breakdown. A thicker oxide prevents this phenomenon, but reduces the electrical performance of the termination structure, as shown later in this chapter.

Because of its relatively simple fabrication process, the field plate termination is widely used in the power devices industry, especially for wide band gap devices, such as SiC power Schottky diodes [93].

This chapter investigates three implementations of the field plate concept: the single step field plate (*FP*) termination, the three-step *FP* structure and the ramp oxide termination. All of them were previously demonstrated on several other semiconductors, including silicon and silicon carbide. In this study, their possible implementation on diamond Schottky structures is for the first time proposed. An extensive comparison of their electrical performances, together with an analysis regarding area consumption and risk of premature breakdown are also considered.

The results of the first successful experiments on a diamond Schottky diode with a ramp oxide termination structure are also presented. Finally, the use of high-k dielectrics meant to reduce the risk of premature insulator breakdown is investigated.

6.2 Single step field plate termination

The simplest termination structure suitable for a diamond M-i-P structure using the field plate concept is obtained if an insulator layer is selectively deposited on top of the drift region (**Fig. 6.7**). This structure, called the single step field plate termination, has

two key-parameters: the thickness of the oxide layer (T_{OX}) and the length of the metallization on top of the oxide layer (field plate length – *FP*).

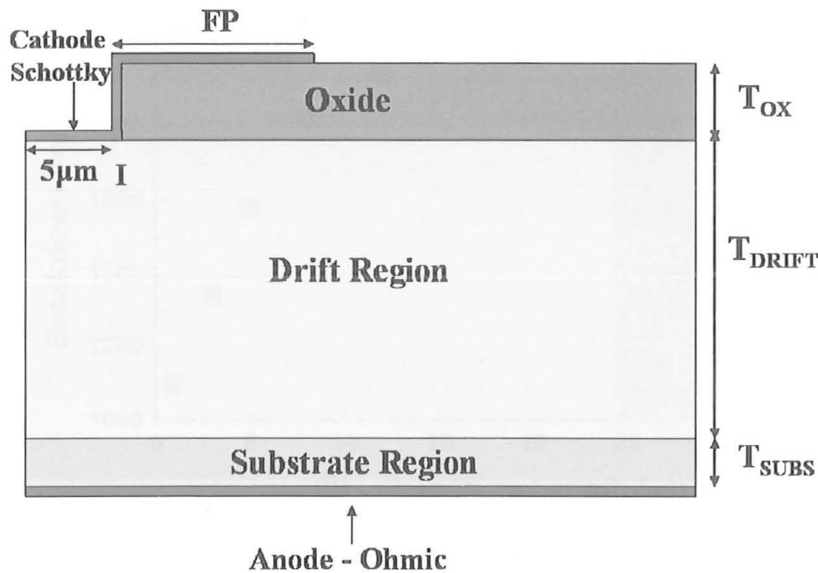

Fig. 6.7 – Cross-section of a diamond M-i-P Schottky diode with single step field plate termination

By adjusting T_{OX} and *FP*, the off-state performance of the structure can be significantly influenced, as presented in **Figs. 6.8** and **6.9**. *BV* increases with *FP* up to 20μm and saturates for larger field plate lengths (**Fig. 6.8**). With respect to the oxide layer thickness, the breakdown voltage has a maximum around 1.5μm, and is significantly smaller when changing T_{OX} by +/- 0.5μm.

Numerical simulations predict that for FP = 25μm and T_{OX} = 1.5μm, and for the geometrical parameters and doping levels defined in **Section 6.1** (T_{DRIFT} = 18μm, T_{SUBS} = 2μm, $10^{11}cm^{-3}$ drift boron doping and $2*10^{19}cm^{-3}$ boron substrate doping), the diamond M-i-P with field plate termination exhibits a maximum breakdown voltage of 2059V.

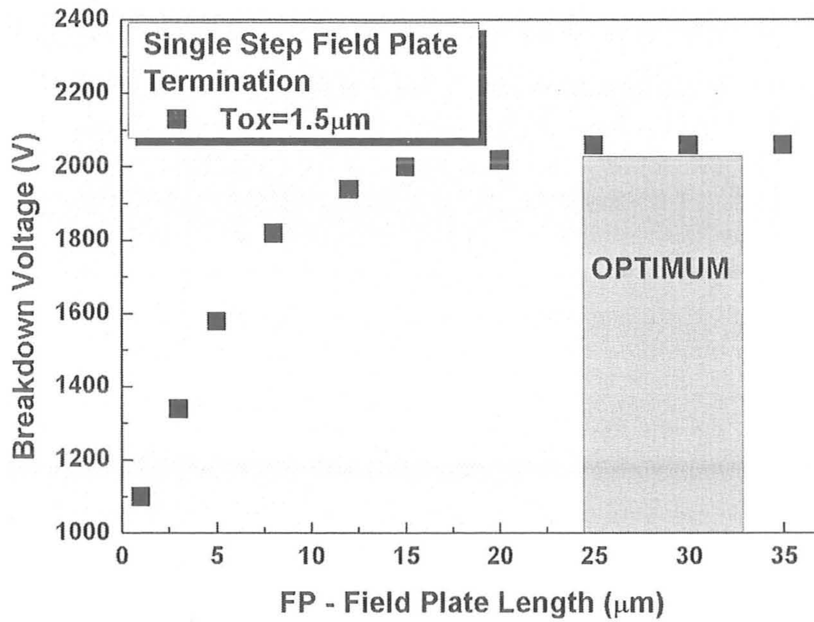

Fig. 6.8 – Breakdown voltage versus field plate length at $T_{DRIFT} = 18\mu m$

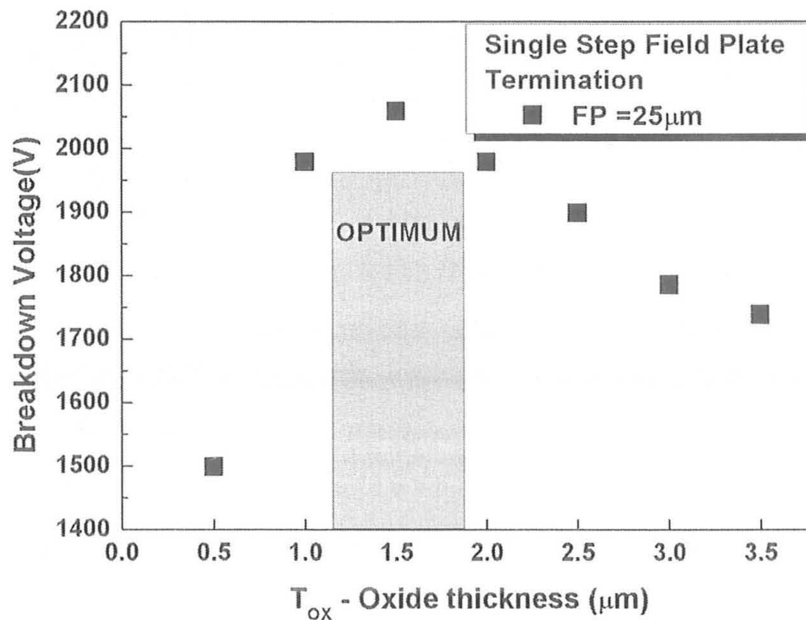

Fig. 6.9 – Breakdown voltage versus oxide thickness at $T_{DRIFT} = 18\mu m$

Due to the sharp edge of the oxide layer, the electric field distribution within the semiconductor has a peak below this edge (**Fig. 6.10**). By increasing *FP*, the potential

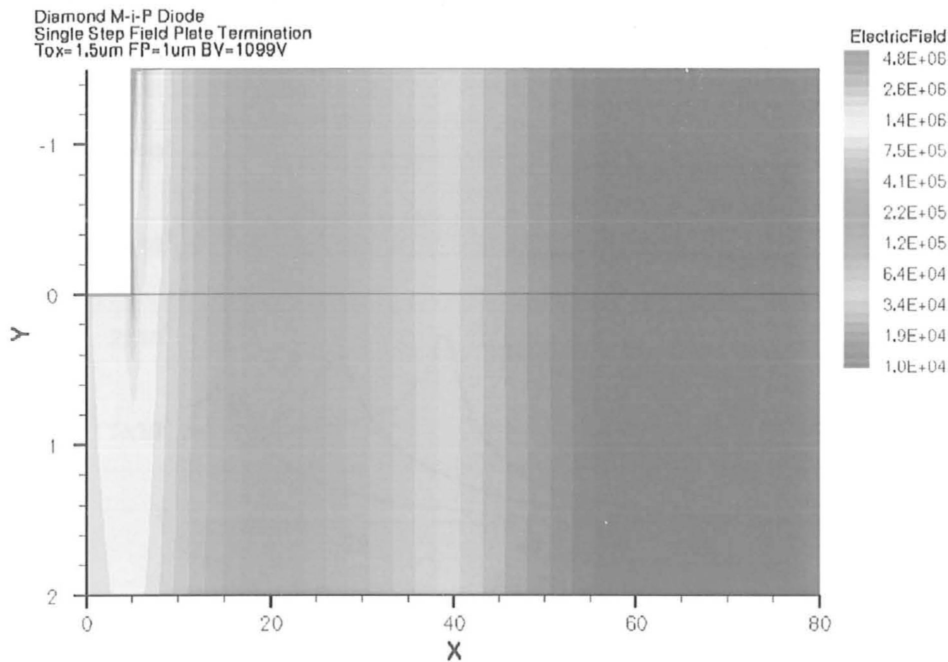

Fig. 6.10 – Electric field distribution for a diamond M-i-P diode with single step termination structure at T_{DRIFT} = 18µm - ZOOM

distribution in diamond has a smoother distribution, therefore the peak of the electric field is reduced and the device has better off-state capability. Even though the breakdown voltage is nearly twice higher when FP = 25µm (2059V) than the case when FP = 1µm (1099V), the peak of the electric field at breakdown is lower (4.03MV/cm for FP = 25µm, 4.78MV/cm for FP = 1µm - **Fig. 6.11**). The difference is even more significant when comparing the field at the same reverse voltage (at V_R = 1000V, the maximum electric field within diamond is 1.99MV/cm for FP = 25µm, and 4.35MV/cm for FP = 1µm - **Fig. 6.12**). At the same time, as *FP* increases, another peak of the electric field distribution, the one which corresponds to the edge of the field plate metal, becomes also significant and, for FP = 25µm, is nearly equal with the other field peak (**Fig. 6.11**). However, even for larger *FP*, this peak does not overcome the one at the beginning of the ramp. This change of maximums is obtained only if the oxide thickness is lowered below 1µm. For the case considered in this study, T_{OX} = 1.5µm, *BV* saturates for *FP* larger than 25µm.

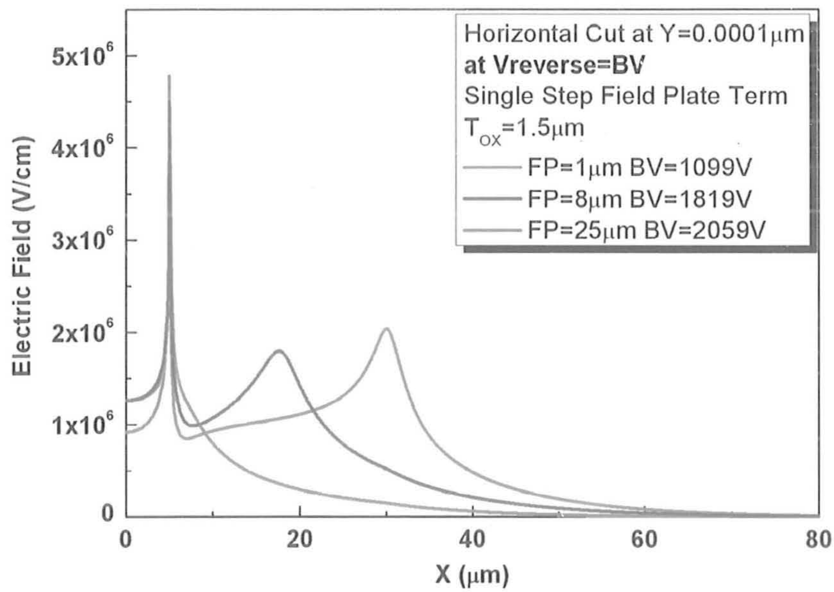

Fig. 6.11 – Electric field distribution at the surface of the diamond drift layer for different FP, at breakdown

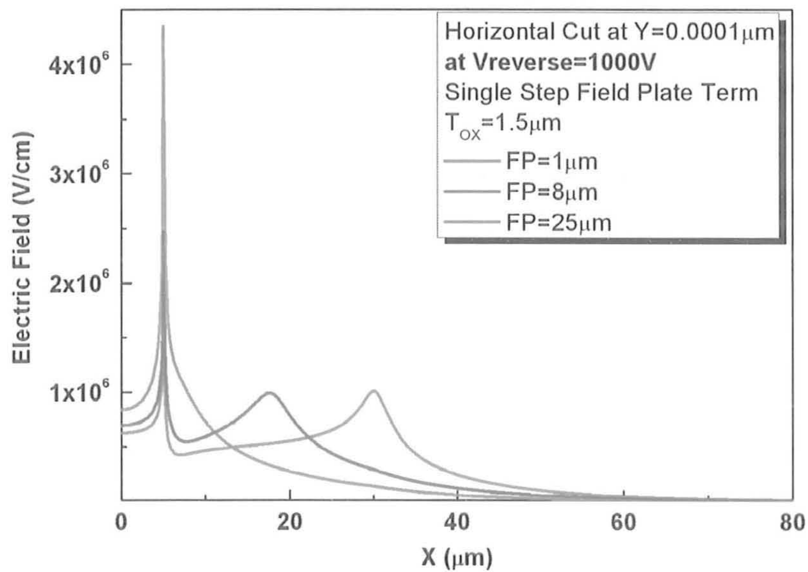

Fig. 6.12 – Electric field distribution at the surface of the diamond drift layer for different FP at V_R=1000V

In terms of variation with T_{OX}, the breakdown voltage has an optimum around 1.5μm (**Fig. 6.9**). As shown in **Figures 6.13-6.16**, both at breakdown and at the same reverse bias (V_R = 1000V), if the thickness is reduced down to 0.5μm, then the peak of the electric field at the beginning of the termination (X = 5μm) becomes lower than the one at the edge of the metal (X = 30μm) and the breakdown is induced by the crowding of the potential lines at the latter point. If, on the contrary, the thickness is increased beyond 3μm, then the high field peak level at X = 5μm lowers the off-state capability of the device.

In order to properly estimate the performance of a termination structure, we define a parameter called termination efficiency (η), as the ratio between the BV of the M-i-P Schottky structure when terminated and the BV of the ideal, plane parallel, structure (as defined in **Fig. 6.1**). The efficiency which corresponds to the optimum design of the single step field plate structure is 64.9% (maximum BV of the termination = 2059V; ideal BV = 3171V) and is obtained for FP = 25μm and T_{OX} = 1.5μm. This is a 22% improvement compared to the non-terminated structure (BV = 1331V, η = 42%), but is still far from the performance of an efficient termination structure. Therefore, two more sophisticated implementations of the field plate concept, the three-step field plate and the ramp oxide, are investigated in the following sections of this chapter.

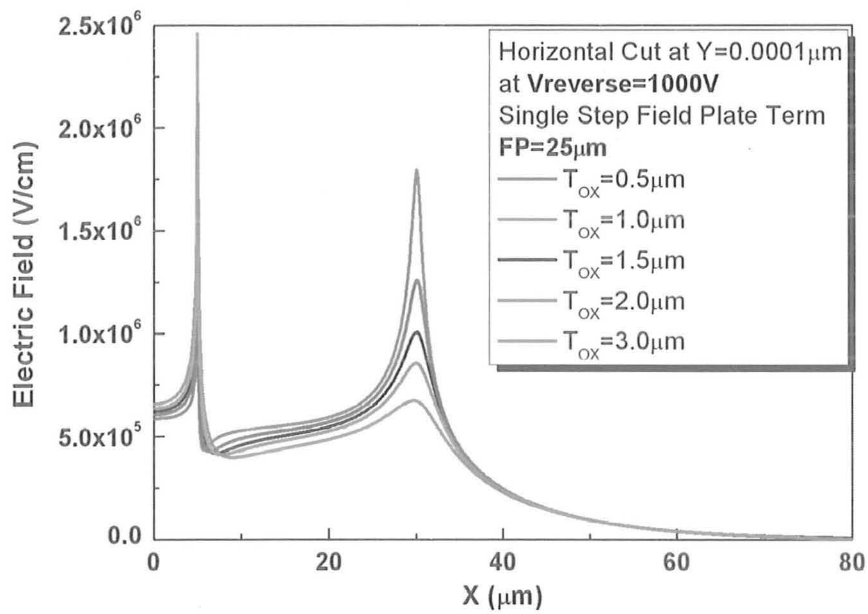

Fig. 6.13 – Electric field distribution at the surface of the diamond drift layer for different T_{OX} at V_R=1000V

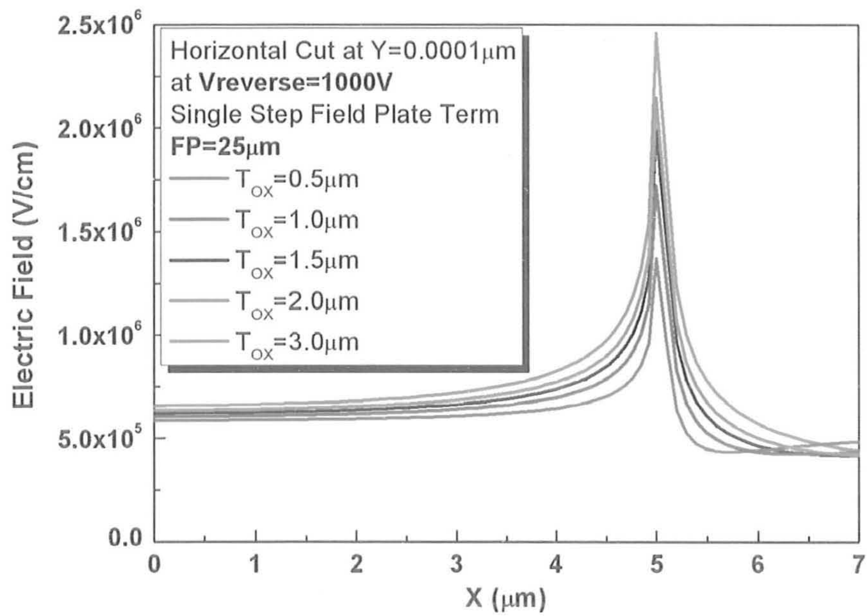

Fig. 6.14 – Electric field distribution at the surface of the diamond drift layer for different T_{OX} at V_R=1000V - ZOOM

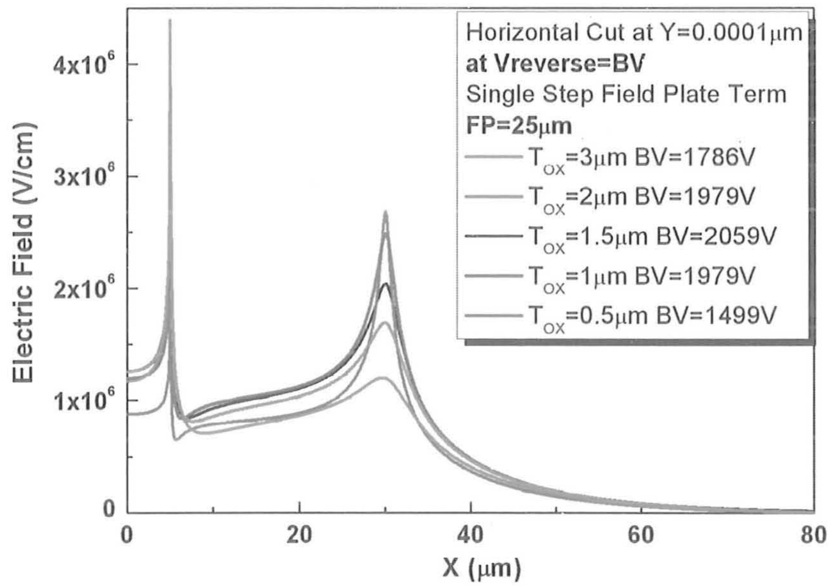

Fig. 6.15 – Electric field distribution at the surface of the diamond drift layer for different T_{OX} at breakdown

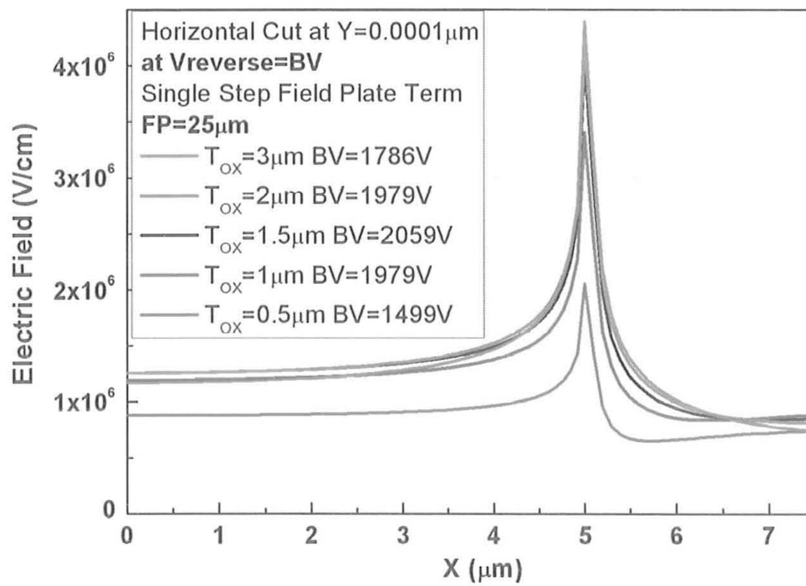

Fig. 6.16 – Electric field distribution at the surface of the diamond drift layer for different T_{OX} at breakdown - ZOOM

6.3 Three-step field plate termination

Another possible implementation of the field plate is the three-step termination [98]. More complex than the ramp oxide, this structure has six key-parameters (**Fig. 6.17**): the thickness of each oxide layer (T_{F1}, T_{F2}, T_{F3}), the lengths of ramps 1 and 2 (X_{F1}, X_{F2}) and the length of the field plate (X_{F3}). In order to optimize its performance, the influence of each parameter needs to be considered. By conveniently choosing their values, not only the breakdown voltage can be influenced, but also the position within the drift diamond layer where the avalanche breakdown is triggered. X_{F3} has the most significant effect on the electrical performance of the diode, determining a 15% variation of BV when changing from 1μm to 25μm (**Fig. 6.18**). The overall X_{F3} versus BV dependence is quite similar to the FP versus BV variation corresponding to the one step field plate termination (**Fig. 6.8**), which is a consistent result, taking into account that both parameters define the field plate length.

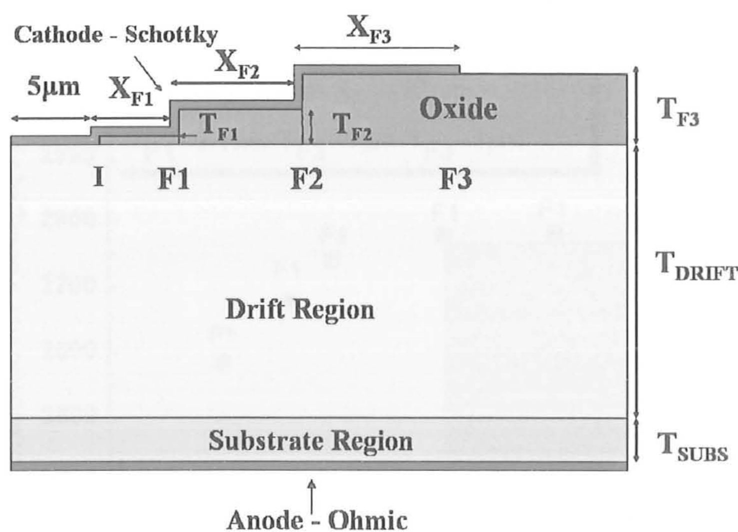

Fig. 6.17 – Cross-section of a diamond M-i-P Schottky diode with three-step field plate termination

X_{F2} has an optimum range of values between 15 and 20μm (**Fig. 6.19**). Lengths lower than 4-5μm are required for the thinner oxide layer, in order to maximize the breakdown voltage (**Fig. 6.20**). An optimal design should consider X_{F1} less than 5μm, X_{F2} in the range 15-20μm and X_{F3} larger than 15μm. While maintaining T_{F1}=0.1μm, T_{F2}=1μm and T_{F3}=3μm, the breakdown always occurs at the edge between the first and the second oxide step (F1, **Fig. 6.18-6.20**). When increasing T_{F1}, premature breakdown within the diamond drift layer is triggered at the beginning of the first oxide layer (I) and BV drops (**Fig. 6.21**). Reverse effects are obtained if increasing T_{F2} above 1μm (**Fig. 6.22**). Finally, the thickness of the third step has a behaviour similar to the one of T_{OX} from the single step field plate termination, exhibiting an optimum range of values between 3 and 4μm (**Fig. 6.23**). Another interesting phenomenon is that, as T_{F3} increases, the breakdown position moves from I to F2, in the same manner as the breakdown position moves from the edge of the oxide layer towards the end of the field plate as T_{OX} is elevated in the case of the single step *FP* (**Fig. 6.11**).

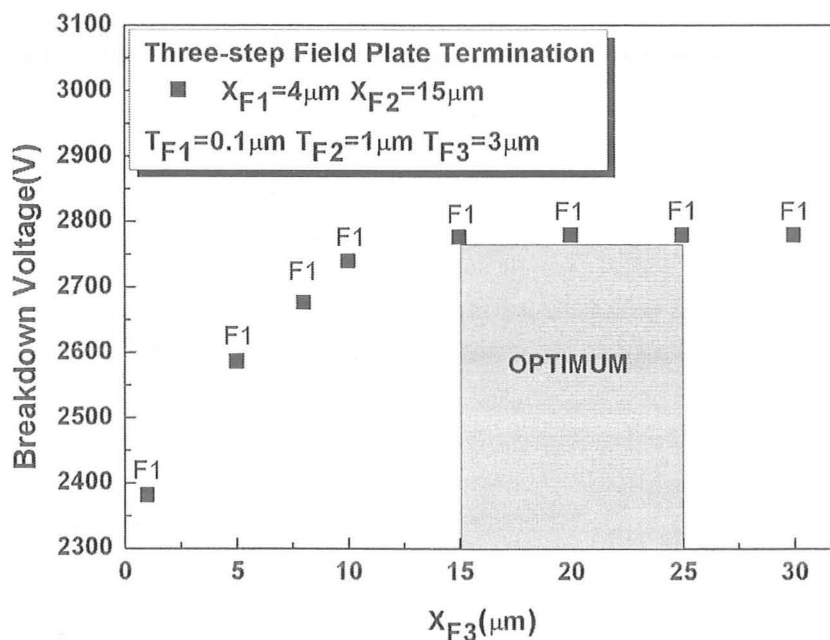

Fig. 6.18 – Three-step field plate termination: BV versus X_{F3}

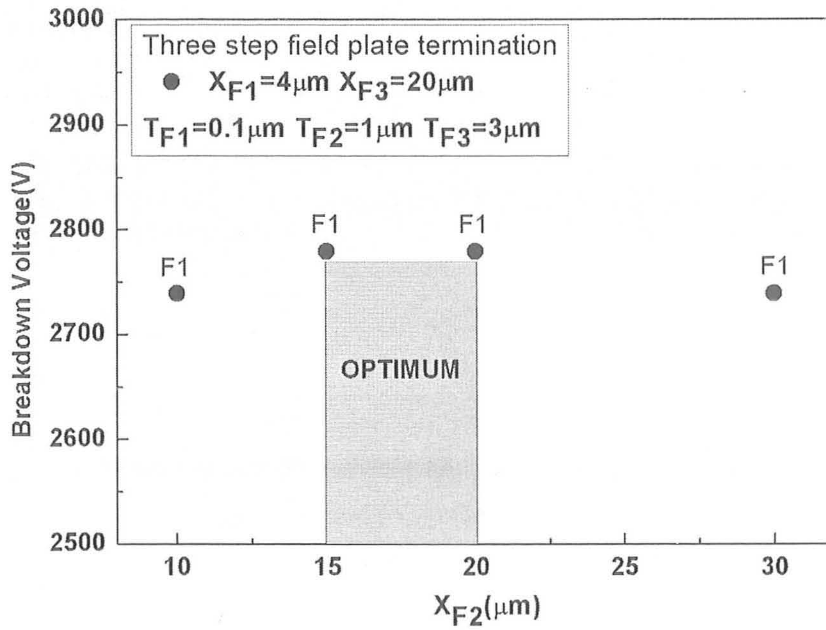

Fig. 6.19 – Three-step field plate termination: BV versus X_{F2}

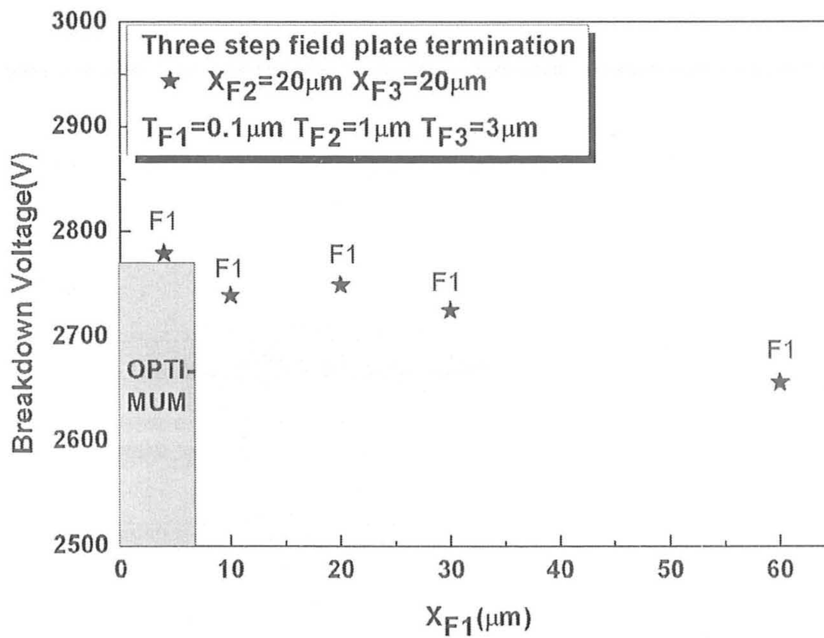

Fig. 6.20 – Three-step field plate termination: BV versus X_{F1}

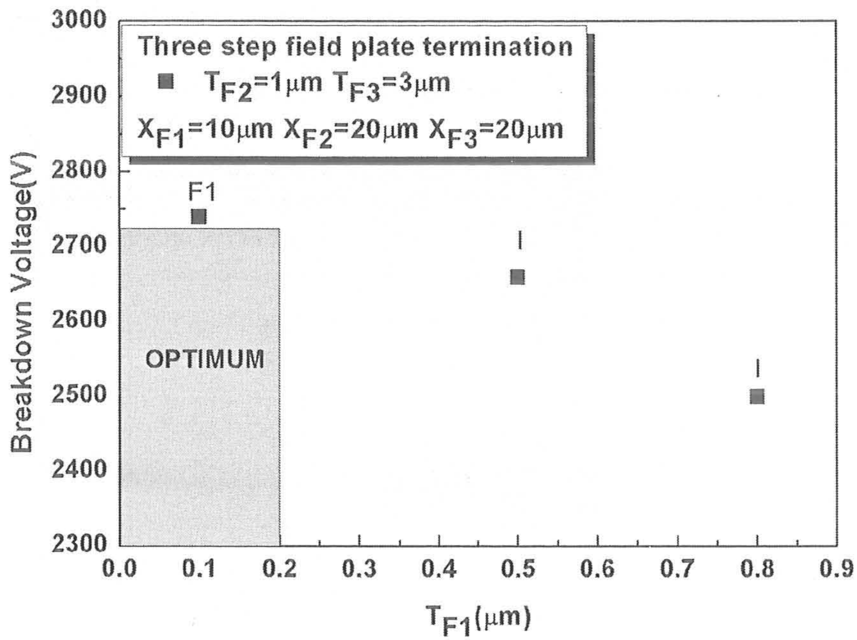

Fig. 6.21 – Three-step field plate termination: *BV* versus T_{F1}

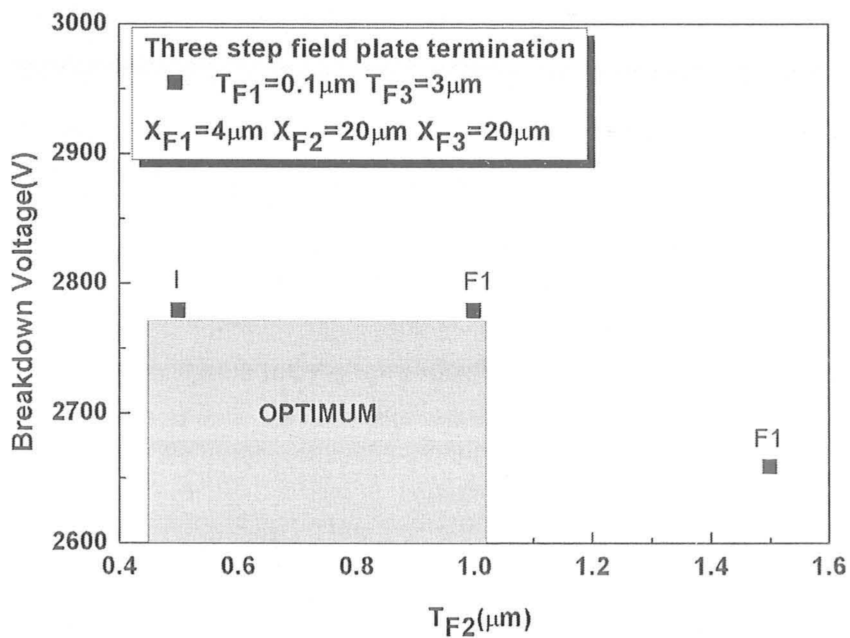

Fig. 6.22 – Three-step field plate termination: *BV* versus T_{F2}

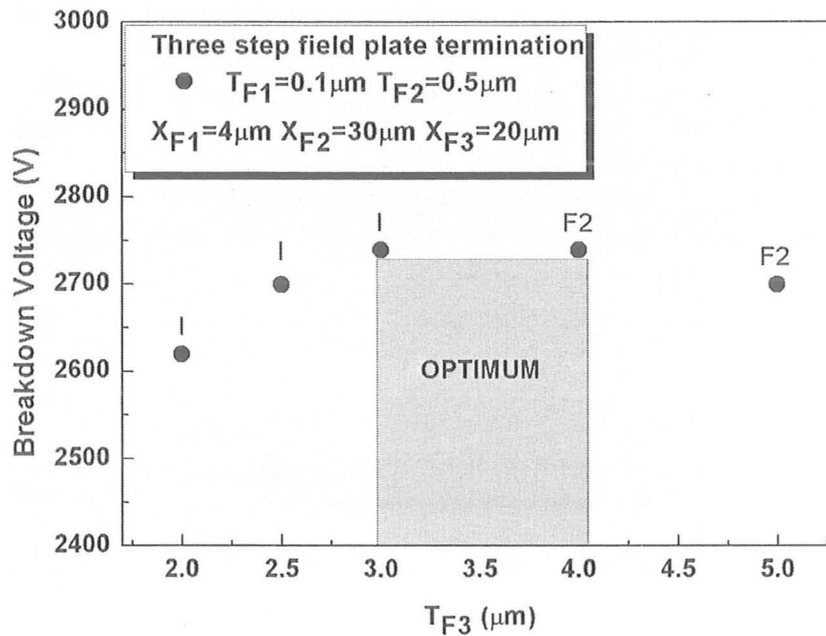

Fig. 6.23 – Three-step field plate termination: BV versus T_{F3}

The best structure, which holds 2779V (efficiency = 87.6%), has the following parameters: X_{F1} = 4μm, X_{F2} = 15μm, X_{F3} = 20μm, T_{F1} = 0.1μm, T_{F2} = 1μm and T_{F3} = 3μm. The potential lines are uniformly distributed (**Fig. 6.24**), while the electric field has a maximum at F1, and three other peaks at I, F2 and F3 (**Fig. 6.25**).

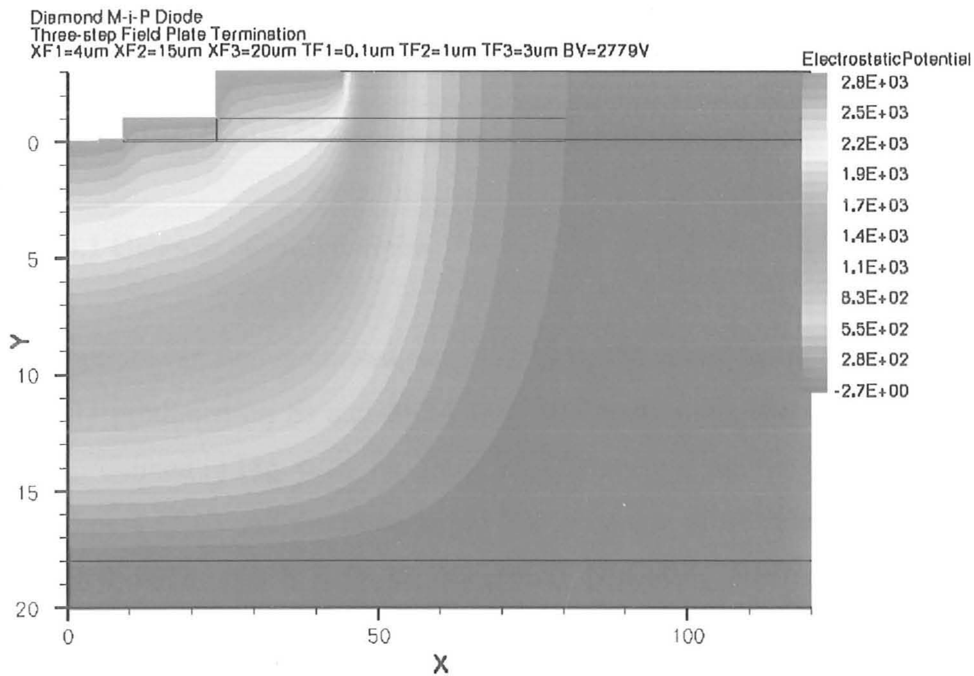

Fig. 6.24 – Potential distribution at breakdown for the best three-step field plate structure

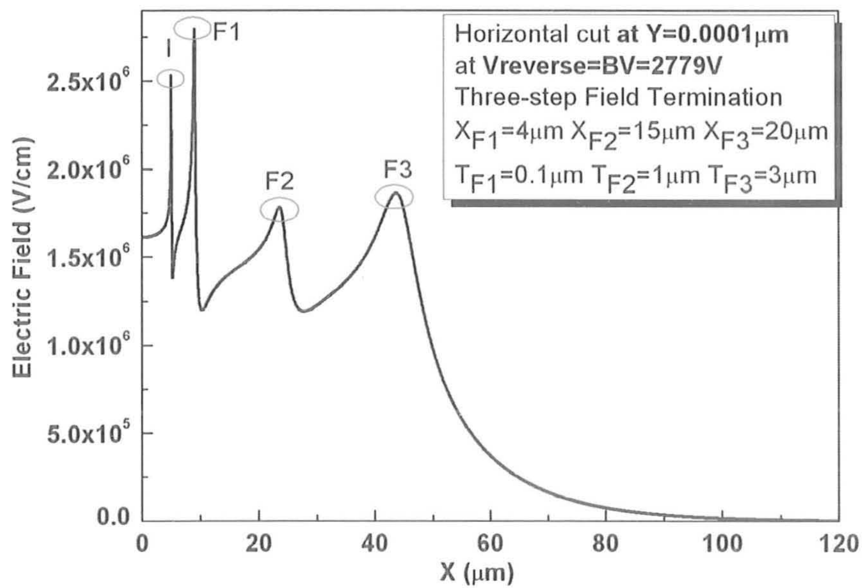

Fig. 6.25 – Field plate distribution at the surface of the diamond drift layer for the best three-step field plate structure at $V_R = BV = 2779V$

6.4 Ramp oxide termination

6.4.1 General considerations

Since it was first proposed, in 1993 [99], the ramp oxide termination has been successfully produced on Si and SiC [100, 101], exhibiting efficiencies up to 90%. Its structure, presented in **Fig. 6.26**, has three key-parameters: the field plate length (*FP*), the oxide thickness (T_{OX}) and the ramp angle (α). An angle of 45^0 can be easily obtained if the deposited oxide layer is isotropically etched. However, simulation results which will be presented in this section show that better electrical performance are obtained for lower ramp angles. This can be experimentally fabricated if several oxide layers with different impurity concentrations are deposited on the diamond drift region. The etching rate of an undoped SiO_2 layer is lower than that of a phosphorus-doped SiO_2 layer and the etching rate increases with the impurity concentration. If, for example, a sandwich of three oxide layers (**Fig. 6.27**), each of them with distinct thickness and impurity concetration, are deposited on top of the diamond drift layer, then, with the aid a P-etch solution, the insulator stack is anistropically etched and a ramp with angles lower than 45^0 is fabricated. In order to hit this target, the impurity concentration of the second layer (*concentration 2*) needs to be smaller than one of the third layer (*concentration 3*). The value of α is controlled via the thickness and impurity level in each oxide layer [89].

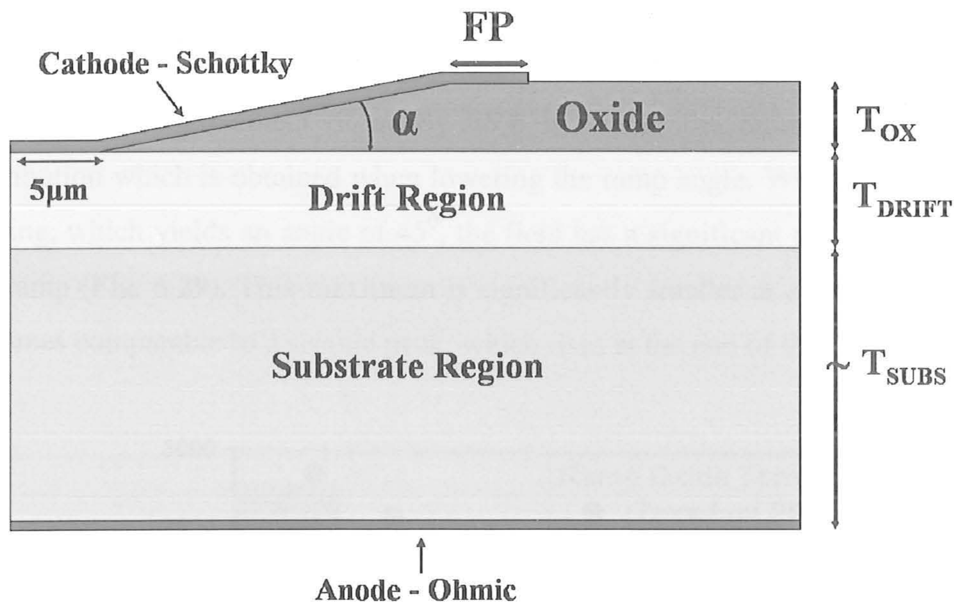

Fig. 6.26 – M-i-P Schottky diode with ramp oxide termination

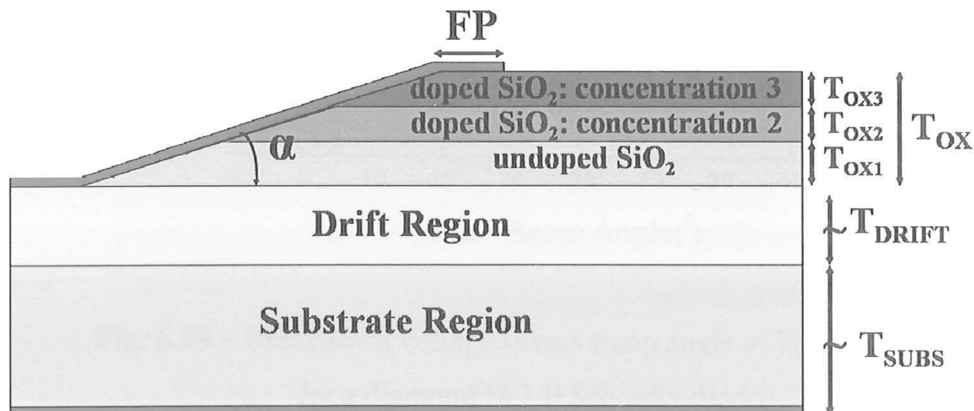

Fig. 6.27 – Ramp oxide termination with a sandwich with three SiO_2 layers

6.4.2 Structure optimisation

Optimisation of the ramp oxide structure by means of numerical simulations has led to improved performance with lower ramp angles (**Fig. 6.28**). The important role played by the anisotropic etching technique in obtaining better electrical performance is

clearly demonstrated: for $\alpha = 45^0$, BV = 1783V, while for angles lower than 7-8^0, BV = 2939V. This improvement of nearly 65% is due to the more uniform electric field distribution which is obtained when lowering the ramp angle. When employing isotropic etching, which yields an angle of 45^0, the field has a significant peak at the beginning of the ramp (**Fig. 6.29**). This maximum is significantly smaller at an angle of 5.7^0, when it becomes comparable to a second peak, which rises at the end of the field plate.

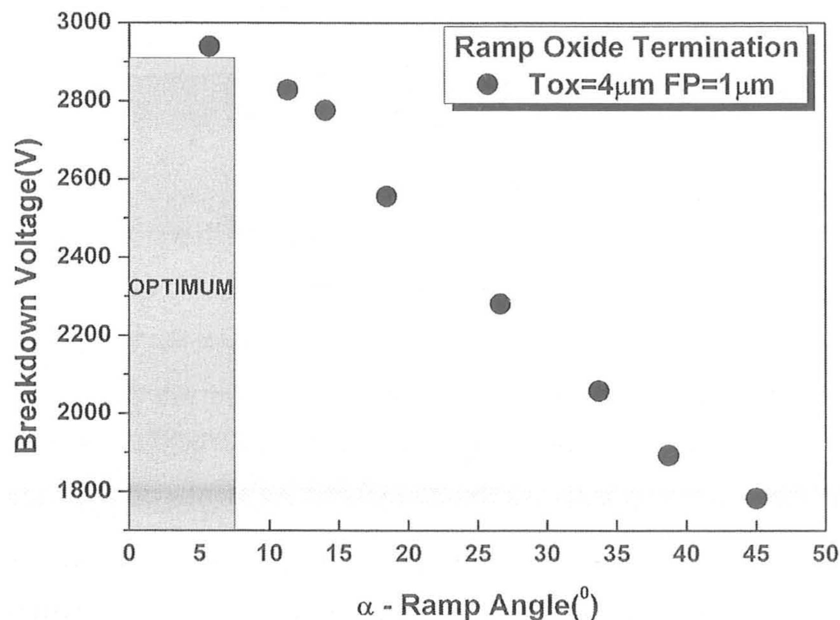

Fig. 6.28 – Breakdown voltage versus ramp angle at $T_{DRIFT} = 18\mu m$ for a diamond M-i-P Schottky diode with the geometrical dimensions and doping profiles defined in **Section 6.1**

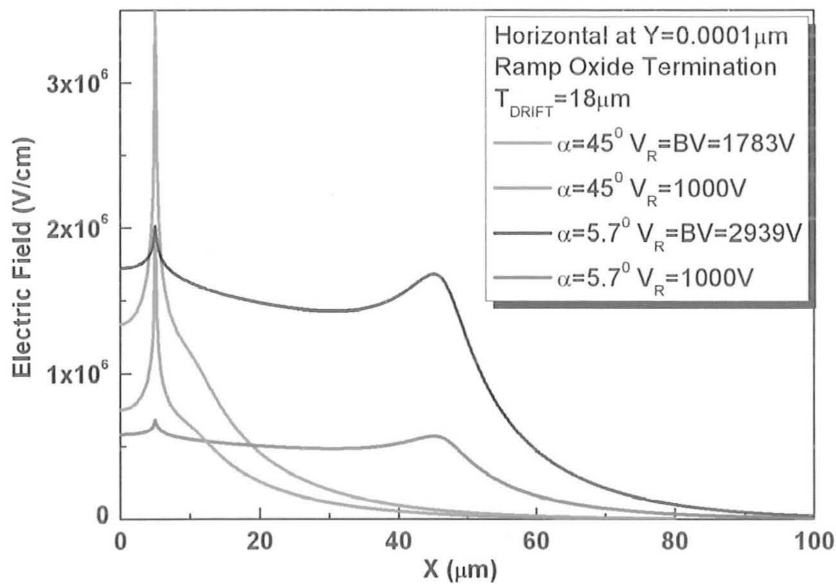

Fig. 6.29 – Field plate distribution along the surface of the diamond drift layer at for ramp oxide termination, at 45^0 and 5.7^0, with FP = 1μm

With respect to the thickness of the ramp, the breakdown voltages increases significantly for T_{OX} lower than 3μm and then saturates (**Fig. 6.30**). This is in contradiction with the tendency noticed at the single step field plate structure, where there is an ideal range of values for T_{OX}, between 1 and 2μm, out of which BV falls far from optimum (**Fig. 6.9**). The difference is due to the low angle of the ramp oxide termination ($\alpha = 5.7^0$) at which the comparison is performed, which prevents the decrease of the off-state capability as T_{OX} overcomes a certain value. The same significant role is played by the angle value when the influence of FP is quantified. Although for large angles ($\alpha = 45^0$), a longer field plate metallization induces an increase of the BV (**Fig. 6.31**), simulations predict that for $\alpha = 5.7^0$ the breakdown voltage is constant with FP larger than 1μm for $T_{OX} > 2$μm. Therefore, the largest breakdown voltage of a diamond M-i-P diode with ramp oxide termination is exhibited by a structure with FP = 1μm, $T_{OX} = 4$μm and $\alpha = 5.7^0$. For $T_{DRIFT} = 18$μm, this maximum BV is 2939V, which corresponds to an efficiency of 92.7%, superior to the ones exhibited by the single and three-step field plate structures. The potential distribution of the optimum design is included in **Fig. 6.32**.

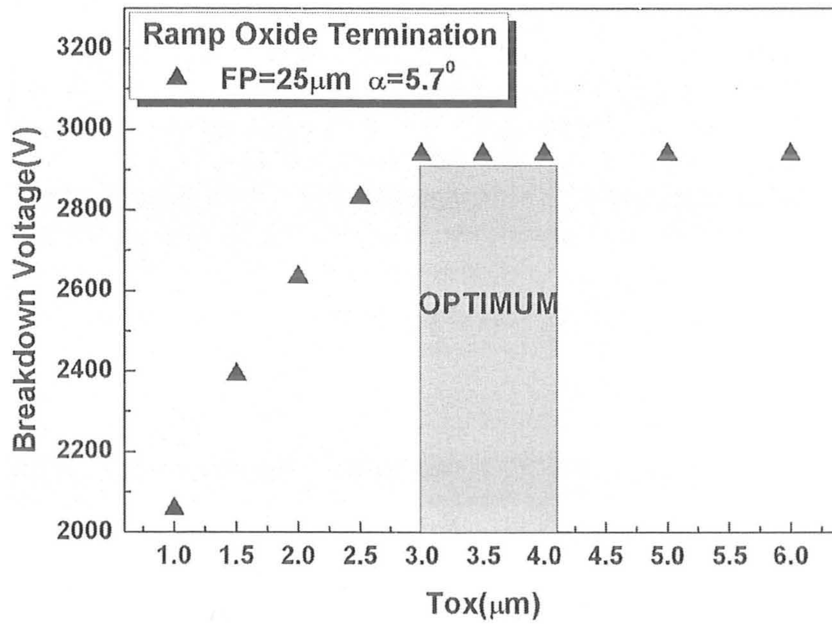

Fig. 6.30 – BV versus oxide thickness at T_{DRIFT} = 18μm

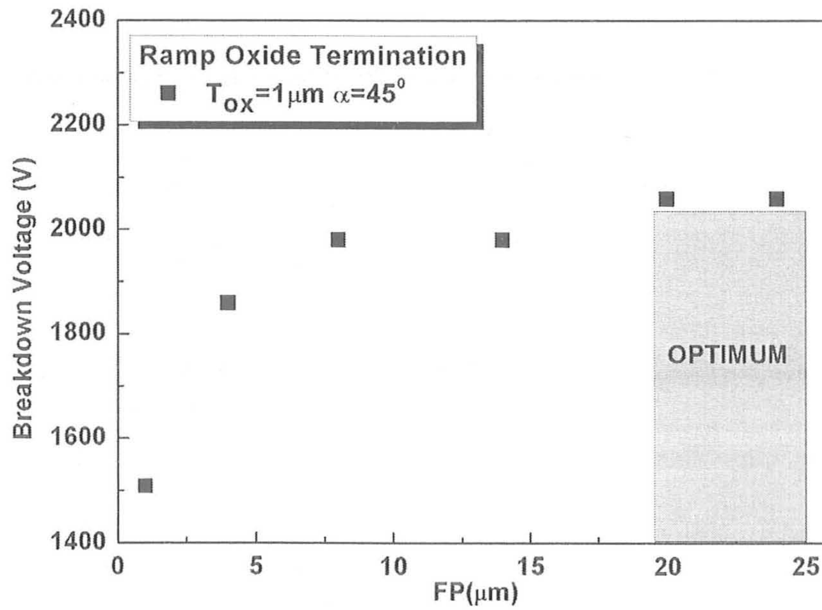

Fig. 6.31 – BV versus field plate length at T_{DRIFT} = 18μm

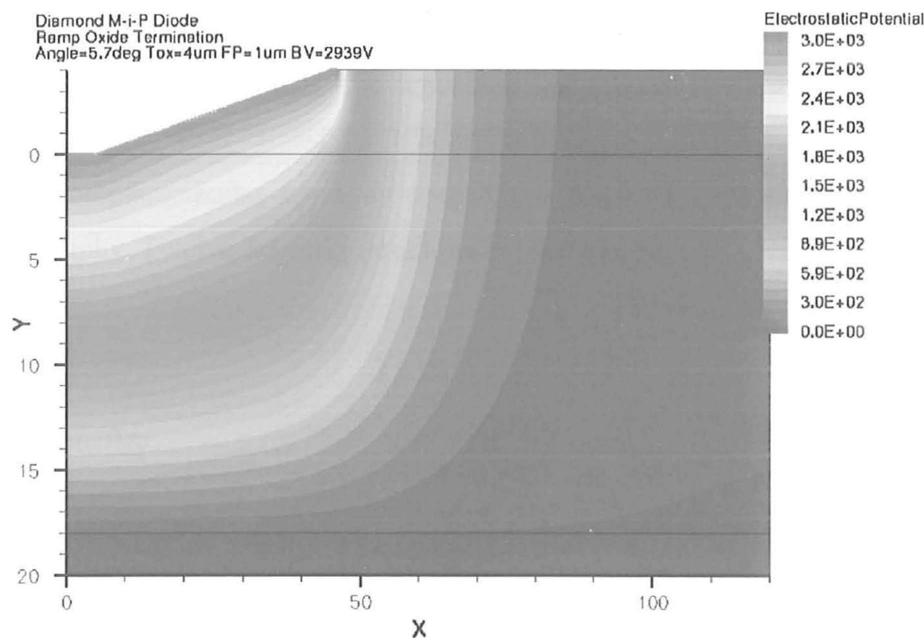

Fig. 6.32 – Potential distribution at breakdown for the best ramp oxide structure

6.4.3 Experimental results

Two years ago, within the CAPE (Carbon Power Electronics Programme) project, the ramp oxide termination was for the first time produced on a diamond sample. The sample consisted of a drift, quasi-intrinsic, layer with 13μm nominal thickness and a 268μm thick substrate, having $2*10^{20}cm^{-3}$ boron doping level. SIMS (Secondary Ion Mass Spectroscopy) measurements showed that the impurities concentration levels (Ni, H, B and Si) in the drift layer were lower than the detection limit ($10^{13}cm^{-3}$). The total area of the sample was $10mm^2$.

As mentioned in **Section 6.4.1**, in order to obtain a small ramp angle, which would allow increased electrical performance, anisotrotropical etching has to be employed. Therefore, three SiO_2 layers, with different impurity levels and geometries, were deposited on top of the diamond drift region. After the deposition of an undoped, 0.8μm thick, SiO_2 layer, two doped oxide layers were added, each of them 0.7μm thick, the first having $10^{12}cm^{-3}$ phosphorus concentration and the second $5*10^{13}cm^{-3}$ (**Fig. 6.33**). All the depositions were performed via the LPCVD (Low Pressure Chemical Vapour

Deposition) technique, at 600^0C. The second and third oxide layers were doped with phosphorus via ion implantation. The deposition was followed by a thermal implantation treatment at 600^0C which lasted for 1 hour. In order to produce several M-i-P diodes across the sample, circular windows with 40μm diameter were defined in SiO_2 via photolithography. Twelve Schottky structures were obtained.

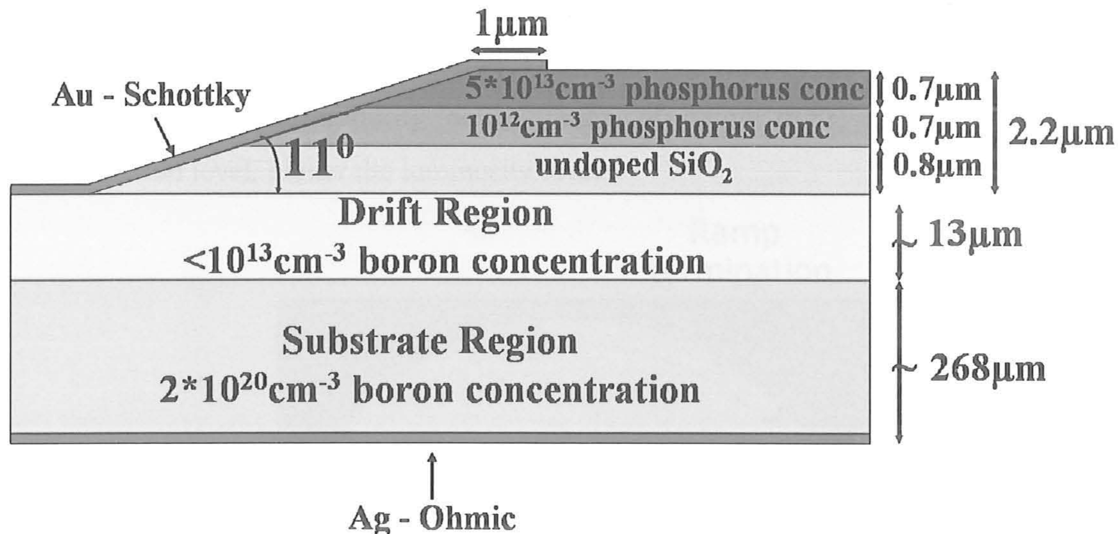

Fig. 6.33 – Cross section of first ever fabricated diamond M-i-P diode with ramp oxide termintion

Next, the anisotropic etching via a P-etch solution was performed. The P-etch consisted of 300 parts deionized water, 10 parts acid (HNO_3) acid with 70% concentration and 15 parts hydrofluoric acid: ammonium fluoride buffer ($HF{:}NH_4F$, ratio 1:6). The etching average speed was 75nm/minute. The etching rate increases with the impurity concentration level. A ramp angle of 11^0 was obtained. However, due to the rough surface of the diamond drift layer, the low quality of the diamond-oxide interface prohibited the fabrication of the ramp termination for all the 12 diodes defined via photolithography. Therefore, only two terminated diodes were obtained.

The ramp building stage was followed by the contact deposition step. First, the Schottky contact was produced, via E-gun metal gold deposition, followed by contact

definition using the lift-off technique, wafer cleaning with hot deionized water and annealing in a nitrogen atmosphere, at 600^0C. A similar process was followed for the ohmic contact, which covered the substrate diamond layer, only that no lift-off was employed and the annealing was performed at 450^0C. Silver was used to define the ohmic contact.

In **Fig. 6.34**, a top-view picture of one of the fabricated diodes is inserted. The round white circle represents the 40μm diameter Schottky contact, while the round yellow contour is the ramp termination. The contour has three different luminosity levels, corresponding to the impurity concentration of oxide layer: higher the impurity concentration level, higher the luminosity level.

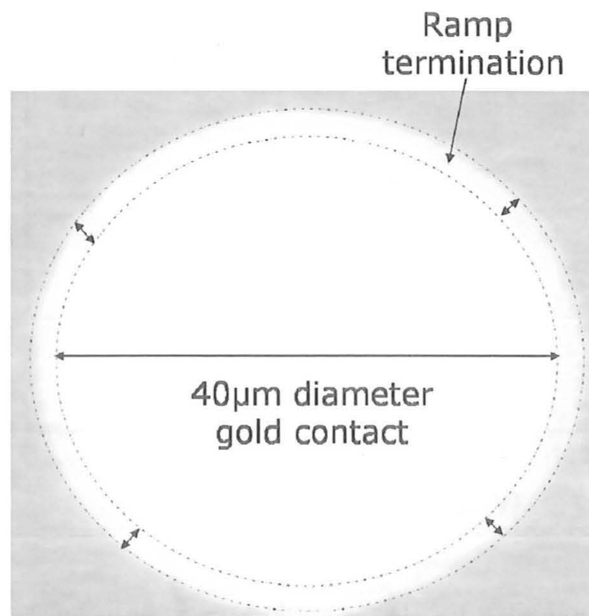

Fig. 6.34 – Top-view of a fabricated diamond M-i-P structure with ramp oxide termination

In terms of electrical performance, the diode presented in **Fig. 6.34** has a measured breakdown voltage of around 1100V, while the other diode fabricated holds approximately 1000V. The off-state characteristic of the first is inserted in **Fig. 6.35** and shows a breakdown voltage around 1100V. When trying to match this value with the simulations, a comparable BV was obtained for T_{DRIFT} = 7μm, as highlighted in **Fig. 6.36**.

This discrepancy may be due to the high tolerance with which T_{DRIFT} was measured, or to defects which might have appeared during the diamond growth or to the fact that the simulator implementation of diamond needs further refinement parameters. Reliable ionization coefficients for diamond still need to be determined. The ionization coefficients used in this work were obtained via extrapolation from silicon and silicon carbide based on band gap. Therefore, they are prone to errors.

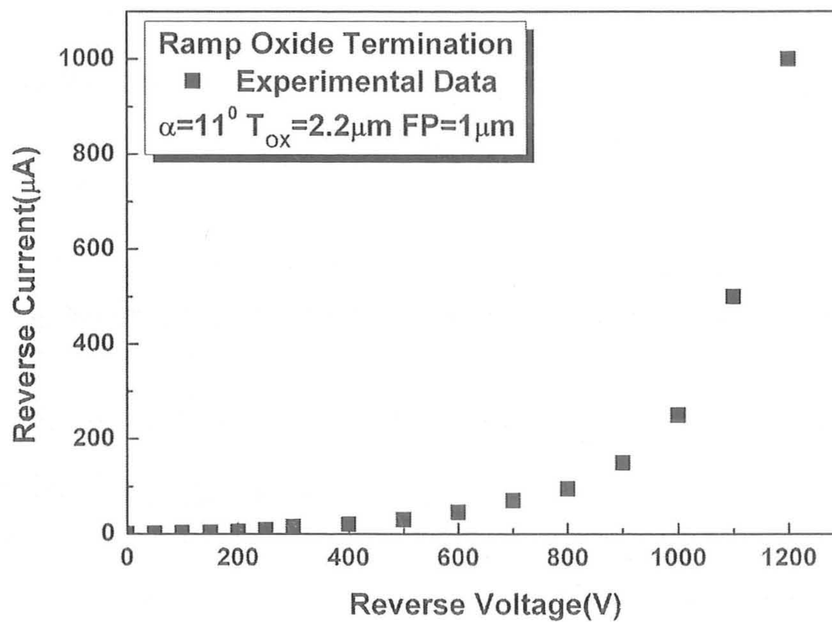

Fig. 6.35 –Measured reverse characteristic of a diamond M-i-P diode with ramp oxide termination (nominal drift thickness=13μm)

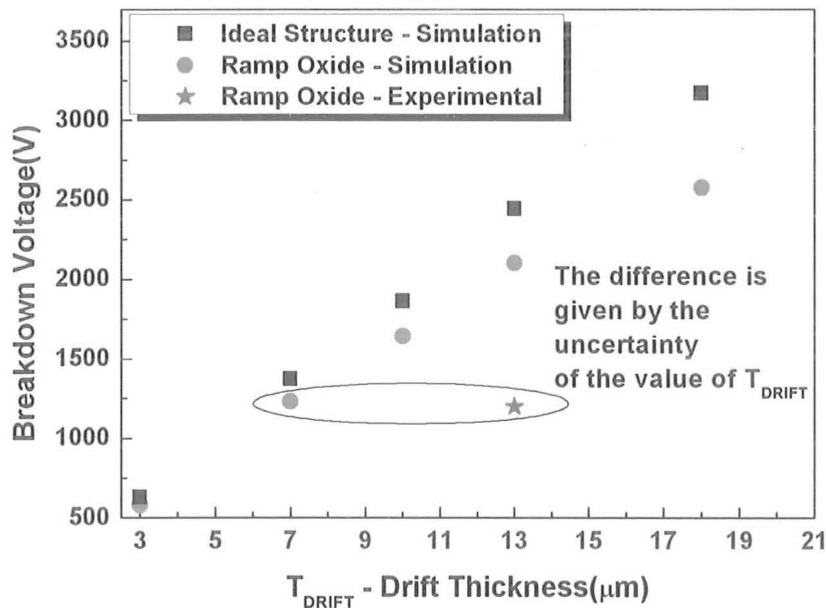

Fig. 6.36 – BV versus T_{DRIFT} for the plane-parallel diamond M-i-P diode (simulation) and for the M-i-P with ramp oxide termination (simulation and experimental)

The technological process which led to the ramp oxide termination presented above is also called wet etching process. This process, which was previously used on silicon and silicon carbide power devices, can be employed for diamond samples having a an i-layer with smooth surface. For wafers with high density of non-uniformities at the surface, the classical wet etching process can not be used to create the oxide ramp. High rate etching centers are formed around these non-uniformities, which can lead to undesirable etching underneath the oxide layer.

Therefore, an alternative technological route, specific for diamond devices, based on Reactive Ion Etching (RIE), has to be followed. As in the case of the previous process, the first step after the wafer cleaning was the LPCVD deposition of an undoped SiO_2 layer at 600^0C. In this case, the thickness of the oxide was much higher, 2.8μm, compared to 0.8μm in the other case. Then the oxide endured a thermal treatment at 600^0C for one hour in N_2 ambient in order to insure a good adhesion to the diamond surface. Circular windows with 40μm diameter were defined over the SiO_2 layer using photolithography and positive photoresist (AZ1350).

Five RIE steps were then employed in order to produce the ramp. The etching was done in CF_4 and CF_4+O_2 atmosphere, varying the RIE chamber pressure between 10Pa and 20Pa and the RF power between 200W and 250W. The entire RIE process lasted 21 minutes. After that, the positive photoresist was plasma stripped in O_2 atmosphere, with a chamber pressure of 30Pa and an RF power of 300W. A ramp structure with an angle of 15^0 was obtained this way.

The wafer was cleaned with hot deionised water and a 1μm thick Al layer was deposited using E-gun evaporation. The Schottky contact was defined by lift-off technique and, after another cleaning in hot deionised water, annealing was performed in N_2+H_2 atmosphere, at 450^0C, for 30 minutes. The backside ohmic contact metal (silver-Ag) was then deposited, followed by a second annealing in N_2 atmosphere, at 450^0C. An image of the front-side of the wafer at the end of the process is presented in **Fig. 6.37**. The small black circles represent the Schottky contact of each diode. The ramp oxide is clearly shown in **Fig. 6.38**, where an SEM image of the ramp and of the Schottky contact corresponding to a diamond M-i-P Schottky structure is inserted.

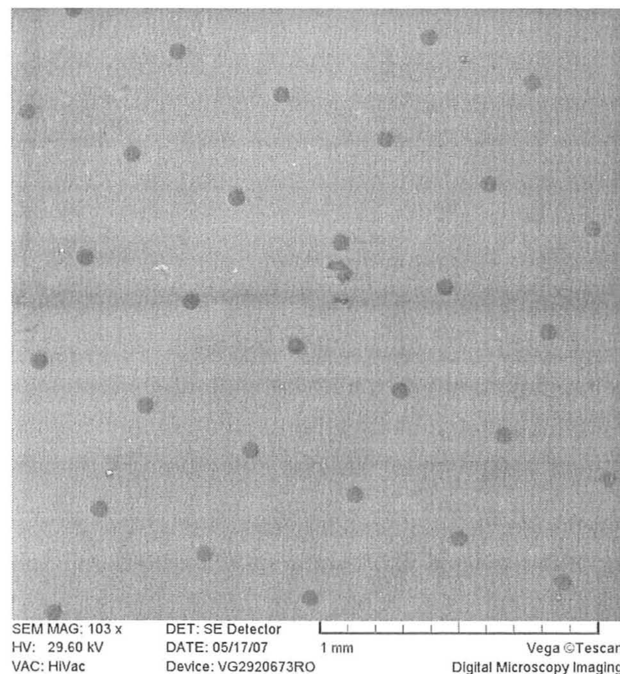

Fig. 6.37 – Diamond wafer with several M-i-P Schottky structures with ramp oxide termination

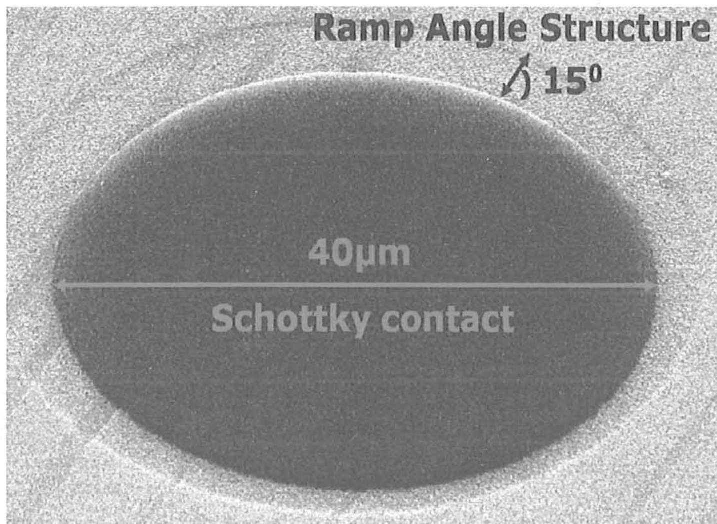

Fig. 6.38 – SEM image of a diamond M-i-P diode with oxide ramp termination with an angle of 15^0, on a diamond M-i-P Schottky structure obtained via RIE process

In **Fig. 6.39**, experimental off-state characteristics for three diodes with ramp oxide terminations obtained via the RIE process are presented. For all samples, the reverse leakage current has a weak dependence on voltage up to 1000V. The measured breakdown voltages were approximately 1100V, 1300V and 1400V, respectively, for a drift thickness of approximately 18µm. The RIE process yielded more reliable results, seven diodes from the same wafer exhibiting breakdown voltages in excess of 1kV. The off-state capability of the other diodes was extremely low. The significant difference in breakdown voltage between diodes of the same wafer is due to the variable material defects concentrations throughout the diamond drift layer and to the non-optimized deposition process of the Schottky contact.

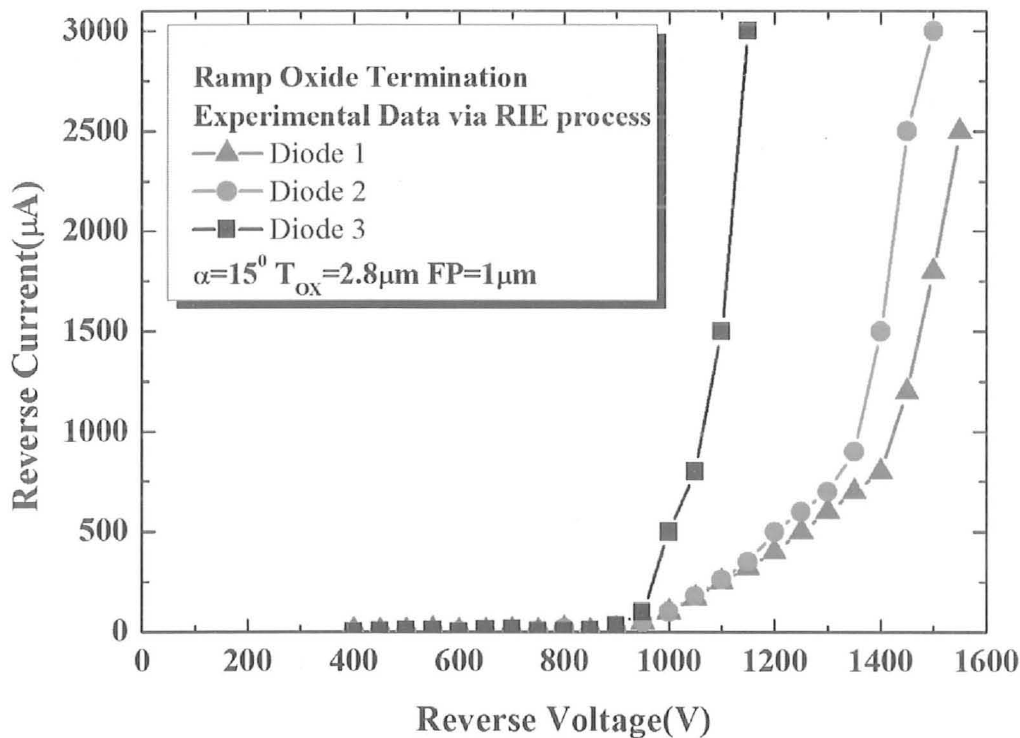

Fig. 6.39 – Measured reverse characteristics of three diamond M-i-P diodes with ramp oxide termination built via RIE process

6.5 Comparison between different termination structures

6.5.1 Electrical performance

In the previous sections of this chapter, the optimum design of each termination structures was included. For the single step field plate structure, the highest efficiency predicted by the numerical simulations is 64.9% (for FP = 25μm and T_{OX} = 1.5μm). For the three-step field plate termination, the optimum design (X_{F1} = 4μm, X_{F2}= 15μm, X_{F3} = 20μm, T_{F1} = 0.1μm, T_{F2} = 1μm and T_{F3} = 3μm) yields an efficiency of 87.6%. Finally, for FP = 1μm, T_{OX} = 4μm and α = 5.7^0, the diamond M-i-P diode with ramp oxide termination holds 2939V, which corresponds to an efficiency of 92.7%. The results are

included in **Table 6.1**. It is clear that the ramp oxide termination exhibits the best electrical behaviour. While the three-step field plate structure has also a remarkable efficiency, the single step, although the easiest to produce from the technological point of view, is far from being an acceptable solution for terminating the diamond structure. However, in order to perform a thorough comparison between the three structures, other aspects need to be taken into consideration, as detailed in the following sections of this chapter.

Termination	**BV**	**Efficiency**
Single Step Field Plate	2059 V	64.9%
Three-step Field Plate	2779 V	87.6%
Ramp Oxide	**2939 V**	**92.7%**

Table 6.1 – Best performance of different termination structures at $T_{DRIFT} = 18\mu m$

6.5.2 Area consumption comparison

When performing the optimisation of a termination structure, apart from maximizing the breakdown capability, the area consumption issue also needs to be addressed. This comes to finding the optimum potential distribution within a limited space. A termination with outstanding electronic parameters which occupies a large area may not be the optimum solution. To quantify the area required by the best structure of each of the three terminations, horizontal cuts through the 2-D potential distributions at the surface of the diamond drift layer for V_R = 1800V (T_{DRIFT} = 18μm) were examined and are shown in **Fig. 6.40**. Although it has the worst electrical performance, the single field plate termination requires an area with 20% smaller than the three-step and ramp oxide structures, which have quite similar behaviour. However, the latter two structures exhibit termination efficiencies with 25% and 30%, respectively, higher than the first one.

The trade-off which needs to be done between high electrical performance and small occupied area is more clearly presented in **Fig. 6.41**, where the best breakdown

voltage of each structure is plotted against the length required so that all the potential lines are closed via the oxide layer at breakdown. As in the case of all the structures analysed in this chapter, the length of the plane-parallel structure is considered 5μm, the rest being occupied by the termination structure. The ramp oxide termination requires approximately 111μm structure length for a drift thickness of 18μm, while the single step field plate only needs 81μm. The difference between the ramp oxide and the three-step field is of nearly 10μm in favour of the first one. This drawback is compensated by the better electrical performance (efficiency is with 5% higher for the ramp oxide).

In terms of efficiency of occupying the area, the three terminations are comparable. The last column of **Table 6.2** presents the ratio between the breakdown voltage and the required length and its values show that the three-step field plate has the best efficiency (27.2V/μm), while the single step has the worse (25.4V/μm). However, the values are extremely close to each other.

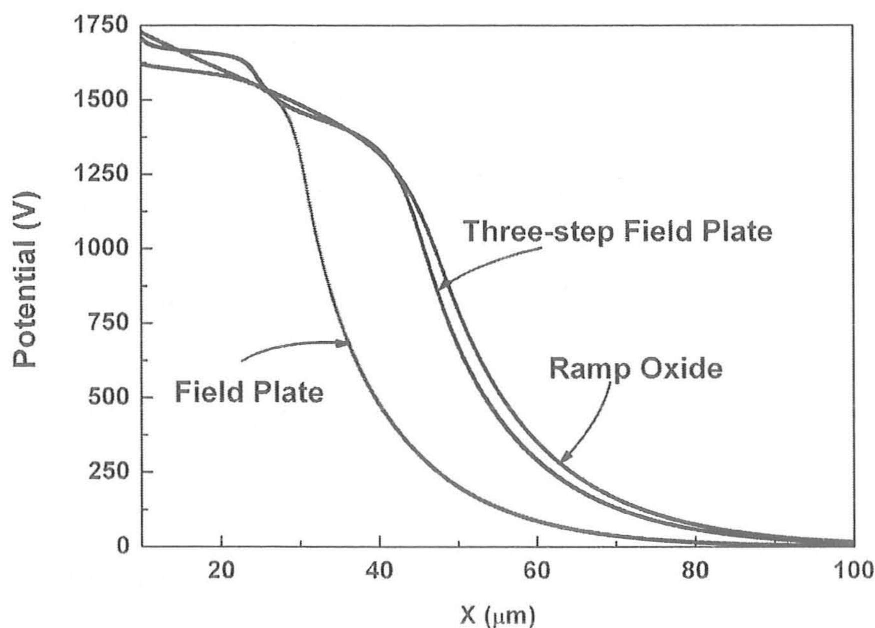

Fig. 6.40 - Horizontal cuts through the potential distributions of the best structure of each termination, at the surface of the drift diamond layer ($V_R = 1800V$, $T_{DRIFT} = 18\mu m$)

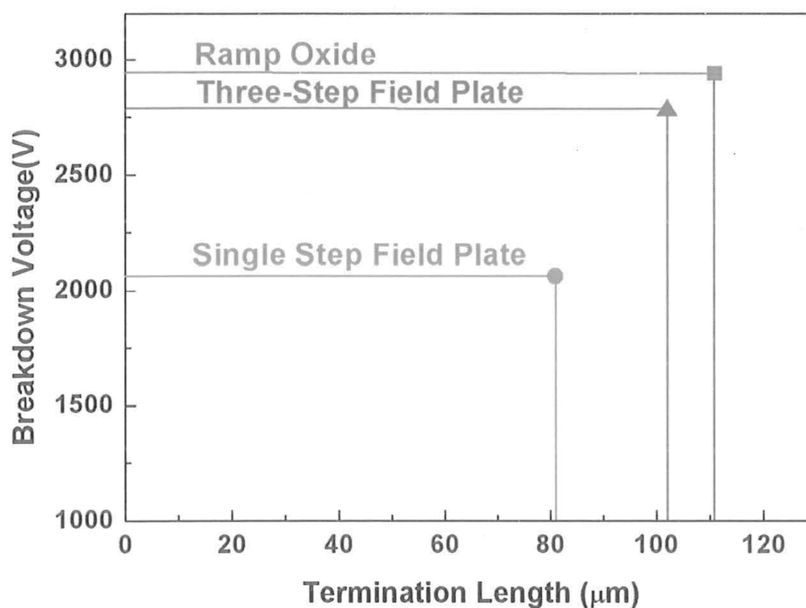

Fig. 6.41 – Breakdown voltage versus required termination length, at breakdown, for the optimum designs of the three structures at $T_{DRIFT} = 18\mu m$

Termination	BV	Length required by the termination	**BV/Length required by the termination**
Single Step Field Plate	2059V	81μm	**25.4V/μm**
Three-step Field Plate	2779V	102μm	**27.2V/μm**
Ramp Oxide	2939V	111μm	**26.5V/μm**

Table 6.2 – Comparison between the electrical and geometrical performance of the optimum of the three terminations at $T_{DRIFT} = 18\mu m$

6.5.3 Scaling with drift thickness

Another crucial issue when analysing the performance of each termination structure is whether the electrical performance are influenced by the drift layer thickness. As expected, the breakdown voltage increases with the drift thickness (**Fig. 6.42**). For the ideal, plane-parallel, structure, the increase is linear, for the real, terminated diodes, the

trend, although non-linear, is still clearly ascendant. However, when varying T_{DRIFT} from 5μm to 30μm, while maintaining other parameters constant, a 10%-20% decrease of the termination efficiency of each structure can be noticed (**Fig. 6.43**). This result is due to the fact that, by increasing T_{DRIFT}, the surface electric field stress at the edge of each termination is larger. Therefore, diamond critical field value and, by consequence, the avalanche breakdown, are reached for smaller reverse voltages. However, even for T_{DRIFT} = 30μm, the ramp oxide and the three-step field plate structures have termination efficiencies larger than 75%, which is an acceptable value.

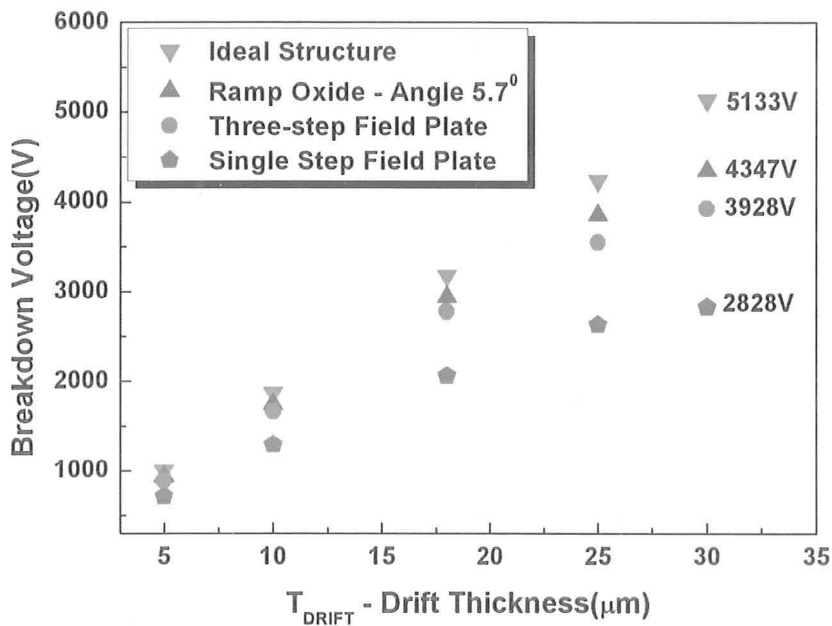

Fig. 6.42 – Breakdown voltage versus drift thickness for three terminated M-i-P diodes, and for the ideal, plane-parallel, structure

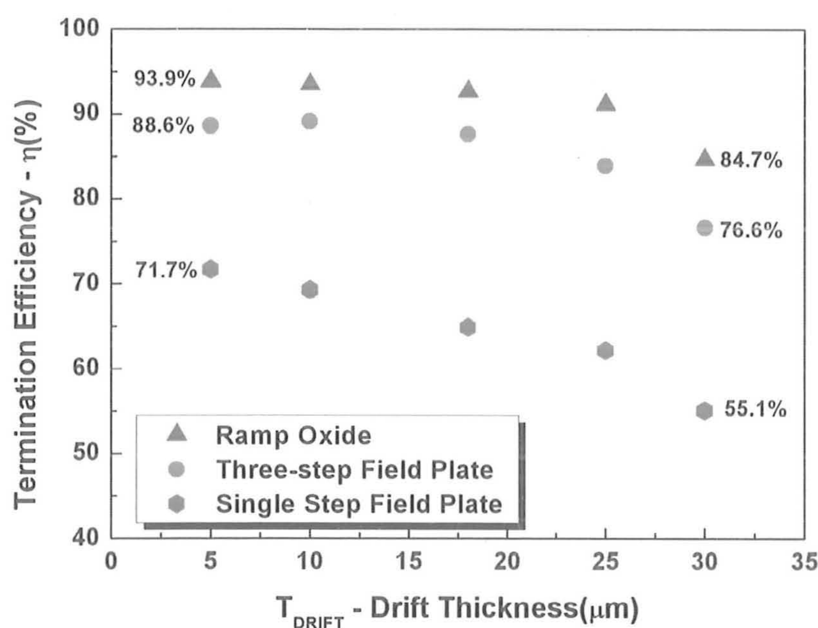

Fig. 6.43 – Termination efficiency versus drift thickness for three termination structures

6.6 Use of high-k dielectrics for oxide ramp termination

The numerical results presented in this chapter so far trigger the hope that diamond M-i-P Schottky diodes terminated with three-step field plate or ramp oxide structures could have excellent electrical performance. However, the electrical behaviour of these devices can be seriously affected by the appearance of premature oxide breakdown. This risk is considerable given the high critical field (10MV/cm) in diamond. According to Gauss' law, the product between the relative dielectric constant (ε_r) and the normal electric field of two materials has to be constant at their interface. For silicon dioxide (SiO_2), which is the only oxide used both in simulations and experiments in this study so far, the relative dielectric constant is 3.9, while the typical operational field (E_O) is 2 MV/cm [102]. This gives a product $\varepsilon_r E_O$ of 7.8MV/cm, significantly lower than 57MV/cm, the corresponding limit for diamond ($\varepsilon_r = 5.7$, $E_O = 10$MV/cm).

If we consider the optimum structures of the terminations analyzed in the previous sections, the maximum electric field within the oxide layer at breakdown is 6.8MV/cm

for the single step field plate, 6.5MV/cm for the three-step field plate, and 6.6MV/cm for the ramp oxide termination. These values are significantly larger than the operational field of SiO_2 (2MV/cm), therefore the risk for premature dielectric breakdown is extremely high.

One solution to overcome this problem is to modify the parameters of the terminations in order to lower the oxide field at breakdown. For example, for the ramp oxide, by only increasing the ramp angle from 5.7^0 to 11.3^0 the maximum oxide field decreases from 6.6MV/cm to 5.2MV/cm. The price to pay for this result is a loss in the off-state capability, which drops from 2939V to 2828V (3.5% in terms of termination efficiency). However, more severe modifications of the termination optimum design need to be performed in order to get the oxide field close to 2MV/cm, modifications which are expected to induce a more significant deterioration of the breakdown voltage.

Another approach to overcome the risk of premature dielectric breakdown is the replacement of SiO_2 with high-k dielectrics. Due to the extremely high operational field of diamond (10MV/cm), materials with dielectric constants larger than that of diamond (5.7) have to be taken into consideration, so that their $\varepsilon_r E_O$ product should exceed the limit for diamond.

We have analyzed the impact of using two high-k dielectrics, silicon nitride (Si_3N_4) and hafnium dioxide (HfO_2), as insulators for the ramp termination on diamond M-i-P structures. Silicon nitride ($\varepsilon_r = 7.5$, $E_O = 2$MV/cm, [103]) has been, in the last few years, subject of extensive research regarding its possible use in termination structures for power devices on SiC, while hafnium dioxide ($\varepsilon_r = 24$, $E_O = 2.6$MV/cm, [103]) is considered one of the main candidates for replacing SiO_2 as the gate insulator in CMOS technology. The study was performed for a Schottky diamond M-i-P diode with 18μm drift thickness, $2*10^{19}$cm^{-3} boron substrate doping and a ramp with $\alpha = 5.7^0$ and FP = 25μm. In order to avoid confusions, starting from here we shall call the thickness of the ramp oxide T_{DIE}, instead of T_{OX}, the notation used so far. This is because we now consider that the ramp can be manufactured from all sorts of dielectrics, not necessarily an oxide.

As expected, the electric field in the dielectric at breakdown decreases when using high-k dielectrics (**Fig. 6.44**). Values of the maximum dielectric field comparable to the

operational field are obtained for HfO_2 ramps with insulator thicknesses (T_{DIE}) in excess of 3.5μm. For these structures, the risk of premature dielectric breakdown is minimum. The price to pay for this improvement in reliability is a small degradation of the electrical performances of the termination. The efficiency drops by 5-7% to 85-87% when using HfO_2 instead of SiO_2 (**Fig. 6.45**), but remains high enough to yield a competitive termination structure.

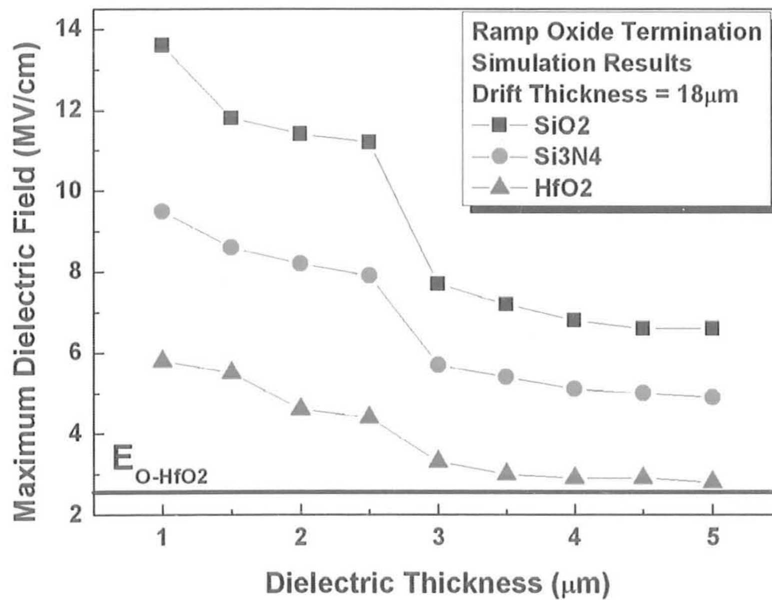

Fig. 6.44 – The electric field in the dielectric at breakdown for different dielectrics types and thicknesses

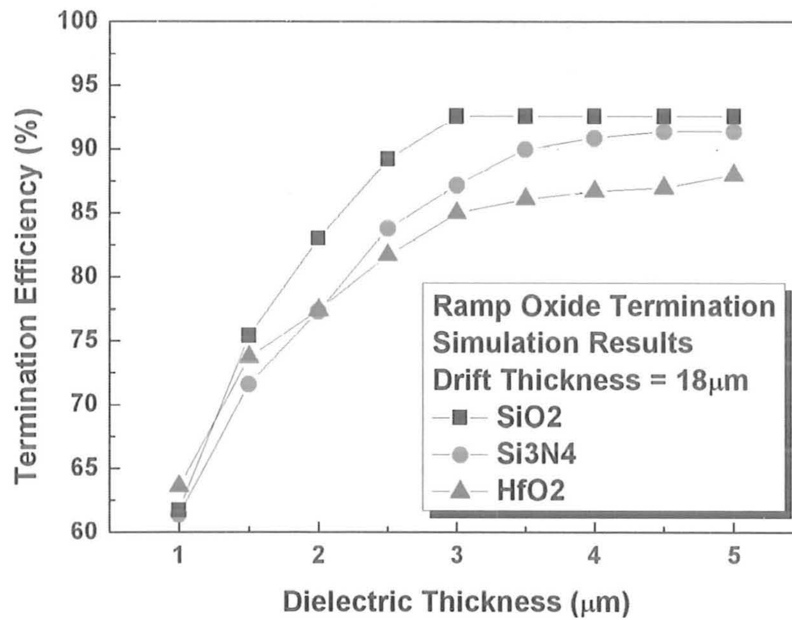

Fig. 6.45 – Termination efficiency versus dielectric thickness for a diamond M-i-P with ramp oxide termination

When using high-k dielectrics in Si and SiC devices, the deposition of a thin SiO_2 transition layer between the semiconductor and the high-k dielectric is common [104]. This technique takes full advantage of the vast knowledge of the interface issues between silicon dioxide and different semiconductors, while avoiding the problems which might occur at a direct high-k dielectric – semiconductor interface. Simulation results show that by introducing a 0.2μm thick SiO_2 layer the termination efficiency of the structure and the maximum electric field in the stack of dielectrics are not significantly influenced (**Figs. 6.46-6.47**), for both high-k dielectrics considered.

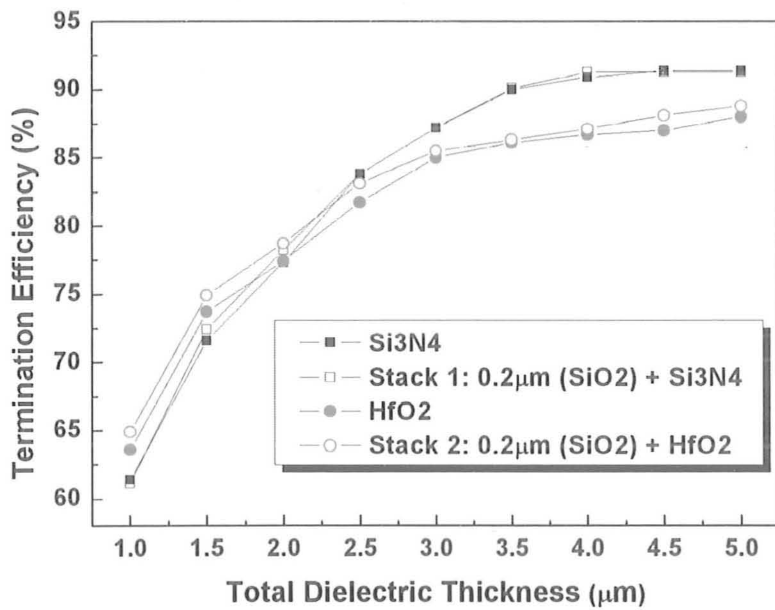

Fig. 6.46 – The effect of using SiO_2–high-k dielectric stacks on the termination efficiency

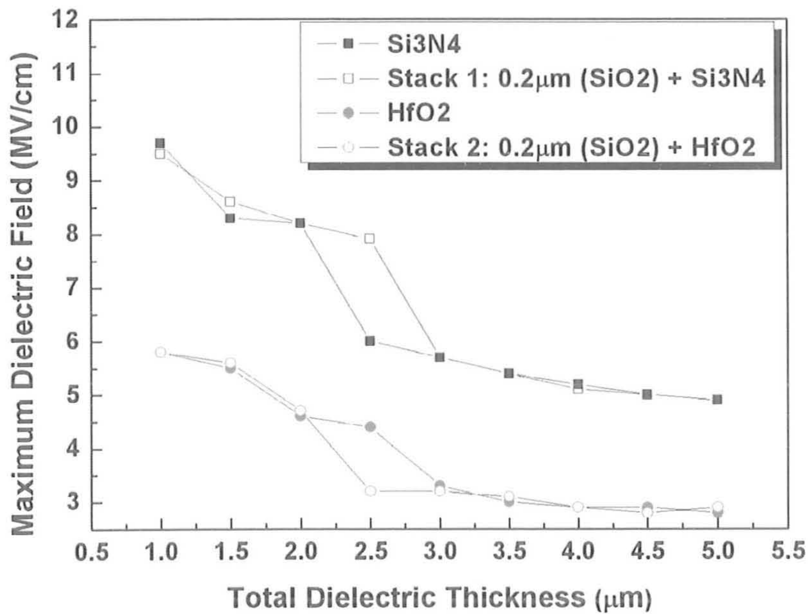

Fig. 6.47 – The effect of using SiO_2–high-k dielectric stacks on the maximum electric field in the insulators, at breakdown

Another important result is that, at breakdown, the maximum electric field in the SiO_2 layer is lower than 2MV/cm for T_{DIE} > 4.5μm in the case of Si_3N_4, and for T_{DIE} larger > 3μm in the case of HfO_2 (**Fig. 6.48**). Therefore, if the ramp is carefully designed, the supplementary thin silicon dioxide layer does not increase the risk of premature dielectric breakdown and does not affect the electrical parameters of the structure, but has the advantage of not having a direct interface between the high-k dielectric and diamond, interface which may otherwise be prone to high defect concentrations.

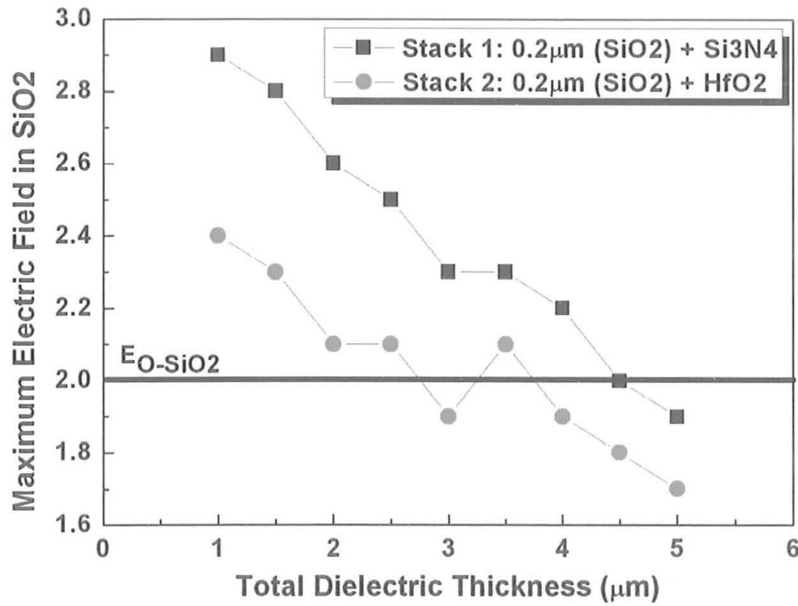

Fig. 6.48 – The maximum electric field
in the SiO_2 layer at breakdown, when using a SiO_2 – high-k dielectric stack

Chapter 7

Conclusions and future work

CHAPTER 7

Conclusions and future work

The fabrication of power Schottky barrier diodes on synthetic diamond is one of the hottest topic within the academic research on power electronics. The remarkable results exhibited by SiC SBDs which are already commercially available enable the hope that wide band gap semiconductors can indeed become a reliable alternative to Si devices in the range of medium to high voltage applications, requiring high frequency and more often high temperature operation.

In terms of physical properties, diamond is the hardest known material, has extremely high boiling and melting points, and is highly transparent to light in the visible range (**Chapter 2**). It has also one of the highest band gaps among semiconductors (5.47eV). This leads to an extremely low intrinsic concentration, which enables the operation at higher temperatures compared to Si and SiC and yields significantly lower leakage currents. Synthetic diamond exhibits as well the highest critical electric field, thermal conductivity and intrinsic carrier concentration of any semiconductor. These remarkable properties lead to outstanding figure of merits for diamond power devices. Due to the lack of shallow n-type dopants, research has mainly focused on diamond devices with unipolar conduction mechanism and in particular on Schottky diodes. Different types of diamond Schottky barrier diodes and field effect transistors have been already demonstrated (**Chapter 2**).

Numerical simulations are an essential tool when searching for optimum device designs to be implemented in diamond. Due to its relative novelty, diamond is not included in the material libraries available in simulators, therefore it had to be defined by the author in order to obtain the results presented in this thesis. The severe decrease of the mobility with the doping level and the temperature needs to be carefully taken into consideration when designing a diamond device (**Chapter 3**). The incomplete ionization of dopants, due to the material's tight atomic structure, induces low carrier concentrations at room temperature. Since reliable ionization coefficients in diamond were not yet

measured, the estimated values of these parameters used in simulations were obtained via extrapolation from silicon and silicon carbide, based on the band gap of each material.

It is the purpose of this thesis to thoroughly investigate the diamond M-i-P Schottky structure, introduced in **Chapter 4**. In order to overcome the dopant incomplete ionization drawback, the drift region of the M-i-P diode is designed to be extremely lowly doped, ideally intrinsic. This takes full advantage of the high intrinsic hole concentration ($3800cm^2/Vs$). At the same time, the substrate doping level is normally higher than $10^{19}cm^{-3}$ boron atoms which approaches the limit of $10^{20}cm^{-3}$ above which all the atoms are ionized at room temperature. Such a structure has the potential of beating the performance of SiC Schottky barrier diodes in the range of medium to high voltages.

The on-state characteristic of a diamond M-i-P Schottky diode has a complex shape, which can be divided into three regions (**Chapter 5**). At low forward biases, as the drift layer is not purely intrinsic, the charge injected from the substrate can be compensated by the charge within the drift layer, therefore the device acts as a classical power Schottky diode with moderately drift doping level (10^{15}-$10^{16}cm^{-3}$). The current obeys the thermionic emission theory and has an exponential variation with the voltage. As the voltage increases, the injected charge cannot be compensated anymore and the current becomes space-charge limited, thus turning to a quadratic dependence on the voltage. Finally, for large current levels, the voltage drop on the internal resistances of the device becomes predominant and the current-voltage curve becomes linear.

In terms of temperature variation, diamond M-i-P structures exhibit both negative and positive temperature coefficients. For small current levels, the strong increase of the saturation current (which has a linear impact on the forward current) with temperature is the leading effect, resulting in an overall negative temperature coefficient. As the current rises, the degradation of the mobility with temperature plays a more significant role, as it induces an increase in the on-state resistance of the drift and substrate layers, thus elevating the voltage drops on these regions. This leads to a change towards a positive temperature coefficient for high current and voltage levels. The point which corresponds to the crossing between the two trends of variation with temperature is called the zero temperature coefficient point and its coordinates (forward current and voltage) can be adjusted by changing the metal used for forming the Schottky contact.

Apart from the promising on-state results reported so far (current densities up to $100A/cm^2$ for 5V forward voltage drop), diamond M-i-P exhibit even more attractive off-state performance. Breakdown voltages up to 2500V were reported on diamond samples with 18μm drift thickness and large area Schottky contacts, while point measurements carried out of the same type of samples led to breakdown voltages of 4.1kV. All these results were measured on structures which lacked a termination structure, thus being prone to edge effects.

Finding termination structures suitable for diamond devices is not an easy task, due to the unavailability of n-type regions with decent electron concentration at room temperature. Several implementations of the field plate concept are compared in **Chapter 6**. The single step field plate termination requires the less complex technological process, but has electrical performance significantly lower than the three step field plate and ramp oxide structures. The optimum design of the latter exhibits a breakdown voltage with only 7% lower than the value corresponding to an ideal structure with the same geometrical properties and doping profile. Diamond M-i-P Schottky structures with ramp oxide termination were for the first time produced and experimental results confirm the potential of the termination structure.

Due to the high critical electric field of the material, power diamond devices are prone to premature breakdown within the insulator (i.e. field oxide) used for the ramp oxide termination. High-k dielectrics such as Si_3N_4 and HfO_2 can be used instead or together with SiO_2 in order to reduce this risk, without significantly affecting the electrical performance of the termination.

In conclusion, research carrier out in the last five years in synthesizing electronic quality single crystal diamond together with the results presented in this thesis have proved the extraordinary potential of this material for power electronics. Although not entirely confirming the theoretical predictions for 'ideally pure' diamond, the experimental investigations have shown the ability of thin diamond M-i-P diodes (drift thicknesses lower than 25μm) to withstand breakdown voltages up to 4kV. On-state current densities approaching $100A/cm^2$ have also been demonstrated. Key-issues such as reducing crystalline defects, optimising the contact deposition procedure and measuring reliable ionization coefficients remain the focus on ongoing research and development.

The results obtained so far point to a diamond M-i-P Schottky diode rated up to 3000V being an exciting alternative to replace silicon p-i-n and especially silicon carbide Schottky diodes in power electronic systems in medium term.

Further work

The work presented in this thesis can be continued on several directions:

- A thorough analysis of the bulk and surface defects related to synthetic diamond layers, together with the optimization of Schottky contact deposition process. Many of the experimental results obtained so far on diamond M-i-P Schottky diodes could not be matched by simulations. Extremely high turn-on voltage and abnormally shaped on-state characteristics were among the most often reported undesired experimental data. These results are mainly due to the poor quality of the Schottky contacts, which has a great influence especially on the turn-on characteristic. At the same time, samples with good on-state behaviour exhibited poor breakdown voltage and diodes with excellent off-state capability showed low forward currents. The traps and vertical dislocations within the diamond drift layer are believed to be responsible for these unsatisfactory results. A complete analysis of the diamond defects would also help in better calibrating the simulations. If clearly defined, the main material defects can be inserted in the simulated device, thus increasing the quality of the simulation-experimental matching.

- Measurement of reliable ionization coefficients for diamond. The values used now in the simulators are empirically extrapolated from the values corresponding to silicon and silicon carbide. This introduces errors when calculating the breakdown voltage and estimating the capability of different termination structures.

- Fabrication of diamond M-i-P Schottky diodes with ramp oxide termination using high-k dielectrics. Simulations show the capability of HfO_2 and Si_3N_4 to successfully replace SiO_2 as insulator for the ramp oxide structure, thus reducing

the risk for premature breakdown. However, experimental data are needed to confirm these results, since issues like defects and traps at the high-k dielectric – diamond interface might occur when fabricating such a structure.

- A complete model for the mobility dependence with temperature and doping. The severe decrease of mobility with both doping level and temperature seriously affects the performance of diamond devices. A model able to incorporate both effects in a single set of equations would be extremely valuable for correctly predicting the performance of such devices when operating in extreme conditions.

The research work included in this thesis was part of the CAPE (CArbon Power Electronics) project, which ran between January 2004 and June 2007 [105]. CAPE was a development project undertaken by a consortium comprising Elements Six Ltd., Dynex Semiconductor Ltd. and the University of Cambridge. The project was funded under the Department of Trade and Industry (DTI) Link BASIC Technologies for Industrial Applications (BTIA) program. The project aimed to develop technologies for novel power electronic components based on semiconducting synthetic diamond. The fabrication of a diamond M-i-P Schottky diode capable of operating at 1700V and 10A/cm^2 was one of the main achievements of this project.

REFERENCES

[1] R.N. Hall, *Power rectifiers and transistors*, Proc. IRE, Vol. 40, 1952, pp. 1512

[2] E.I. Caroll, Power electronics for very high power applications, IEEE Trans. On Pow. Elec., Vol. 15, No. 6, 2000, pp. 1102

[3] S.C. Sun and J.D. Plummer, *Modeling of the on-resistance of LDMOS VDMOS and VMOS power transistor*, IEEE Trans on Electr Dev, Vol. 27, 1980, pp. 356.

[4] B.J. Baliga, *Power Semiconductor Devices*, PWS Publishing Company, 1996, pp. 373

[5] B.J. Baliga, *Silicon Carbide Power Devices*, World Scientific Publishing, 2005

[6] J.A. Cooper and A. Agarwal, *SiC-Power Switching Devices – The Second Electronic Revolution?*, Proc. of IEEE, Vol. 90, 2002, pp. 956

[7] D. Nakamura et al., *Ultrahigh quality silicon carbide single crystals*, Nature, Vol. 430, 2004, pp. 1009

[8] K.V. Vasillevski et al., 4H-SiC rectifiers with dual metal planar Schottky contacts, IEEE Trans. on El. Dev, Vol. 49, 2002, pp. 947

[9] www.infineon.com

[10] www.cree.com

[11] K. Asano et al., 5.5kV normally-off low Ron 4H-SIC SEJFET, Proc. ISPSD 2001, pp. 23

[12] J. Isberg et al., *High carrier mobility on single-crystal plasma-deposited diamond*, Science, Vol. 297, 2002, pp. 1670

[13] G.A.J. Amaratunga, *A dawn for carbon electronics?*, Science, Vol. 297, 2002, pp. 1657

[14] Robert M. Hazen, *The diamond makers*, Cambridge University Press, 1999

[15] H.T. Hall, *The Synthesis of diamond*, Journal of Chemical Education, Vol. 38, 1961, pp. 484

[16] F.P. Bundy, H.T. Hall, H.M. Strong and R.H. Wentorf, *Man-made diamonds*, Nature, Vol. 176, 1955, p. 51

[17] M.N. Yoder, Naval Research Reviews, Office of Naval Research Two, 1987 XXXIX, pp. 27

[18] B.T. Kelly, *Physics of Graphite*, Applied Science Publishers, 1981

[19] W. Crookes, *A New Formation of Diamond*, Proc of the Royal Society in London, Vol. 76, 1905, pp. 458

[20] Z. Guofang, S. Fazheng, T. Weizhong, L. Fanxiu, *Preparation of high quality transparent chemical vapor deposition diamond films by a DC arc plasma jet method*, Dia. and Rel. Mat., Vol. 9, 2000, pp. 1678

[21] J. Walker, *Optical absorption and luminescence in diamond*, Rep. Prog. Phys., Vol. 42, 1979

[22] S.E. Coe and R.S. Sussmann, *Optical, thermal and mechanical properties of CVD diamond*, Dia. and Rel. Mat., Vol. 9, 2000, pp. 1726

[23] G.E. Harlow, R.M. Davies, *Diamonds*, Elements, Vol. 1, No. 2, 2005, pp. 67

[24] C.E. Nebel, *Electronic properties of CVD diamond*, Semicond. Sci. Technol., Vol. 18, 2003, S1-S11

[25] S.M. Sze, *Physics of semiconductor devices*, John Wiley and Sons, 1981

[26] S. Salvatori et al., *High-temperature performances of diamond-based UV-photodetectors*, Dia. and Rel. Mat., Vol. 9, 2000, pp. 982

[27] G. Knuyt et al., *Photoconductivity observations on phosphorous-doped n-type CVD diamond at low temperature and varying electric field*, Dia. and Rel. Mat., Vol. 15, 2006, pp. 29

[28] M. Brezeanu, *Ramp oxide termination structure using high-k dielectrics for high voltage diamond Schottky diodes*, Dia. and Rel. Mat., Vol. 16, 2007, pp. 1020

[29] C.E. Nebel, M. Stutzmann, *Transport properties of diamond: carrier mobility and resistivity*, Handbook (Dia. And Rel Mat.), May 2000

[30] J. Isberg, A. Lindblom, A. Tajani, D. Twitchen, *Temperature dependence of hole drift mobility in high-purity single-crystal CVD diamond*, Phys. Stat. Solidi A, Vol. 202, 2005, pp. 2194

[31] H. Umezawa et al., *Potential applications of surface channel diamond field-effect transistors*, Dia. and Rel. Mat., Vol. 10, 2001, pp. 1743

[32] J.E. Butler et al., *Exceptionally high voltage Schottky diodes and low boron doping*, Semicond. Sci. Tech, Vol. 18, 2003, S67

[33] H. Taniuchi et al., *High-frequency performance of diamond field-effect transistor*, IEEE Elec. Dev Let., Vol. 22, 2001, pp. 390

[34] A. Aleksov et al., *RF performance of surface channel diamond FETs with sub-micron gate length*, Dia. and Rel. Mat., Vol. 11, 2002, pp. 382

[35] T. Kashiwagi et al., *Investigation of Basic Characteristic of Synthetic Diamond Radiation Detectors*, IEEE Trans. on Nuclear Sci., Vol. 53, 2006, pp. 630

[36] H. Kagan, *Diamond radiation detectors might be forever!*, Nucl. Instr. and Meth in Phys. Research A 546 (2005), pp. 222

[37] C. Wang et al., *Boron-doped diamond film homoepitxally grown on high-quality chemical-vaport-deposited diamond (100)*, Jpn. Journ. Appl. Phys., Vol. 40, 2001, pp. 4145

[38] J.P. Goss, P.R. Briddon, *Theoretical study of Li and Na as n-type dopants for diamond*, Phys. Rev. B, Vol. 75, 2007, 075202

[39] E.O. Johnson, *Physical limitations on frequency and power parameters of transistors*, RCA Rev, Vol. 26, 1965, pp. 163

[40] R.W. Keyes, *Figure of merit for semiconductors for high speed switches*, Proc. IEEE, Vol. 60, 1972, pp. 225

[41] B.J Baliga, *Semiconductors for high-voltage, vertical channel FETs*, Journ. Appl. Phys., Vol. 53, 1982, pp. 1759

[42] D.J. Twitchen et al., *High-Voltage Single-Crystal Diamond Diodes*, IEEE Trans. on El. Dev., Vol. 51, 2004, pp. 826

[43] R.J. Nemanich et al., *Electron emission properties of crystalline diamond and III-nitride surfaces*, Appl. Surf. Sci., Vol. 130-132, 1998, pp. 694

[44] J. Ristein, *Surface science of diamond: familiar and amazing*, Surf. Sci., Vol. 600, 2006, pp. 3677

[45] J.P. Goss, P.R. Briddp, R.J. Eyre, *Donor levels for selected n-type dopants in diamond: A computational study of the effect of the supercell size*, Phys. Rev. B, Vol. 74, 2006, pp. 245217

[46] A. Aleksov et al., *Diamond diodes and transistors*, Semicond. Sci. Tech, Vol. 18, 2003, S59

[47] M. Brezeanu, J. Rashid, A. Tajani, A. Garraway, *Diamond Schottky Diodes for Power Electronics*, Elec. World, August 2006, pp. 20

[48] M. Brezeanu et al., On-state behaviour of diamond M-i-P structures, Proc. IEEE CAS Conf., 2006, pp. 311

[49] A. Vescan et al., *Very high temperature operation of diamond Schottky diode*, IEEE El. Dev. Lett., Vol. 18, 1997, pp. 556

[50] A. Balducci et al., *Extreme ultraviolet single-crystal diamond detectors by chemical vapour deposition*, Appl. Phys. Lett., Vol. 86, 2005, pp. 193509

[51] A. Balducci et al., *Extreme UV single crystal diamond photodetectors by chemical vapour deposition*, Dia and Rel. Mat.., Vol. 14, 2005, pp. 1980

[52] M. Brezeanu et al., Optically triggered Schottky barrier diodes in single crystal diamond, Dia and Rel. Mat.., Vol. 14, 2005, pp. 499

[53] H. Kawarada, Hydrogen-terminated diamond surfaces and interfaces, Surf. Sci. Rep., Vol. 26, 1996, pp. 205

[54] E. Kohn, A. Denisenko, *Concepts for diamond electronics*, Thin Solid Films, Vol. 515, 2007, pp. 4333

[55] K. Ueda et al., *Diamond FET using high-quality polycrystalline diamond with f_T of 45GHz and f_{MAX} of 120GHz*, IEEE El. Dev. Lett., Vol. 27, 2006, pp. 570

[56] M. Kubovic et al., *Microwave performance evaluation of diamond surface channel FETs*, Dia. and Rel. Mat., Vol. 13, 2004, pp. 802

[57] M. Kasu, *Microwave operation of diamond field-effect transistor*, NTT Tech. Rev., Vol. 2, 2004, pp. 19

[58] K. Hirama et al., *RF diamond MISFETs using surface accumulation layer*, Proc. ISPSD 2006, pp. 1

[59] A. Denisenko and E. Kohn, *Diamond power devices. Concepts and limits*, Dia. and Rel. Mat., Vol. 14, 2005, pp. 491

[60] ISE TCAD Manuals version 10.0, 2006

[61] S.J. Rashid et al., *Modelling of single-crystal diamond Schottky diodes for high-voltage applications*, Dia. and Rel. Mat., Vol. 15, 2006, pp. 317

[62] S.J. Rashid et al., *Numerical and experimental analysis of single crystal diamond Schottky barrier diodes*, Proc. ISPSD 2005, pp. 315

[63] G. Maseti, M. Severi, S. Solmi, *Modeling of carrier mobility against carrier concentration in Arsenic-, Phosphorus- and Boron-doped Silicon*, IEEE Trans. on El. Dev., Vol. 30, 1983, pp. 764

[64] K. Somogyi, *Classical approximations for ionised impurity scattering applied to diamond monocrystals*, Dia. and Rel. Mat., Vol. 11, 2002, pp. 686

[65] R. van Overstraeten, H. de Man, *Measurements of ionization rates in diffused silicon p-n junctions*, Solid State Elec., Vol. 13, 1970, pp. 583

[66] W. Schottky, *Halbleitertheorie der Sperrschicht*, Naturwissenschaften, Vol. 26, 1938, pp. 843

[67] S.M. Sze, *Semiconductor devices. Physics and technology*, John Wiley and Sons, 1985

[68] B.G. Streetman, S. Banerjee, *Solid state electronic devices*, Prentice Hall International, 2000

[69] B.J. Baliga, *The future of power semiconductor device technology*, Proc. of the IEEE, Vol. 89, 2001, pp. 822

[70] B.J. Baliga, *Power semiconductor device figure of merit for high frequency applications*, IEEE El. Dev. Lett.,., Vol. 10, 1989, pp. 455

[71] N. Mohan, T.M. Undeland, W.P. Robbins, *Power Electronics: Converters, Applications, and Design*, Wiley, 2006

[72] M. Bhatnagar, B.J. Baliga, Silicon carbide high voltage (400V) Schottky barrier diodes, IEEE Elec. Dev. Lett., Vol. 13, 1992, pp. 501

[73] D. Alok, B.J. Baliga, A simple edge termination for silicon carbide devices with nearly ideal breakdown voltage, IEEE Elec. Dev. Lett., Vol. 15, 1994, pp. 394

[74] http://www.cree.com/press/press_detail.asp?i=1171029691679

[75] http://www.cree.com/products/power_docs2.asp

[76] http://www.cree.com/products/pdf/CID150660.A.pdf

[77] M. Brezeanu et al., *Single Crystal Diamond M-i-P Diodes for Power Electronics*, Proc. ISPS 2006, pp. 103

[78] O.W. Richardson, *Thermionic phenomena and the laws which govern them*, Nobel Lecture, 12 December 1929

[79] Thomas Edison, US Patent 214,636 for *Improvement in Electric Lights*, Issue Date 22 April 1879

[80] O.W. Richardson, *On the negative radiation from hot platinum*, Proc. of the Cambridge Phil. Soc., Vol. 11, 1902, pp. 286

[81] O.W. Richardson, *The electron theory of contact electromotive force and thermo-electricity*, Phil. Mag., Vol. 23, 1912, pp. 263

[82] O.W. Richardson, *Some applications of the electron theory of matter*, Phil. Mag., Vol. 23, 1912, pp. 594

[83] H.A. Bethe, MIT Radiation Laboratory Report No. 43-12, 1942

[84] C.D. Child, *Discharge from hot CAO*, Phys. Rev. 32, 1911, pp. 492

[85] I. Langmuir, *The Effect of Space Charge and Residual Gases on Thermionic Currents in High Vacuum*, Phys. Rev. 2, 1913, pp. 450

[86] N.F. Mott, R.W. Gurney, *Electronic processes in ionic crystals*, Oxford Univ. Press, 1940

[87] I. Ben-Yacoov, U.K. Misra, *Unipolar space charge limited transport*, Univ. Of California Santa Barbara lecture notes

[88] W.A. Mackie, J.E. Plumlee, A.E. Bell, *Work function measurements of diamond film surfaces*, Jour. Vac. Sci. Tech. B, Vol. 14, 1996, pp. 2041

[89] M. Brezeanu et al., *Termination Structures for Diamond Schottky Barrier Diodes*, Proc. ISPSD 2006, pp. 73

[90] D. C. Sheridan et al., *Design and Fabrication of Planar Guard Ring Termination for High Voltage SiC Diodes*, Solid State Electron., Vol. 44, 2000, pp1367.

[91] F. La Via et al., *Comparation Between Different Schottky Diode Edge Termination Structures: Simulation and Experimental Results*", Mat. Sci. Forum, Vols. 433-436, 2003, pp.827

[92] M. C. Tarplee, V.P. Madangagly, Q. Zhang, T.S. Surdarshan, *Design Rules for Field Pate Edge Termination in SiC Schottky Diodes*, IEEE Trans. El. Dev., Vol. 48, 2001, pp 2659

[93] V Saxena et al., *High Voltage Ni - and Pt - SiC Schottky Diodes Utilising Metal Field Plate Termination*, IEEE Trans. El. Dev., Vol. 46, 1999, pp. 456

[94] G. Brezeanu et al., *Electrical Characteristics Modeling of Large Area boron compensated 6H-SiC pin Structures*, Solid State El.., Vol. 44, 2000, pp. 571

[95] K. J. Schoen, J.M. Wodall, J.A. Cooper jr., M.R. Mellach, *Design Considerations and Experimental Analysis of High Voltage SiC Schottky Barrier Rectifiers*, IEEE Trans El. Dev., vol. 45, 1998, pp.1595

[96] I. Snackin, J.B. Dufrene, J.N. Meret, J.B. Casadi, *Fabrication and Simulation of 4H-SiC pin Diodes Having MESA Guard-ring Edge Termination*, Mat. Sci. Forum, Vols. 433-436, 2003, pp.879

[97] G. Brezeanu et al., *High Performance SiC Diodes Based on an Efficient Planar Termination*, Proc. IEEE CAS 2003, pp. 27

[98] J. Korec, R. Held, *Comparison of DMOS/IGBT-Compatible High-Voltage Termination Structures and Passivation Techniques*, IEEE Trans. El. Dev., Vol. 40, 1993, pp. 1845

[99] M. Badila, G. Brezeanu, Double Epitaxial Layer Power Schottky Diodes with End in the Ramp Oxide Technique, Proc. IEEE CAS 1993, pp. 255

[100] G. Brezeanu et al., *Accurate Modelling and Parameter Extraction for 6H-SiC Schottky Barrier Diodes (SBDs) with Nearly Ideal Breakdown Voltage*, IEEE Trans. El. Dev., Vol. 48, 2001, pp 2148

[101] M. Badila, G. Brezeanu, F. Mitu, *Schottky Oxide Ramp Diodes*, John Wiley Encycl. of Electrical and Electronics Eng, Vol. 18, 1999, pp. 710

[102] L. Lipkin, J. Palmour, *Insulator investigation on SiC for improved reliability*, IEEE Trans. on El. Dev., Vol. 46, 1999, pp. 525

[103] S. Saddow, A. Agarwal, *Advances in Silicon Carbide Processing and Applications,* Artech House Inc., 2004

[104] R. Ribes et al., *Review of high-k dielectric reliability issues*, IEEE Trans. on Dev. and Mat. Reliab., Vol. 5, 2005, pp. 5

[105] http://www-g.eng.cam.ac.uk/cape

APPENDIX A
Diamond parameters
implemented in ISE-TCAD simulator

```
Material = "Diamond" {

Epsilon
{ * Ratio of the permittivities of material and vacuum

  * epsilon() = epsilon
      epsilon = 5.7 # [1]
}


RefractiveIndex
{ * Optical Refractive Index

  * refractiveindex() = refractiveindex * (1 + aplpha * (T-Tpar))
      refractiveindex = 2.684 # [1]
      alpha    = 4.04e-06    # [1/K]
      Tpar     = 3.0000e+02    # [K]
}


Kappa
{ * Lattice thermal conductivity

  * Formula = 1:
  * kappa() = kappa + kappa_b * T + kappa_c * T^2
      kappa    = 24 # [W/(K cm)]
      kappa_b = 0.0000e+00    # [W/(K^2 cm)]
      kappa_c = 0.0000e+00    # [W/(K^3 cm)]
}


Ionization
{
      E_As_0        = 0.1   # [eV]
      alpha_As      = 3.1000e-08    # [eV cm]
      g_As          = 2    # [1]
      Xsec_As = 1.0000e-12    # [cm^2/sec]
```

```
    E_P_0          = 0.62   # [eV]
    alpha_P        = 3.1000e-08    # [eV cm]
    g_P          = 2    # [1]
    Xsec_P         = 1.0000e-12    # [cm^2/sec]

    E_Sb_0         = 0.1   # [eV]
    alpha_Sb       = 3.1000e-08    # [eV cm]
    g_Sb           = 2     # [1]
    Xsec_Sb        = 1.0000e-12    # [cm^2/sec]

    E_B_0          = 0.37   # [eV]
    alpha_B        = 3.1000e-08    # [eV cm]
    g_B           = 4     # [1]
    Xsec_B         = 1.0000e-12    # [cm^2/sec]

    E_In_0         = 0.2   # [eV]
    alpha_In       = 3.1000e-08    # [eV cm]
    g_In          = 4     # [1]
    Xsec_In        = 1.0000e-12    # [cm^2/sec]

    E_N_0  = 0.1   # [eV]
    alpha_N        = 3.1000e-08    # [eV cm]
    g_N    = 2    # [1]
    Xsec_N = 1.0000e-12    # [cm^2/sec]

    E_NDopant_0     = 0.1   # [eV]
    alpha_NDopant  = 3.1000e-08    # [eV cm]
    g_NDopant       = 2     # [1]
    Xsec_NDopant    = 1.0000e-12    # [cm^2/sec]

    E_PDopant_0     = 0.2   # [eV]
    alpha_PDopant  = 3.1000e-08    # [eV cm]
    g_PDopant       = 4     # [1]
    Xsec_PDopant    = 1.0000e-12    # [cm^2/sec]

    NdCrit         = 1.0000e+18    # [cm-3]
    NaCrit         = 1.0000e+18    # [cm-3]
}
```

Bandgap

```
{ * Eg = Eg0 + dEg0 + alpha Tpar^2 / (beta + Tpar) - alpha T^2 / (beta + T)
  * dEg0(<bgn_model_name>) is a band gap correction term. It is used together with
  * an appropriate BGN model, if this BGN model is chosen in Physics section
  * Parameter 'Tpar' specifies the value of lattice
  * temperature, at which parameters below are defined
```

```
 * Chi0 is electron affinity.
    Chi0    = 1.3  # [eV]
    Bgn2Chi = 0.5  # [1]
    Eg0     = 5.47  # [eV]
    dEg0(Bennett)  = 0.0000e+00   # [eV]
    dEg0(Slotboom) = 0.0000e+00   # [eV]
    dEg0(OldSlotboom)      = 0.0000e+00   # [eV]
    dEg0(delAlamo) = 0.0000e+00   # [eV]
    alpha   = 0    # [eV K^-1]
    beta    = 0.0000e+00   # [K]
    Tpar    = 0.0000e+00   # [K]
}
```

Scharfetter * relation and trap level for SRH recombination:

```
{ * tau = taumin + ( taumax - taumin ) / ( 1 + ( N/Nref )^gamma)
 * tau(T) = tau * ( (T/300)^Talpha )          (TempDep)
 * tau(T) = tau * exp( Tcoeff * ((T/300)-1) ) (ExpTempDep)
      taumin = 0.0000e+00 ,          0.0000e+00   # [s]
      taumax= 1.0000e-05 , 3.0000e-06     # [s]
      Nref    = 1.0000e+16 ,         1.0000e+16    # [cm^(-3)]
      gamma= 1 ,    1        # [1]
      Talpha = -1.5000e+00 ,          -1.5000e+00   # [1]
      Tcoeff = 2.55 ,          2.55    # [1]
      Etrap   = 0.0000e+00 # [eV]
}
```

OldSlotboom

```
{ * deltaEg = dEg0 + Ebgn ( ln(N/Nref) + [ (ln(N/Nref))^2 + 0.5]^1/2 )
 * dEg0 is defined in BandGap section
    Ebgn    = 9.0000e-03    # [eV]
    Nref    = 1.0000e+17    # [cm^-3]
}
```

Slotboom

```
{ * deltaEg = dEg0 + Ebgn ( ln(N/Nref) + [ (ln(N/Nref))^2 + 0.5]^1/2 )
 * dEg0 is defined in BandGap section
    Ebgn    = 6.9200e-03    # [eV]
    Nref    = 1.3000e+17    # [cm^-3]
}
```

delAlamo

```
{ * deltaEg = dEg0 + Ebgn  ln(N/Nref)
 * dEg0 is defined in BandGap section
    Ebgn    = 0.0187        # [eV]
    Nref    = 7.0000e+17    # [cm^-3]
```

```
}

Bennett
{ * deltaEg = dEg0 + Ebgn (ln(N/Nref))^2
  * dEg0 is defined in BandGap section
      Ebgn    = 6.8400e-03    # [eV]
      Nref    = 3.1620e+18    # [cm^-3]
}

eDOSMass
{
  * For effective mass specificatition Formula1 (me approximation):
  * or Formula2 (Nc300) can be used :
      Formula = 2     # [1]
  * Formula1:
  * me/m0 = [ (6 * mt)^2 *  ml ]^(1/3) + mm
  * mt = a[Eg(0)/Eg(T)]
  * Nc(T) = 2(2pi*kB/h_Planck^2*me*T)^3/2 = 2.540e19 ((me/m0)*(T/300))^3/2
       Nc300       = 5e+18        # [2]
}

hDOSMass
{
  * For effective mass specificatition Formula1 (mh approximation):
  * or Formula2 (Nv300) can be used :
      Formula = 2     # [1]
  * Formula1:
  * mh =  m0*{[(a+bT+cT^2+dT^3+eT^4)/(1+fT+gT^2+hT^3+iT^4)]^(2/3) + mm}
  * Nv(T) = 2(2pi*kB/h_Planck^2*mh*T)^3/2 = 2.540e19 ((mh/m0)*(T/300))^3/2
       Nv300       = 1.8e+19        # [2]
}

ConstantMobility:
{ * mu_const = mumax (T/T0)^(-Exponent)
      mumax   = 4500 ,  3800     # [cm^2/(Vs)]
      Exponent      = 3.0 ,  3.0      # [1]
}

DopingDependence:
{
  * For doping dependent mobility model three formulas
  * can be used. Formula1 is based on Masetti et al. approximation.
  * Formula2 uses approximation, suggested by Arora.
      formula = 1 ,   1      # [1]
  * If formula=1, model suggested by Masetti et al. is used:
  * mu_dop = mumin1 exp(-Pc/N) + (mu_const - mumin2)/(1+(N/Cr)^alpha)
```

```
 *                         - mu1/(1+(Cs/N)^beta)
 * with mu_const from ConstantMobility
     mumin1  = 20 ,  103        # [cm^2/Vs]
     mumin2  = 0.0000e+00 ,  70      # [cm^2/Vs]
     mu1     = 0.0000e+00 ,  48.5      # [cm^2/Vs]
     Pc      = 0.0000e+00 ,  0.0000e+00      # [cm^3]
     Cr      = 4.5000e+17 ,  1.0000e+14      # [cm^3]
     Cs      = 3.4300e+20 ,  5.6000e+14      # [cm^3]
     alpha   = 0.45 ,        0.57     # [1]
     beta    = 2 ,   10       # [1]
}
```

HighFieldDependence:

```
{ * Caughey-Thomas model:
 * mu_highfield = mu_lowfield / ( 1 + (mu_lowfield E / vsat)^beta )^1/beta
 * beta = beta0 (T/T0)^betaexp.
     beta0   = 2 ,   2       # [1]
     betaexp = 0.0000e+00 ,  0.0000e+00      # [1]

 * Smoothing parameter for HydroHighField Caughey-Thomas model:
 * if Tl < Tc < (1+K_dT)*Tl, then smoothing between low field mobility
 * and HydroHighField mobility is used.
     K_dT    = 0.2 , 0.2      # [1]
 * Transferred-Electron Effect:
 * mu_highfield = (mu_lowfield+(vsat/E)*(E/E0_TrEf)^4)/(1+(E/E0_TrEf)^4)
     E0_TrEf = 4.0000e+03 ,  4.0000e+03      # [1]
     Ksmooth_TrEf    = 1 ,   1       # [1]

 * For vsat either Formula1 or Formula2 can be used.
     Vsat_Formula    = 1 ,   1       # [1]
 * Formula1 for saturation velocity:
 *           vsat = vsat0 (T/T0)^(-Vsatexp)
 * (Parameter Vsat_Formula has to be not equal to 2):
     vsat0   = 2.0000e+07 ,  2.0000e+07      # [1]
     vsatexp = 0.5 , 0.5      # [1]
}
```

PooleFrenkel

```
{ * TrapXsection = Xsec0*(1+Gpf)
 * Gpf = (1+(a-1)*exp(a))/a^2-0.5
 * where
 *      a = (1/kT)*(q^3*F/pi/e0/epsPF)^0.5,
 *      F is the electric field.
     epsPF   = 5.7 ,         5.7    # [1]
}
```

```
vanOverstraetendeMan * Impact Ionization:
{ * G_impact = alpha_n n v_drift_n  +  alpha_p p v_drift_p
  * with alpha = gamma a  exp(-b gamma/E) for E<E0 (low) and E>E0 (high)
  *  with gamma = tanh(hbarOmega/(2kT0)) / tanh(hbarOmega/(2kT))
       a(low)  = 1.89e+05 ,  5.48e+06      # [1/cm]
       a(high) = 1.89e+05 ,  5.48e+06      # [1/cm]
       b(low)  = 1.7e+07 ,  1.42e+07       # [V/cm]
       b(high) = 1.7e+07 ,  1.42e+07       # [V/cm]
       E0      = 4.0000e+05 ,  4.0000e+05      # [V/cm]
       hbarOmega       = 1.0000e+03 ,  1.0000e+03      # [eV]
}


}
```

APPENDIX B

List of publications and patents

Papers published in journals

1. **M. Brezeanu**, T. Butler, N. Rupesinghe, S.J. Rashid, M. Avram, G.A.J. Amaratunga, F. Udrea, M. Dixon, D. Twitchen, A. Garraway, D. Chamund, P. Taylor, *"Single Crystal Diamond M-i-P Diodes for Power Electronics"*, published IET Circuits, Devices & Systems, Vol. 1, No. 5 (2007), pp. 380-386

2. **M. Brezeanu**, T. Butler, N. L. Rupesinghe, G. A. J. Amaratunga, S. J. Rashid, F. Udrea, M. Avram, G. Brezeanu, *"Ramp Oxide Termination Structure using High-k Dielectrics for High Voltage Diamond Schottky Diodes"*, presented at the 17th European Conference on Diamond, Diamond-Like Materials, Carbon Nanotubes, Nitrides & Silicon Carbide (Diamond 2006), 3-8 Sept. 2006, Estoril, Portugal, published in Diamond & Related Materials, Vol. 16, Issues 4-7 (2007), pp. 1020-1024

3. **M. Brezeanu**, J. Rashid, A. Tajani, A. Garraway, *"Diamond Schottky Diodes for Power Electronics"*, published in Electronics World magazine, August 2006, pp. 20-24

4. **M. Brezeanu**, M. Badila, G. Brezeanu, F. Udrea, C. Boianceanu, G.A.J. Amaratunga, K. Zekentes, *"Theoretical study of an Effective Field Plate Termination for SiC Devices Based on High-k Dielectrics"*, presented at the International Conference on Silicon Carbide and Related Materials (ICSCRM 2005), 18-23 Sept. 2005, Pittsburgh, USA, published in Materials Science Forum, Vol. 527-529 (2006), pp. 1087-1090

5. S. J. Rashid, A. Tajani, L. Coulbeck, **M. Brezeanu**, A. Garraway, T. Butler, N. L. Rupesinghe, D. J. Twitchen, G. A. J. Amaratunga, F. Udrea, P. Taylor, M. Dixon, J. Isberg, *"Modelling of single-crystal diamond Schottky diodes for high-voltage applications"*, presented at the 8th Applied Diamond Conference (ADC 2005), May 2005, Chicago, USA, published in Diamond & Related Materials, Vol. 15 (2006), pp. 317-323

6. **M. Brezeanu**, S. J. Rashid, T. Butler, N. L. Rupesinghe, F. Udrea, K. Okano, G. A. J. Amaratunga, D. J. Twitchen, A. Tajani, C. Wort, *"Optically Triggered Schottky Barrier Diodes in Single Crystal Diamond"*, presented at the 15th European Conference on Diamond, Diamond-Like Materials, Carbon Nanotubes, Nitrides &

Silicon Carbide (Diamond 2004), 12-17 Sept. 2004, Riva del Garda, Trentino, Italy, published in Diamond & Related Materials , Vol. 14, Issue 3-7 (2005), pp. 499-503

7. G. Brezeanu, **M. Brezeanu**, F. Udrea, G. A. J. Amaratunga, M. Badila, K. Zekentes, *"Comparison between Schottky Diodes with Oxide Ramp Termination on Silicon Carbide and Diamond"*, presented at the 6th European Conference on Silicon Carbide and Related Materials (ECSCRM 2006), 3-7 Sept. 2006, Newcastle, UK, published in Material Science Forum, vols. 556-557 (2007), pp. 865-868

8. G. Brezeanu, C. Boianceanu, **M. Brezeanu**, A. Mihaila, F. Udrea, G. A. J. Amaratunga, *"Performance of SiC Cascode Switches with Si MOS Gate"*, presented at the 5th European Conference on Silicon Carbide and Related Materials (ECSCRM 2004), 31 Aug.-4 Sept. 2004, Bologna, Italy, published in Material Science Forum, vols. 483-485 (2005), pp. 825-828

Papers published in international conferences

9. **M. Brezeanu**, S. J. Rashid, G.A.J. Amaratunga, N.L. Rupesinghe, T. Butler, F. Udrea, G. Brezeanu, *"On-state behaviour of diamond M-i-P structures"*, presented at the 29th IEEE International Semiconductor Conference (CAS 2006), 27-29 Oct. 2006, Sinaia, Romania, published in the Proceedings of CAS 2006, pp. 311-314

10. G. Brezeanu, A. Visoreanu, **M. Brezeanu**, F. Udrea, G.A.J. Amaratunga, I. Enache, I. Rusu, *"Off-state performances of ideal Schottky barrier diodes (SBD) on diamond and silicon carbide"*, presented at the 29th IEEE International Semiconductor Conference (CAS 2006), 27-29 Oct. 2006, Sinaia, Romania, published in the Proceedings of CAS 2006, pp. 319-322

11. **M. Brezeanu**, T. Butler, N. Rupesinghe, S.J. Rashid, M. Avram, G.A.J. Amaratunga, F. Udrea, M. Dixon, D. Twitchen, A. Garraway, D. Chamund, P. Taylor, *"Single Crystal Diamond M-i-P Diodes for Power Electronics"*, presented at the 8th IEEE International Seminar on Power Semiconductors (ISPS 2006), 29 Aug.-1 Sept. 2006, Prague, Czech Republic, published in the Proceedings of ISPS 2006 (ISPS 2006), pp. 103-108

12. **M. Brezeanu**, M. Avram, S. J. Rashid, G. A. J. Amaratunga, T. Butler, N. L. Rupesinghe, F. Udrea, A. Tajani, M. Dixon, D. J. Twitchen, A. Garraway, D. Chamund, P. Taylor, G. Brezeanu, *"Termination Structures for Diamond Schottky Barrier Diodes"*, presented at the 18th International Symposium on Power Semiconductor Devices and ICs (ISPSD 2006), 4-8 June 2006, Napoli, Italy, published in the proceedings of ISPSD 2006, pp. 73-76

13. **M. Brezeanu**, S. J. Rashid, T. Butler, N. L. Rupesinghe, F. Udrea, A. Garraway, L. Coubeck, P. Taylor, G. A. J. Amaratunga, D. J. Twitchen, A. Tajani, M.P. Dixon,

"Highly Efficient Edge Terminations for Diamond Schottky Diodes", presented at the 28th IEEE International Semiconductor Conference (CAS 2005), 3-5 Oct. 2005, Sinaia, Romania, published in the Proceedings of CAS 2005, pp. 319-322

14. G. Brezeanu, M. Badila, **M. Brezeanu**, F. Udrea, C. Boianceanu, I. Enache, F. Draghici, A. Visioreanu, *"Breakdown Performance Improvements of SiC Diodes Using High-k Dielectrics"*, presented at the 28th IEEE International Semiconductor Conference (CAS 2005), 3-5 Oct. 2005, Sinaia, Romania, published in the Proceedings of CAS 2005, pp. 357-360

15. M. Avram, G. Brezeanu, A. Avram, O. Neagoe, **M. Brezeanu**, C. Iliescu, C. Codreanu, C. Voitincu, *"Contributions to Development of High Power SiC-IGBT"*, presented at the 28th IEEE International Semiconductor Conference (CAS 2005), 3-5 Oct. 2005, Sinaia, Romania, published in the Proceedings of CAS 2005, pp. 365-368

16. S. J. Rashid, L. Coulbeck, A. Tajani, **M. Brezeanu**, A. Garraway, T. Butler, N. L. Rupesinghe, D. J. Twitchen, G. A. J. Amaratunga, F. Udrea, P. Taylor, M. Dixon, J. Isberg, *"Numerical and Experimental Analysis of Single Crystal Diamond Schottky Barrier Diodes"*, presented at the 17th International Symposium on Power Semiconductor Devices and ICs (ISPSD 2005), 22-26 May 2005, Santa Barbara, USA, published in the proceedings of ISPSD 2005, pp. 315-318

17. S. J. Rashid, A. Tajani, L. Coulbeck, **M. Brezeanu**, A. Garraway, T. Butler, N. L. Rupesinghe, D. J. Twitchen, F. Udrea, P. Taylor, J. Isberg, G. A. J. Amaratunga, *"Analysis of Carrier Transport in Synthetic Single Crystal Diamond Schottky Diodes"*, presented at the 3rd International Conference on Materials for Advanced Technologies (ICMAT 2005), July 2005, Singapore

18. **M. Brezeanu**, S. J. Rashid, T. Butler, N. L. Rupesinghe, F. Udrea, K. Okano, G. A. J. Amaratunga, D. J. Twitchen, A. Tajani, C. Wort, A. Garraway, L. Coubeck, P. Taylor and D. G. Hasko, *"High Voltage Schottky Barrier Diodes in Synthetic Single Crystal Diamond"*, presented at the 27th IEEE International Semiconductor Conference (CAS 2004), 4-6 Oct. 2004, Sinaia, Romania, published in the Proceedings of CAS 2004, pp. 385-388

19. C. Boianceanu, G. Brezeanu, F. Udrea, G. Amaratunga, **M. Brezeanu**, A. Mihaila, F. Draghici, I. Enache, A. Visoreanu, *"SiC Device Parameters Effects on the Electrical Behaviour of MCascode Switch"*, presented at the 27th IEEE International Semiconductor Conference (CAS 2004), 4-6 Oct. 2004, Sinaia, Romania, published in the Proceedings of CAS 2004, pp. 389-392

20. G. Brezeanu, M. Badila, F.Udrea, J. Millan, P. Godignon, A. Mihaila, G. A. J. Amaratunga, **M. Brezeanu**, C. Boianceanu, *"High Performance SiC Diodes Based on an Effiecient Plannar Termination"*, Invited Paper presented at the 26th IEEE

International Semiconductor Conference (CAS 2003), 28 Sept.-02 Oct. 2003, Sinaia, Romania, published in the Proceedings of CAS 2003, pp. 27-38

21. C. Boianceanu, **M. Brezeanu**, A. Palfi, A. Mihaila, G. Brezeanu, F. Udrea, G. A. J. Amaratunga, I. Enache, *"Transient Analysis of Si-MOS and SiC-J-FET Cascode Power Switches"*, presented at the 26th IEEE International Semiconductor Conference (CAS 2003), 28 Sept.-02 Oct. 2003, Sinaia, Romania, published in the Proceedings of CAS 2003, pp. 227-230

22. **M. Brezeanu**, A. Rusu, L. Dobrescu, *"MOS Channel Length Modulation in Weak Inversion"*, presented at the 25th IEEE International Semiconductor Conference (CAS 2002), 8-12 Oct. 2002, Sinaia, Romania, published in the Proceedings of CAS 2002, pp. 301-304

23. G. Brezeanu, F. Udrea, A. Mihaila, G. A. J. Amaratunga, J. Millan, P. Godignon, M. Badila, F. Draghici, C. Boianceanu, **M. Brezeanu**, *"Numerical and Analytical Study of 6H-SiC Detectors with High UV Performance"*, presented at the 25th IEEE International Semiconductor Conference (CAS 2002), 8-12 Oct. 2002, Sinaia, Romania, published in the Proceedings of CAS 2002, pp. 185-188

24. A. Rusu, **M. Brezeanu**, L. Dobrescu, *"Advanced Modeling of MOS Transistors in Weak Inversion"*, presented at the 1st Balkan Workshop on Applied Physics (IBWAP 2002), Targoviste, Romania, September 2002, published in the Proceedings of IBWAP 2002

25. L. Dobrescu, **M. Brezeanu**, A. Rusu, A.M. Ionescu, *"On the limit between subthreshold and strong inversion regions in the EKV model using the nonlinear electrical conduction theorem"*, presented at the 24th IEEE International Semiconductor Conference (CAS 2001), October 2001, Sinaia, Romania, published in the Proceedings of CAS 2001, pp. 421-424

Papers presented at international conferences

26. **M. Brezeanu**, P. Servati, G. A. J. Amaratunga, F. Udrea, D. Chamund, A. Garraway, *"Transport characteristics of synthetic single crystal diamond Schottky diamond structures"*, presented at the 58th De Beers Diamond Conference, July 2007, Warwick, UK

27. G. A. J. Amaratunga, T. Butler, N. L. Rupesinghe, S. J. Rashid, **M. Brezeanu**, F. Udrea, A. Tajani, D. J. Twitchen, C. Wort, L. Coulbeck, P. Taylor, J. Isberg, *"High Voltage Synthetic Single Crystal Diamond metal-intrinsic-p+ (MIP) diodes"*, presented at the 16th European Conference on Diamond, Diamond-Like Materials,

Carbon Nanotubes, Nitrides & Silicon Carbide (Diamond 2005), Sept. 2005, Grenoble, France

28. L. Coulbeck, A. Garraway, P. Taylor, T. Butler, N. L. Rupesinghe, S. J. Rashid, **M. Brezeanu**, F. Udrea, G. A. J. Amaratunga, A. Tajani, M. Dixon, D. J. Twitchen, *"Diamond for High Voltage High Power Electronics, a Comparison to other Semiconductors"*, invited paper presented at the 16th European Conference on Diamond, Diamond-Like Materials, Carbon Nanotubes, Nitrides & Silicon Carbide (Diamond 2005), Sept. 2005, Grenoble, France

Patents

1. G.A.J Amaratunga, **M. Brezeanu**, S.J. Rashid, N.L. Rupesinghe, A. Tajani, D.J. Twitchen, F. Udrea, C. Wort, *"Switching Device"*, International Application Number PCT/IB2005/002654, International Publication Number WO2006/027669, filed on 08.08.2005 (pending)

CAMBRIDGE UNIVERSITY LIBRARY